A PROPOSED GROUND MOTION SELECTION AND SCALING PROCEDURE FOR NONLINEAR RESPONSE HISTORY ANALYSIS

by

Esra Zengin

B.S., Civil Engineering, Middle East Technical University, 2008

M.S., Civil Engineering, Boğaziçi University, 2010

Submitted to the Kandilli Observatory and Earthquake Research Institute

in partial fulfillment of the requirements for the degree of

Doctor of Philosophy

Graduate Program in Earthquake Engineering

Boğaziçi University

2016

ACKNOWLEDGEMENTS

I would like to express my sincere thanks to my supervisor, Prof. Dr. Sinan Akkar for his invaluable guidance and support, throughout this research.

I would like to thank the members of my dissertation committee, Prof. Dr. Erdal Şafak, Assoc. Prof. Dr. Beyza Taşkın, Assist.Prof. Dr. Ufuk Yazgan, and Assist. Prof. Dr. Özer Ay for their valuable comments and suggestions.

I would like to thank all the professors, colleagues and friends at the Department of Earthquake Engineering for their support and help.

Finally, I would like to express my sincere gratitude to my family. Thank you for the support, unconditional love, and encouragement throughout my life.

Dedicated to my beloved mother and father…

ABSTRACT

A PROPOSED GROUND MOTION SELECTION AND SCALING PROCEDURE FOR NONLINEAR RESPONSE HISTORY ANALYSIS

With the advancement in performance-based earthquake engineering, nonlinear response history analysis of structures has become more common in recent years. The selection and scaling of ground motions for use in nonlinear response history analysis is one of the most critical steps in performance-based seismic assessment procedures. This study presents ground motion selection and scaling procedure that addresses the uncertainty in the spectral demand with the preserved dispersion within the ground motion set. The candidate ground motion sets are constructed based on dispersion statistics about the target spectral demand. The optimum ground-motion set is linearly scaled by using an optimization algorithm that minimizes the error between scaled median and target spectra. The scaling stage ensures that the median record spectrum provides a reasonable match to target median in a previously defined period interval. This procedure allows performing further modification on each scaled ground motion in order to match the target variance of the scenario-based spectrum. In this study, a novel probabilistic framework is presented to propagate the uncertainties in both ground motion intensity and the structural response on fragility curve estimations. To investigate the effects of uncertainties on seismic damage estimations, the results of this study are compared with those obtained by the conventional fragility curve approach.

ÖZET

ZAMAN TANIM ALANINDA DOĞRUSAL OLMAYAN ANALİZ İÇİN ÖNERİLEN KAYIT SEÇİM VE ÖLÇEKLENDİRME YÖNTEMİ

Performans esaslı deprem mühendisliğindeki gelişmelerle, zaman tanım alanında doğrusal olmayan analiz yöntemlerinin uygulanması son yıllarda yaygın hale gelmiştir. Doğrusal olmayan yapısal davranış analizlerinde kullanılacak yer hareketlerinin seçimi ve ölçeklendirilmesi, performans esaslı sismik değerlendirme yöntemlerinin en kritik adımlarından biridir. Bu çalışma, hedef şiddet ölçüsündeki belirsizliği, seçilen yer hareketi setinin spektral değişkenliği ile temsil eden bir kayıt seçim ve ölçeklendirme yöntemi sunmaktadır. Aday deprem kayıt setleri hedef spektral talepteki saçılım (standard sapma) değerlerine göre oluşturulmuştur. Optimum kayıt seti, belli bir periyot aralığında, medyan kayıt spektrumu ile hedef spektrumu arasındaki hatayı en aza indirecek bir optimizasyon algoritması kullanılarak ölçeklendirilmiştir. Ölçeklendirme aşamasında medyan kayıt spektrumu ile hedef spektrumu arasında makul bir eşleşme sağlanmaktadır. Bu prosedür, senaryo-bazlı spektrumdaki hedef şiddet dağılımını yakalayan bir ölçeklendirme aşamasına da imkan vermektedir. Bu çalışmada, yer hareketi şiddeti ölçüsündeki ve yapısal tepkideki belirsizlikleri kırılganlık eğrisi hesaplamalarında göz önüne alan istatistiksel bir model sunulmuştur. Göz önüne alınan belirsizliklerin sismik hasar tahminleri üzerindeki etkisini incelemek amacıyla, bu çalışmadan elde edilen sonuçlar geleneksel kırılganlık eğrisi yaklaşımıyla elde edilen sonuçlarla karşılaştırılmıştır.

TABLE OF CONTENTS

LIST OF FIGURES

LIST OF TABLES

LIST OF SYMBOLS

df	Degree of freedom
D_{rms}	Root-mean-square difference
F_i	Lateral force at level i
H_0	Null hypothesis
M_w	Magnitude
MDOF	Multi degree of freedom
n_i	i^{th} sample size
N_{obs}	Number of observations
R_{jb}	Source to site distance
Sd,i	Inelastic spectral displacement
Sd,e	Elastic spectral displacement
SDOF	Single degree of freedom
$S.E.$	Standard error
SF_{final}	Final scale factor
SF_{median}	Median scale factor
s_i^2	i^{th} sample variance
SSE	Sum of the squared error
T_R	Return period
T_1	Fundamental period of the structure
V_1	First-mode base shear
w_j	Lumped seismic weight at j^{th} level
$\bar{X}_i$	i^{th} Sample mean
α	Significance level
β	Standard deviation estimation of the fitted fragility curve
γ_{ik}	Posterior probability of the ith observation belonging to the k-th mixture component

ε	Epsilon
ϕ_{j1}	Amplitude of the first mode at the jth level
θ	Median estimation of the fitted fragility curve
$\lambda(DV)$	Mean annual frequency of a decision variable
μ_k	Mean vector of the kth population
π_k	Mixing coefficients for the kth population
ρ	Pearson correlation coefficient
$\sigma_{\ln Sdi}$	Variability in the inelastic spectral displacement
Σ_k	Covariance matrix of the kth population

LIST OF ACRONYMS / ABBREVIATIONS

CDF	Cumulative distribution function
CMS	Conditional Mean Spectrum
CP	Collapse prevention
CS	Conditional Spectrum
DM	Damage measure
DSHA	Deterministic seismic hazard analysis
DV	Decision variable
EDP	Engineering demand parameter
EM	Expectation-Maximization
GMM	Gaussian mixture model
GMPE	Ground motion prediction equation
GMSM	Ground Motion Selection and Modification
IDR	Interstory drift ratio
IM	Intensity measure
IO	Immediate occupancy
LS	Life safety
MCE	Maximum Credible Earthquake
MDOF	Multi-degree-of-freedom
MIDR	Maximum interstory drift ratio
PBEE	Performance-Based Earthquake Engineering
PDF	Probability density function
PEER	Pacific Earthquake Engineering Research
PFA	Peak floor acceleration
PFD	Peak floor displacement
PGA	Peak ground acceleration
PGD	Peak ground displacement
PGV	Peak ground velocity
PSHA	Probabilistic seismic hazard analysis

RC   Reinforced concrete

RHA   Response history analysis

UHS   Uniform Hazard Spectrum

1. INTRODUCTION

1.1. Background and Motivation

Nonlinear response history analysis is recognized as the most accurate method for assessing the seismic response of structures with emerging trends in Performance-Based Earthquake Engineering (PBEE). The selection of ground motions for use in nonlinear response history analysis (RHA) is the most critical step for both code-based design checks and probabilistic seismic risk assessment of structures. Due to the complexity and time-consuming nature of nonlinear RHA, the analyst seeks to reduce the computational effort while not compromising the accuracy and reliability of structural response. One of the objectives of ground motion selection and scaling methodologies is to enable engineers to estimate the median response, or to predict the distribution of structural response, with relatively small number of ground motions. The current ground motion selection and modification (GMSM) methods have generally focused on assembling the real earthquake records as simulated records that can mimic the genuine characteristics of real accelerograms still require an extensive amount of scientific research (e.g., SCEC platform). The records having similar characteristics of the scenario event are typically modified to match the target spectrum to a single period or within a period range of interest.

GMSM procedures should be evaluated according to the purpose of their use. For example, the main objective of the code-based procedures is to predict the average or mean response of the structure for a specified level of ground shaking (e.g., IBC 2006, ASCE 2010, Eurocode 8 (CEN, 2003)). The building codes use uniform hazard spectrum (UHS), or its envelope, to define the target spectral accelerations for certain exceedance probabilities within a predefined exposure time (e.g., 2% in 50 years). Several guidelines are prescribed by the seismic codes for selecting appropriate ground motions for nonlinear response history analysis (e.g., Eurocode 8, ASCE 7-05). The aim of code-based scaling is to obtain ground motions that are compatible with the target spectrum over a period range

of interest such as between $0.2T_1$ and $2.0T_1$ where T_1 is the fundamental period of the structure. The spectral period band accounts for the higher mode effects and period elongation when seismic demands exceed the yield capacity of the structure. Various code-based GMSM methods have been proposed to achieve a reasonably accurate fit between the spectral ordinates of selected accelerograms and target spectrum (Naeim *et al.*, 2004; Iervolino *et al.*, 2006; Reyes and Kalkan, 2012). These methods disregard the variability in the target spectral acceleration because the probabilistic seismic hazard analysis (PSHA) takes epistemic and aleatory variability into account with a certain percentile of hazard distribution after implementing logic-trees in source and ground-motion characterization. Thus, the uncertainties associated with the calculated seismic hazard are not properly captured in the code-based scaling methods.

Alternative to PSHA, the seismic hazard can be represented by deterministic scenario-based events with a particular combination of magnitude, style-of-faulting, source-to-site distance, site conditions etc. The use of deterministic seismic hazard analysis (DSHA) in structural performance assessment is identified as scenario-based assessment in ATC-58-1 (NIST, 2011) in which the typical outcome would be the average structural response and its variability. For such cases, the target spectrum is developed by considering a ground motion prediction equation, GMPE, (or a suite of GMPEs) associated with the standard deviation to account for the ground motion (aleatory) variability. There are several ground motion selection and scaling approaches to capture the distribution of ground motion intensity (due to aleatory variability) in scenario-based assessment. For example, Rathje and Kottke (2007) proposed a ground motion selection and scaling procedure to control the variance about the scenario-based spectrum. Buratti *et al.* (2011) proposed a methodology that scales the records to three spectral levels of the target spectrum with the aim of approximating full distribution of drift response.

The current probabilistic seismic performance assessment methods require e valuating the full distribution of the response measures for different ground-motion intensity levels (Porter, 2003). These procedures mainly utilize the ground-motion hazard in a probabilistic manner and use the ground motion intensity measure (IM) as a proxy to characterize the earthquake damage potential with respect to structural performance

(Bojorquez *et al.*, 2012). Studies show that the elastic spectral acceleration at the fundamental period of the structure, $Sa(T_1)$, is efficient (i.e., small variability of structural response given IM) and sufficient (i.e., structural response is independent of other parameters, e.g. magnitude, distance, for a given IM) intensity measure for seismic structural assessment (Shome and Cornell, 1999; Baker and Cornell, 2006; Luco and Cornell, 2007). Iervolino and Cornell (2005) pointed out that scaling earthquake records to a single spectral ordinate $Sa(T_1)$ is useful in fragility curve computations (i.e., probability of failure at given IM) and it results in unbiased estimate of the structural response with reduced variability. Later, Baker and Cornell (2005) discussed the significance of using $Sa(T_1)$ and epsilon (ε; the number of standard deviations between the spectral acceleration of a record and the mean of a GMPE at the given period) together as a vector-valued IM for scaling of accelerograms as the latter parameter is an indicator of spectral shape that accounts for the shape of target spectrum (i.e., peaks or valleys in a response spectrum) yields better predictions of structural response. The consideration of epsilon in ground-motion scaling led to the proposition of Conditional Mean Spectrum, CMS, (Baker, 2005; Baker and Cornell, 2006; Baker, 2011) that generates the expected (mean) spectral accelerations (Sa) across a period band using their correlation (via epsilon) with the target spectral acceleration ordinate at T_1. In other words, CMS produces mean Sa conditioned on target $Sa(T_1)$ for a given period interval (e.g., $0.2T_1 < T_1 < 2T_1$). The recently proposed Conditional Spectrum (CS) brings improvements over CMS and considers the ground motion variability over the expected spectral accelerations conditioned on structure's fundamental period (Jayaram *et al.*, 2011; Lin *et al.*, 2013). The average of scaled ground motions following the spectral shape imposed by CS (equivalent to mean spectrum by CMS) with dispersion comparable to the ground motion variability dictated by the same spectrum would properly address the probabilistic building response (Haselton *et al.*, 2012). Except for the target spectral acceleration at T_1, the spectral ordinates computed by CMS and CS would be lower than those of UHS because they account for the spectral correlation conditioned on $Sa(T_1)$ specific to the most contributing earthquake scenario obtained from the disaggregation of probabilistic seismic hazard analysis. In this respect, CMS and CS overcome the conservatism imposed by UHS in the definition of target spectrum for ground motion scaling (Bommer *et al.*, 2000; Iervolino and Manfredi, 2008;

Lin *et al.*, 2013) and are recommended as target spectra for ground motion selection and scaling in PBEE (Haselton *et al.*, 2014).

Ground motions scaled to CMS or CS within a given period band have zero dispersion at the target spectral acceleration $Sa(T_1)$ because the ground motion variability is assumed to be fully represented for this spectral ordinate by PSHA. A proper PSHA considers the modelling uncertainty and ground motion variability by implementing complicated logic-tree structures and the resultant target hazard corresponds to a pre-determined percentile of hazard distribution (e.g., 50th percentile) resulting from the logic-tree branches. However, $Sa(T_1)$ computed via this procedure accounts for ground-motion variability and modelling uncertainties to a certain extent. This fact is presented in Figure 1.1 that shows the $T_1=0.2$-second-period spectral acceleration hazard for Diablo Kanyon Power Plant (California) site (Abrahamson, 2015). As seen in the figure, the PSHA calculations result in the form of fractile probabilities (5, 16, 50, 84 and 95%) and mean values over a range of annual probability of exceedance. In this figure, the epistemic uncertainty can be represented by the dispersion in the spectral demand at specified annual probability of exceedance. For example, when the target annual probability of exceedance is 0.001 (i.e., return period of 1000 years), the spectral acceleration ordinates vary from 0.4g (16th fractile) to 1.0g (84th fractile) with a mean value of 0.7g. In some studies, record selection and scaling procedures are proposed in order to account for the ground motion uncertainty stemming from the inherent nature of PSHA as discussed above. For example, Huang *et al.* (2011) presented a distribution scaling (D-scaling) method to capture both the median and dispersion in the spectral demand characterized by PSHA or ground motion prediction model. In their study, ground motions are scaled to a range of target spectral ordinates at the fundamental period of the structure to explicitly address the epistemic uncertainty in UHS. Ay and Akkar (2012) proposed a ground motion selection and scaling procedure that defines the scatter around the target hazard by using the difference between the actual ground motion and its estimation from a representative GMPE. Hines *et al.* (2011) discussed the additional uncertainty associated with the logic-tree calculations in PSHA (i.e., epistemic uncertainty) and the aleatory variability related to disaggregation of hazard into magnitude-distance pairs. In their work, a ground motion selection procedure is proposed to address these uncertainties without amplitude scaling. Bearing the

aforementioned discussion in mind, the primary objective of this study is to develop a ground motion selection and scaling methodology that considers the uncertainties in the intensity measure (i.e., epistemic uncertainty in PSHA-based spectrum, and aleatory variability in scenario-based spectrum). The proposed approach provides site-specific ground motions for use in nonlinear response history analysis for design and seismic performance assessment of buildings.
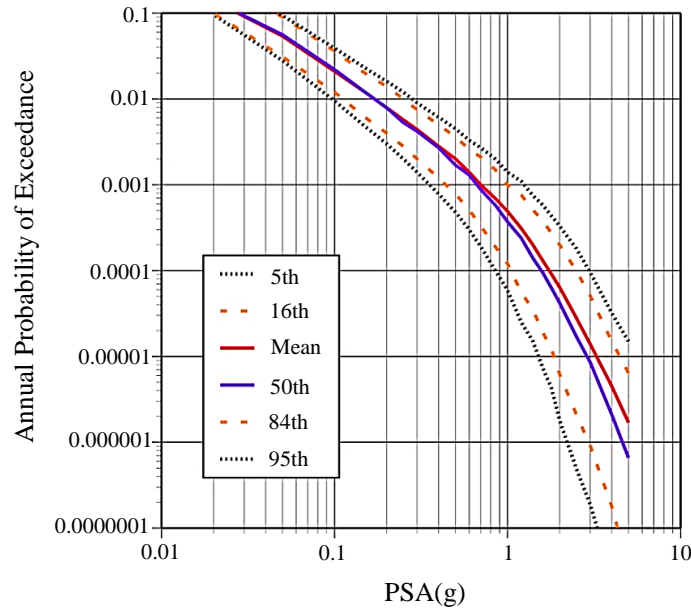
Figure 1.1. T_1=0.2-second-period spectral acceleration hazard for Diablo Kanyon Power Plant site (Abrahamson, 2015).

1.2. Scope and Organization

The proper selection of input motions for use in nonlinear response history analysis is a crucial prerequisite for reliable seismic performance evaluation of structures. The current research effort has been geared towards the development of methodologies for selecting and scaling of earthquake records. The main objective of this dissertation is to present a new ground motion selection and scaling procedure that implicitly takes into account the uncertainty in target intensity measure (i.e., epistemic uncertainty in PSHA) for a given seismic hazard level. The extension of this approach is aimed at scaling ground motions for matching scenario-based target spectrum. This study also introduces a novel

probability density estimation approach that propagates uncertainties in both intensity measure and structural response on analytical fragility curve estimations. This dissertation discusses the proposed ground motion selection and scaling methodology and its applications. The dissertation is composed of six chapters. The subsequent chapters are organized as follows:

Chapter 2 provides a brief background on seismic hazard analysis and CMS/CS concept. It then discusses the record selection criteria and reviews the current ground motion selection and scaling approaches.

Chapter 3 presents the proposed ground motion selection and scaling methodology and its applications. The performance of the proposed procedure for predicting the response of nonlinear single-degree-of-freedom systems is evaluated by comparing the results of this study with those obtained using the most commonly employed ground motion scaling method. In this chapter, the nonlinear response history analyses are conducted using different number of ground motions to determine the required number of ground motions for reliable and accurate estimate of the structural response.

Chapter 4 presents comparative studies to investigate the effect of different ground motion selection and scaling approaches on structural response distributions of 12-story reinforced concrete model building. In this chapter, the heightwise distributions of the selected engineering demand parameters (i.e., interstory drift ratios, peak floor displacements and peak floor accelerations) that are estimated by different scaling methods are compared. The correlations among spectral accelerations and engineering demand parameters are examined in order to understand the effect of different ground motion suites on structural response estimation. The exceedance probabilities of the maximum interstory drift ratios obtained from two different scaling methodologies are evaluated at three specified hazard levels.

Chapter 5 provides overview of the most commonly used probabilistic seismic demand models and proposes a new probabilistic framework to derive analytical fragility functions. The theoretical background of the proposed Gaussian Mixture Model is given

and its application to reinforced concrete model frame structure is demonstrated. The proposed approach implicitly treats the uncertainty in both ground motion intensity and structural response, and then propagates them into fragility curve. The analytical fragility curves obtained by the proposed approach are compared with those obtained using the conventional method. The effects of different fragility curve approaches on seismic damage estimations are investigated. Finally, Chapter 6 presents summary and key conclusions of this dissertation and recommendations for future work.

1.3. Ground Motion Database Used in This Study

To facilitate the use of earthquake records in engineering analysis and design, the analyst requires both an extensive databank of high quality strong-motion accelerograms and access to reliably known ground motion information (e.g., magnitude, source-to-site distance, site class, fault mechanism and usable period range). The use of large volume of earthquake database is important as it may significantly affect the degree of compatibility between the selected record spectrum and target spectrum. In this dissertation, the ground motion database is gathered from Pacific Earthquake Engineering Research (PEER) Ground Motion Database Next Generation Attenuation (Chiou *et al.*, 2008) and RESORCE Database (Akkar *et al.*, 2014). The PEER- Next Generation Attenuation (NGA) database contains 3551 strong-motion multi-component records from 173 shallow active crustal earthquakes with magnitudes from 4.2 to 7.9. The RESORCE (i.e., assembles the most recent pan-European strong-motion databases) includes 5882 multi-component accelerograms from 1814 events ranging in magnitude from 2.8 to 7.8. In this study, the overlapping events from PEER-NGA and RESORCE databases are excluded from the compiled strong motion database. The metadata information that have been included for record selection are earthquake moment magnitude, M_w; fault mechanism; source to site distance, R_{jb} (i.e., the closest distance from the vertical projection of ruptured fault (Joyner and Boore, 1981); local site conditions of the recording stations, Vs_{30} (i.e., average shear wave velocity in upper 30 meters); and usable period information. The resulting ground motion library used in this study includes 4493 records with two-horizontal components. It is important to note that the ground motion database used in this study can be expanded with the updated recordings from recent events (Ancheta *et al.*, 2014).

Figure 1.2 shows the earthquake magnitude and distance distribution of the strong motion records with histograms of each variable. In this figure, the earthquake events with magnitudes between Mw 4.0-7.9 and source to site distances of 0-200km are shown. The magnitude and distance bin widths are 0.30 units and 15km, respectively. Figure 1.3 shows a histogram of the average shear-wave velocity (Vs_{30}) values of the ground motions. The vertical dashed lines in the histogram represent the boundaries between the NEHRP site classes. Values of $760 < Vs_{30} \leq 1500$ m/s, $360 < Vs_{30} \leq 760$ m/s, $180 < Vs_{30} \leq 360$ m/s, and $Vs_{30} \leq 180$ m/s correspond to site classes designated as B, C, D and E, respectively (BSSC, 2009). The main search criteria for selecting recordings suitable for nonlinear response history analysis will be discussed in subsequent chapters.
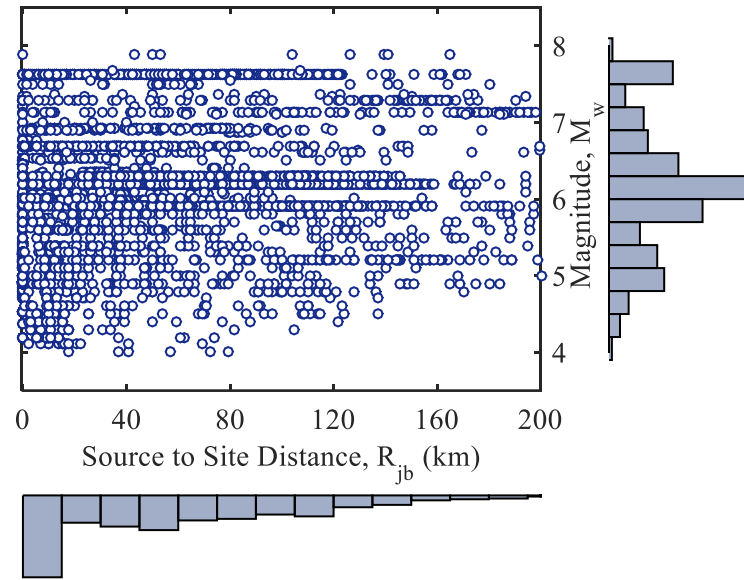
Figure 1.2. Distributions of magnitude versus source to site distance. Histograms of the individual variables are shown in the margins of the plot.
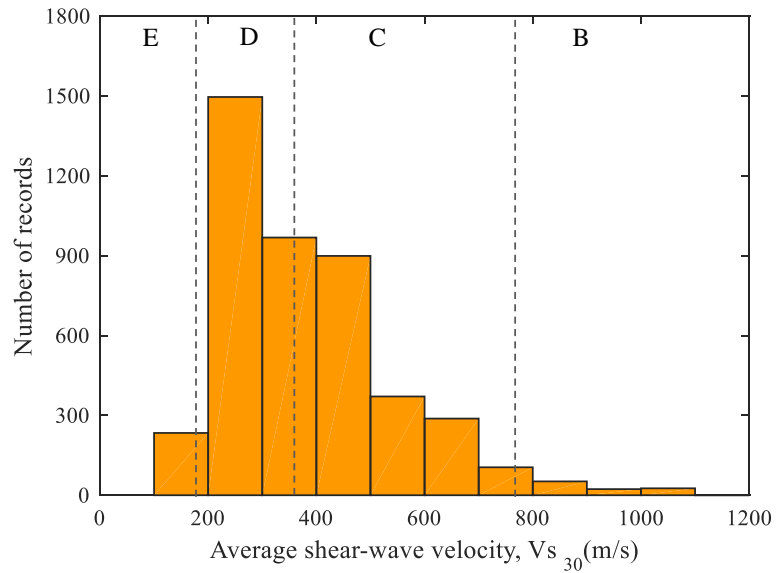
Figure 1.3. Histogram of the average shear-wave velocity (Vs$_{30}$) values of the ground motions.

2. SELECTION AND SCALING OFGROUND MOTIONS FOR SEISMIC RESPONSE ANALYSIS

2.1. Introduction

Over the last two decades, the advancement of performance-based earthquake engineering concepts in seismic design and assessment of buildings has prompted a substantial level of research in characterizing the seismic hazard, estimating the structural response, and assessing the earthquake damage and its implications. The selection and scaling of earthquake records for use in nonlinear response history analysis is the most critical and challenging step in performance-based seismic evaluation and design methodologies. Since the seismic response of structures is highly sensitive to the input motions utilized in the nonlinear response history analysis, it is important to develop robust and reliable tools in order to obtain a suite of motions that can represent the critical aspects of the design motions. In current practice, the ground motions having similar seismological features with target earthquake scenario are typically scaled to match the desired target spectrum by using appropriate ground motion selection and scaling methods. Although several approaches have been developed for selecting and scaling earthquake records, there is still no consensus on a certain method. It is crucial to put the ground motion selection and scaling procedures into context because the different approaches must be adopted depending on the objectives of the structural analyses. This chapter begins with a brief description of seismic hazard analysis and defines the uncertainties associated with the probabilistic seismic hazard analysis. It then presents the detailed information about the record selection criteria and focuses on reviewing the ground motion selection and scaling approaches that are commonly used in engineering practice.

2.2. Definition of the Seismic Hazard and the Target Spectra

The deterministic and probabilistic seismic hazard analyses are two main approaches to develop design ground motions for a given site. The deterministic seismic hazard analysis (DSHA) attempts to determine the earthquake scenario that is expected to produce the largest seismic demand in the structure (referred to as Maximum Credible Earthquake, MCE). It is typically performed by the following steps: (1) identification of the potential earthquake sources (fault or area source), (2) estimation of maximum magnitude on each earthquake source and distance to the site, (3) computation of single-percentile level of ground motion parameter using the attenuation models (e.g., median or 84th percentile). In the deterministic approach, the ground motions are computed separately for each individual source, magnitude and distance. Then, the seismic hazard at the given site is defined as the ground motions resulting from the controlling earthquake (Reiter, 1990; Krinitzsky, 2002). Since there exist uncertainties in earthquake locations, size and frequency of earthquakes, the probabilistic seismic hazard analysis (PSHA) incorporates all these uncertainties and defines the hazard as the mean rate of exceedance of the selected ground motion parameter. It is pointed out that the DSHA is typically independent of time, whereas the PSHA has units of time (Hanks and Cornell, 1994). As depicted in Figure 2.1, the steps of PSHA process involve (1) identification of earthquake sources and geometry, (2) estimation of earthquake magnitude and recurrence relations for each source, (3) computation of the ground motion intensity parameter for a given site by using the ground motion prediction model, and (4) integration of these three steps to develop the seismic hazard curve. The seismic hazard curve relates the design ground motion parameter to the probability of exceedance. In the modern PSHA calculations, the rate of exceedance of ground motion intensity parameter ($\lambda[IM > im]$) is evaluated using the total probability theorem (Cornell, 1968; McGuire, 2008), as given in Equation 2.1.

$$\lambda[IM > im] = \sum_{i=1}^{N} v_i \left\{ \iiint P[IM > im \,|\, m, r, \varepsilon] f_{M,R,\varepsilon}(m, r, \varepsilon) dm dr d\varepsilon \right\}_i \tag{2.1}$$

where N represents the number of earthquake sources contributing to hazard, and ε is the number of logarithmic standard deviations that the logarithmic ground motion intensity

level deviates from the median estimation of the ground motion prediction model. $P[IM > im \mid m, r, \varepsilon]$ is the probability that the ground motion exceeds the level *im* for given magnitude (*m*), distance (*r*), and epsilon (ε). $f_{M,R,\varepsilon}(m, r, \varepsilon)$ corresponds to the probability density function of these variables (m, r, ε) .
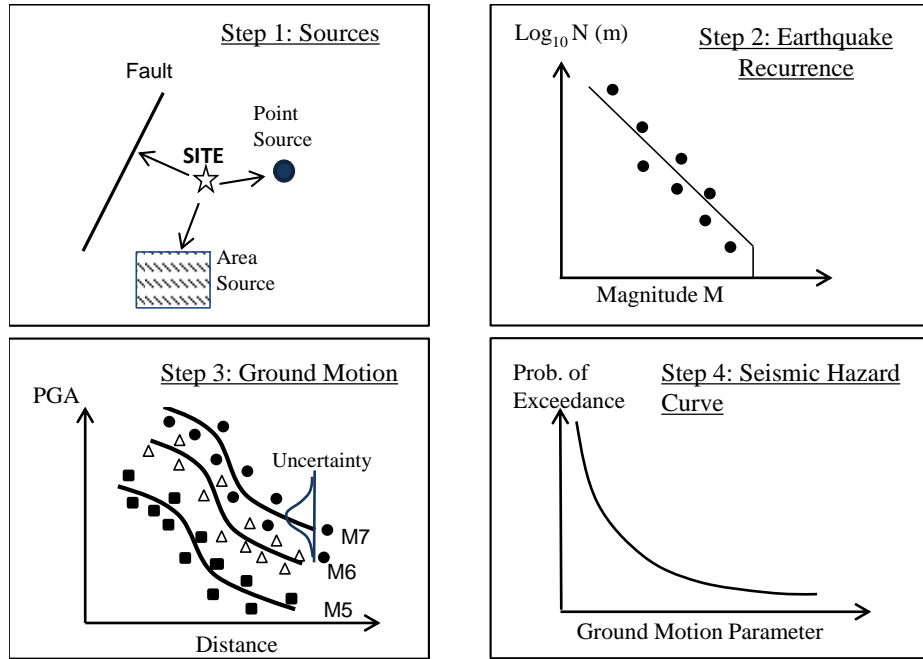
Figure 2.1. Main steps in PSHA (adapted from Reiter, 1990).

It is worth noting that the PSHA framework outlined above identifies and incorporates all aleatory uncertainties that exist in each step of the process. The aleatory uncertainties represent the inherent randomness of the events that are treated and incorporated through the probability distributions. Another type of uncertainty is known as epistemic uncertainty which is associated with the lack of knowledge about the applicability of methods to model the events (Abrahamson and Bommer, 2005; Bommer and Abrahamson, 2006). The logic trees provide a mechanism to systematically assess the uncertainties in models and parameters (e.g., seismic activity, maximum magnitude, ground motion prediction models). Each branch of the logic tree includes different models, parameters and expert opinion-based weights. In this framework, each branch yields a single hazard curve, and thus the probability density function can be fitted to family of

hazards in order to determine the fractiles (e.g., 50th fractile or median). It should be noted that the mean hazard curve represents the weighted average of the hazard, whereas fractiles of the hazard show the range of hazard for alternative source and ground motion prediction models. Note that a representative plot of the mean hazard curve and its fractiles is already given in Chapter 1.

A traditional approach for developing design spectra is based on the mean hazard curve of the PSHA. The PSHA produces a suite of hazard curves for spectral ordinates for different response periods. A set of spectral ordinates can be obtained and plotted as a function of response period to form the elastic response spectrum for the selected design return period (T_R). This spectrum is known as Uniform Hazard Spectrum (UHS). The UHS represents the equal probability of exceedance of ground motions over the entire period range of interest. A schematic illustration for the construction of the UHS is shown in Figure 2.2. The Uniform Hazard Spectrum is typically an envelope of the spectra associated with different sources of seismicity, in which the short period ground motions are controlled by nearby moderate magnitude earthquakes, whereas the long period ground motions are dominated by larger and more distant earthquakes. Accordingly, the motions represented by UHS may not be realistic because no single earthquake can produce a spectrum as high as UHS over the entire frequency range (e.g., Bommer *et al.*, 2000; Naeim and Lew, 1995). In particular, this situation becomes an issue when this spectrum is used as a target for ground motion selection. It has been shown that the UHS leads to conservative estimation of the structural response; however, if an engineering analyst cannot afford to perform expensive analyses or works on a system with multiple sensitive modes, the UHS can effectively be used as a target spectrum (Baker, 2011).
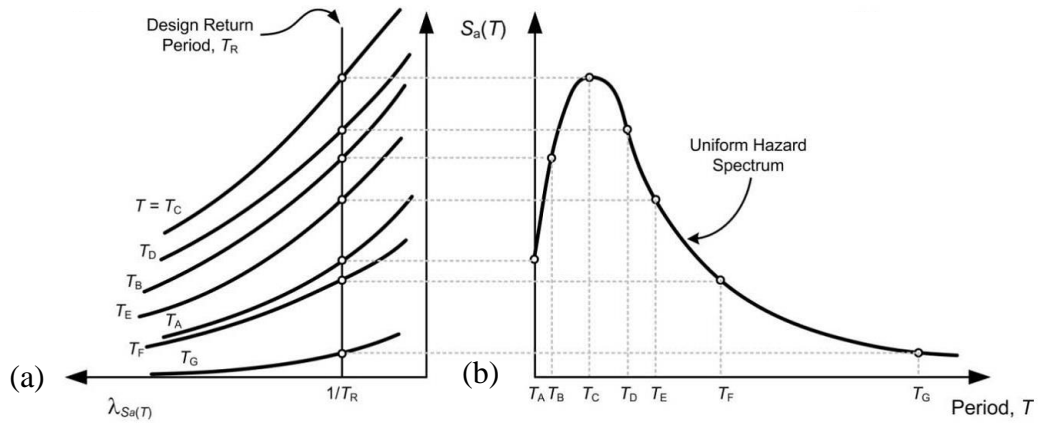
Figure 2.2. Construction of uniform hazard spectrum: (a) Hazard curves for different response periods, (b) Spectral accelerations at design return period (T_R) vs. response period (from Kramer *et al.*, 2012).

Conditional Mean Spectrum (CMS) is proposed as an alternative target spectrum to UHS for selecting ground motions as input to the nonlinear response history analysis (Baker and Cornell, 2006; Baker, 2011). This approach relates the target spectrum to the controlling earthquake scenario events (from the disaggregation of the PSHA) that would no longer assume uniform rate of exceedance. Since the CMS is generated based on the site-specific earthquake scenario, it is more realistic spectrum than the UHS for ground motion selection. As mentioned previously, the CMS provides the expected mean spectrum, conditioned on the target spectral acceleration at the period of interest. The target $Sa(T_1*)$ value (i.e., the spectral acceleration at the fundamental period of the structure, T_1) is determined by performing a site-specific PSHA. Disaggregation of the PSHA is then required to compute the mean M, R, and $\varepsilon(T^*)$ values associated with the target $Sa(T_1*)$. For illustration, the seismic hazard curve and the disaggregation results for a site (T_1=2.6s) located in Palo Alto, California with Vs_{30} =400 m/s are plotted in Figure 2.3. Figure 2.3a shows the hazard curve for Sa at the period of 2.6s. As seen in the figure, the ground motion intensity associated with 2% in 50 year probability of exceedance can be identified through the hazard curve as 0.45g. Figure 2.3b shows the causal M, R, and ε that are obtained from the disaggregation of the PSHA at 2% in 50 year probability of exceedance. The tallest column of the disaggregation histogram represents the controlling (M, R) earthquake parameters that can be used to generate the CMS.
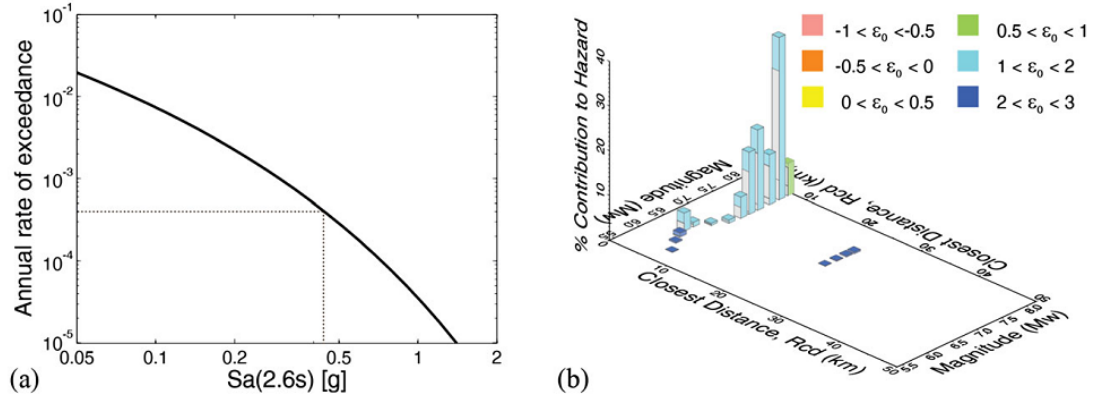
Figure 2.3. (a) Seismic hazard curve for Sa(T_1=2.6s) and, (b) disaggregation at 2% in 50-year probability of exceedance (NIST, 2011).

The conditional mean value of the response spectrum ($\mu_{\ln Sa(T_i)|\ln Sa(T_1^*)}$) can be computed using the Equation 2.2.

$$\mu_{\ln Sa(T_i)|\ln Sa(T^*)} = \mu_{\ln Sa}(M,R,T_i) + \rho(T_i,T^*)\varepsilon(T^*)\sigma_{\ln Sa}(T_i) \tag{2.2}$$

where $\mu_{\ln Sa}(M,R,T_i)$ and $\sigma_{\ln Sa}(T_i)$ are the marginal mean and standard deviation of the $\ln(Sa(T_i))$, respectively, and are estimated by using the ground motion prediction model. Note that the correlation coefficient between two periods ($\rho(T_i,T^*)$) in the above equation can be predicted by regression on empirical observations (Baker, 2005):

$$\rho_{(T_{\min},T_{\max})} = 1 - \cos\left(\frac{\pi}{2} - \left(0.359 + 0.163 I_{(T_{\min}<0.189)} \ln\frac{T_{\min}}{0.189}\right) \ln\frac{T_{\max}}{T_{\min}}\right) \tag{2.3}$$

where $I_{(T_{\min}<0.189)}$ is an indicator function equal to 1 if $T_{\min} < 0.189$ and equal to 0 otherwise, and where $T_{\min}$ and $T_{\max}$ represent the smaller and larger of two periods of interest, respectively (Baker and Cornell, 2006). Later, the Conditional Spectrum (CS) is introduced as a target spectrum for ground motion selection that accounts for both conditional mean and variance of the response spectrum (Lin *et al.*, 2013). Another

selection and scaling approach that incorporates various conditional intensity measures as well as other characteristics of the ground motion (e.g., duration) can be found in Bradley (2010). The conditional standard deviation ($\sigma_{\ln Sa(T_i)|\ln Sa(T_1^*)}$) of the CMS can be computed by using Equation 2.4.

$$\sigma_{\ln Sa(T_i)|\ln Sa(T_1^*)} = \sigma_{\ln Sa(T_i)} \sqrt{1 - \rho^2(T_i, T^*)} \tag{2.4}$$

Figure 2.4a depicts an example Conditional Mean Spectra conditioned on a period of 2.6 seconds as well as three other periods (0.45s, 0.85s, and 5s) for a site located in Palo Alto, California with Vs_{30}=400 m/s. The UHS is also provided for comparison. The spectral value at the conditioning period for each CMS is equal to that of the UHS but less at other periods, as compared to those of the UHS. Figure 2.4b depicts ground motions that are selected and scaled based on the CS for a period of 2.6 seconds. Note that the distribution of Sa at 2.6s has zero standard deviation while Sa at other periods have some uncertainty because they are only partially correlated with $Sa(T_1=2.6s)$. It is recommended that the UHS and CMS can be used when the average or mean estimate of structural responses are sought, and CS can be adopted when the distributions of the structural response are sought (NIST, 2011).

(a)
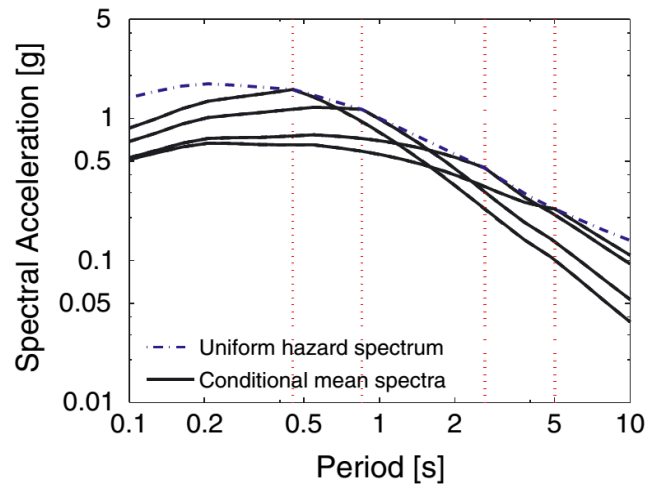
(b)
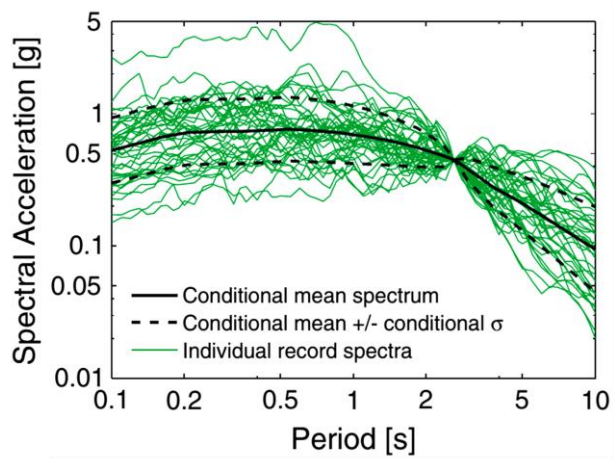
Figure 2.4. (a) CMS at multiple conditioning periods (0.45, 0.85, 2.6, and 5s with UHS superimposed) at the 2% in 50-year intensity level, (b) Response spectra of selected ground motions with CS as target spectra for Sa (T1=2.6s) associated with 2% in 50-year probability of exceedance in log scale (NIST, 2011).

2.3. Ground Motion Selection Criteria

The current practice for ground motion selection is to assemble earthquake records that represent the seismological and geophysical parameters of the scenario event at the site of interest. Once the scenario event is identified by DSHA or disaggregation of the PSHA, the ground motion database can be constrained to select records that are consistent with the parameters of the target earthquake scenario. The selected earthquake records, which have similar implicit causal parameters (e.g., magnitude, source-to-site distance, site class, fault mechanism), are then typically scaled to match the target response spectrum. The magnitude of the earthquake (M) is the most important parameter for the initial selection of the records because this parameter directly influences the frequency content and the duration of the ground motions. Stewart *et al.* (2001) recommended selecting earthquake magnitude within 0.25 magnitude units of target value as obtained from a disaggregation of the PSHA, while Bommer and Acevedo (2004) suggested 0.20 magnitude units either side of the target value. However, many recent studies have focused on selecting the ground motions based on their spectral shape because the response spectrum shape is a better predictor of structural response than the seismological parameter. Therefore, the bound on magnitude may be relaxed and the records can be selected from 0.5 magnitude units of target value in order to give more emphasis to spectral shape parameter in the record selection stage.

In addition to magnitude, the source to site distance (R) is another common parameter to identify the records for use in engineering analyses and design. This parameter is commonly used in combination with the magnitude to select the accelerograms that comply with the earthquake parameters resulting from PSHA disaggregation. It has been shown that the structural response is less sensitive to the distance parameter, whereas the magnitude has a significant effect on the seismic demand, particularly for the displacement-based structural parameters (Carballo and Cornell, 2000; Bommer and Acevedo, 2004; Baker and Cornell, 2005). Nevertheless, some seismic code provisions suggest that the records having source to site distance should be consistent with the target earthquake scenario (e.g., ASCE 7-05 (ASCE, 2006), FEMA P-750 (BSSC, 2009)). It is worth noting that the selection of earthquake records having appropriate

source to site distance is particularly important for the sites located close to the active fault. Since the near-fault ground motions (i.e., distances less than 10-15km from the fault) are strongly influenced by the fault mechanism, rupture propagation and possible ground displacements resulting from the fault slip, they have significantly different characteristics than the ordinary (or distant) ground motions (Stewart *et al.*, 2001). In this case, an appropriate number of selected ground motions should include near-fault and directivity effects, such as velocity pulses that produce large spectral ordinates at long periods. However, it is still challenging to find suites of motions that represent the near fault effects (e.g., directivity, fling-step) due to the scarcity of the recorded accelerograms from large earthquakes at the near fault regions. The detailed information about this topic can be found in NIST (2011).

The site condition (S) at the target site can also be used as a selection criterion while identifying the appropriate ground motions. This parameter is often used in conjunction with the M, R selection criteria. The soil type at the site of interest is generally determined based on the shear-wave velocity at the uppermost 30m (Vs_{30}) which is expected to have an impact on the amplitude and shape of the response spectrum. Ideally, the ground motions corresponding to the specified hazard level should reflect the site condition of the target site. Specifying a close match for this parameter, on the other hand, may not be feasible since the soil profile of strong motion recording stations is not known with a high degree of confidence in most cases (Katsanos *et al.*, 2010). Additionally, finding ground motions that satisfy the magnitude (M), distance (R) and site condition (S) criteria may greatly reduce the number of ground motions available for use in nonlinear response history analysis. Therefore, the matching criteria for the site condition can be relaxed in order to obtain a reasonable number of records (Bommer and Scott, 2000). For example, if the target site is characterized by soft soil, it would be advisable to exclude the rock site recordings from a suite of ground motions for use in nonlinear response history analysis. It is recommended to assemble records from sites that are within one site class (e.g., NEHRP, EC8) either side of the classification of the target site (Bommer and Acevedo, 2004).

In addition to M, R, S parameters, the ground motion database can be searched on the basis of complementary criteria such as fault mechanism and duration. It is pointed out that the frequency content of the ground motions is dependent on the tectonic regime, however the effect of different fault mechanisms (e.g., strike-slip, reverse) on the structural response parameters is not well-studied (Katsanos *et al.*, 2010). Duration of the ground motions may affect the damage measures in different ways. It is demonstrated that the duration is insignificant for displacement-based demand parameters; while it has an impact on energy-based models such as hysteretic energy dissipation demand (Iervolino *et al.*, 2006). Some studies also reported that the long duration ground motions may lead to significant reduction in the structural collapse capacity (Hancock and Bommer, 2006; Raghunandan and Liel, 2013). Due to the lack of consensus on the effect of ground motion duration on structural performance, current seismic design provisions do not explicitly consider this parameter as a selection criterion. Consequently, the common application is to exclude the fault mechanism and duration criteria for ground motion selection as they may significantly reduce the number of records required in nonlinear response history analysis.

The issues related to the seismological criteria and types of the records to be used in nonlinear response history analysis are not properly addressed in the seismic building codes. Guidance on how to select ground motions is mainly based on the compatibility of the response spectrum rather than the seismological criteria at the site of interest. Traditionally, the earthquake records which have similar seismological parameters with the site under consideration are selected to match the target spectrum. However, if the ground motions are selected purely on the basis of seismological characteristics (e.g., magnitude, distance), it would result in large dispersion in the structural response so that the median response cannot be estimated with a high degree of confidence. It is important to note that the ground motions whose response spectrum is similar to target spectrum minimize the need for scaling and prevent possible bias in the estimated structural response. Baker and Cornell (2006) demonstrated that epsilon (ε) is an implicit measure of the spectral shape, and the effect of ε on structural response is greater than that of magnitude and distance. They suggested that if the records are carefully selected by considering the spectral shape (i.e., ε-based or CMS based), they can be scaled without inducing bias in structural

response. To investigate the influence of different ground motion selection procedures on resulting estimated structural response, Baker and Cornell (2006) performed a series of nonlinear response analyses using four selection methods:

1. Method 1 (AR method): Select records randomly without attempting to match any record properties (i.e., arbitrary selection).

2. Method 2 (MR-BR method): Select records with their values of M and R representative of the disaggregation results.

3. Method 3 (ε-BR method): Select records with their values of ε representative of the site hazard (i.e., ε-Based Records).

4. Method 4 (CMS-ε method): Select records with spectral shapes that match the CMS- ε. No direct attempt was made to match M, R, and ε.

With all four methods, the additional restriction in the ground motion database is imposed to select records which have similar site conditions with the site of interest. The Conditional Mean Spectrum is derived using the mean parameters of the scenario event (M=6.4, R=11.5km, and ε=2.1) that are obtained through the disaggregation of the PSHA. Figure 2.5 shows the mean record spectra of the ground motion suits selected using each of the four record selection methods for $Sa(T_1=0.8s)=1.6g$ along with the target mean, CMS-ε spectrum (see Equation 2.2). As seen in Figure 2.5, the mean spectra of the records selected using Method 3 and 4 are very close to the target spectrum, while Method 1 and 2 deviates significantly from the target at almost all periods other than 0.8s. Baker and Cornell (2006) concluded that the ground motions selected using Method 1 and 2 produce much greater probability of collapse estimates compared to other two methods; the results from records selected using Method 3 and 4 are nearly identical. Acknowledging that the CMS-ε spectrum is more realistic target than UHS, the method 3 and 4 would provide more appropriate ground motions for use in nonlinear response history analysis. Baker and Cornell (2006) pointed out that the use of CMS as a target spectrum for record selection may increase the number of available records for nonlinear response history analysis

because the selected records with incorrect M, R, and ε values may have correct spectral shape. Furthermore, it is noted that the records selected based on the CMS have realistic shape at multiple periods, and therefore they produce unbiased estimate of the median structural response (Haselton, 2009; Baker, 2011). In other words, the scaled ground motions produce structural responses that are comparable to responses produced by unscaled ground motions.
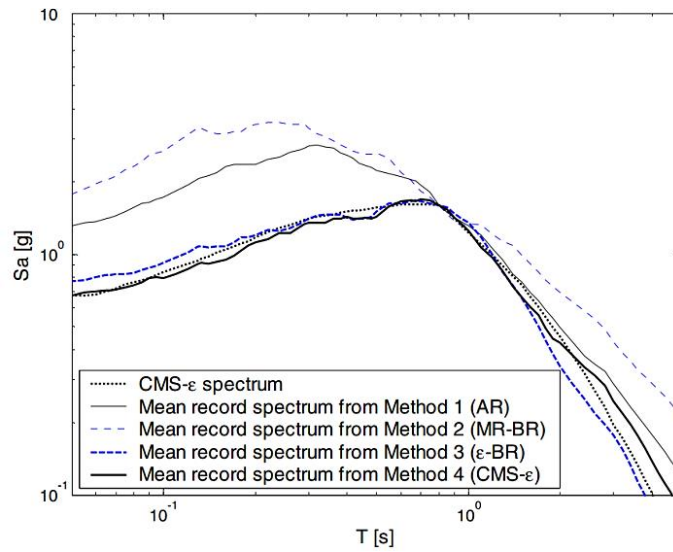
Figure 2.5. Conditional mean spectrum at Sa(0.8s)=1.6g (given M =6.4, R =11.5 km and ε =2.1) and mean response spectra of record sets selected using each of four record selection methods (Baker, 2005).

2.4. Ground Motion Modification Methods

Despite the growing number of strong-motion accelerograms, the number of records available for rare earthquake event is still limited, even for sites located in high seismic regions. Although earthquakes will never cease to occur, it may take many years for the strong-motion databank to expand particularly for the events with low probability of occurrence. It is, thus, necessary to make adjustments to individual ground motions to represent the characteristics of the target scenario event. The modification of ground motions can be performed by amplitude scaling (in time domain) or spectrum matching (in time or frequency domain) to ensure the compatibility of ground motions with the target

spectrum over a period range or some specified intensity level defined from seismic hazard analysis. The amplitude scaling (i.e., linear scaling) is defined as the procedure of applying the constant scale factor to each individual record that increases or decreases the amplitude without changing the frequency content. The amplitude scaling of records allows one to match the spectrum of the record to target spectrum either at single period or the specified period range, whereas the spectrum matching method alters the frequency content and phasing of the ground motions in order to match a smooth target spectrum (e.g., Carballo and Cornell, 2000; Hancock *et al.*, 2006). Thus, the amplitude scaling methods retain the nonstationary characteristics of the ground motions, while spectral matching methods alter the physical characteristics of the records. In the case of spectral matching method, the peaks and troughs of the original time history are suppressed that in turn leads to reduced variability in the structural response. If the objective of the analysis is to assess the percentile values of the structural response, the spectrum matching would be inappropriate, because this method can only be used to estimate the median response and not the distribution of the response. Some key recommendations regarding selection of ground motion for spectrum matching can be found in NIST (2011) document. It is important to note that the arbitrary suppression of the record-to-record variability might affect the accuracy of the analyses in the probabilistic seismic assessment procedures where the variability of the records should be considered in the model. In this respect, the analyst must evaluate the ground motion selection and scaling procedures based on the choice whether to estimate the full distribution or only the central tendency of the structural response (e.g., ASCE, 2010). It should be noted that this study investigates the selection and amplitude-scaling of real earthquake records. The spectral matching of ground motions and artificial accelerograms are beyond the scope of this dissertation but can be found in other studies (e.g., Silva and Lee 1987; Al Atik and Abrahamson, 2010; Gasparini and Vanmarcke, 1976).

2.4.1. Intensity-Based Scaling Methods

The common practice in earthquake engineering relies on identifying the intensity measures that adequately represent the characteristics of the earthquake records such as amplitude, frequency content and duration. The intensity measure (IM) can be used as an

interface variable between the seismic hazard and structural response. A large amount of research has been devoted to the investigation of the efficient and sufficient intensity measure for probabilistic seismic response estimation. The sufficiency refers to the ability of the intensity measure to predict the structural response conditionally independent of the other seismological characteristics of the earthquake shaking (e.g., magnitude, distance), while the efficient IM results in reduced variability of the structural response given IM. In the context of ground motion scaling, intensity measure that is well correlated with seismic demand is desirable because it provides an acceptable confidence level in structural performance assessment. In the past, parameters as Peak Ground Acceleration (PGA), Peak Ground Velocity (PGV) and Peak Ground Displacement (PGD) are the most popular intensity measures. It has been shown that PGA has a high correlation in the short-period range, but it does not provide sufficient information about the damage potential of the earthquake shaking for mid and high-rise buildings (Trifunac, 2012). The PGV, on the other hand, provides relatively high correlations between intensity and structural response in the intermediate and long period ranges. The PGD provides a good correlation in long period range only, and thus controls the damage at long periods. Several studies show that scaling ground motions to target PGA produce biased estimates with large scatter in structural response (Shome and Cornell, 1998). Kurama and Farrow (2003) provided a comprehensive review of the other scaling methods such as scaling to Effective Peak Acceleration, Arias intensity-based parameter, Effective Peak Velocity, and Maximum Incremental Velocity. It has been concluded that the effectiveness of the scaling approaches depend on the site conditions (e.g., soil profile and epicentral distance) as well as the structural characteristics (e.g., yield strength, period and hysteretic behavior). However, it is pointed out that the Maximum Incremental Velocity (MIV) scaling method results in less scatter in structural response compared to other considered intensity measures, but the implementation of this method in current seismic design procedures may not be feasible due to the lack of methods to estimate the mean annual frequency of exceedance of MIV.

All of the aforementioned IMs are independent of the dynamic characteristics of the structure, and thus they may produce large dispersion in the structural response. Bazurro and Luco (2005) pointed out that the spectral quantities enhance the estimation of

structural response compared to previously mentioned intensity measures. It has been demonstrated that seismic demands are strongly correlated with the elastic single degree of freedom (SDOF) oscillator response acceleration at the fundamental period of the structure (Shome and Cornell, 1998). The intensity measure, i.e. $Sa(T_1)$, is used as an efficient predictor of the structural performance particularly for the first-mode dominated structures. It is noted that $Sa(T_1)$ is widely adopted IM for record scaling due to its simplicity and relative accuracy. This is also because the most of the seismic hazard maps quantify the seismic threat in terms of probability of exceedance of this quantity. Nevertheless, $Sa(T_1)$ has some limitations to accurately describe the seismic demands of a multi degree of freedom (MDOF) structure because it does not capture the effects of the period elongation during nonlinear response and the contribution of the higher modes to the structural response. Furthermore, several studies show that scaling ground motions to $Sa(T_1)$ may lead to large scatter in the structural response for near-fault ground motions (Cordova *et al.*, 2001; Tothong and Luco, 2007; Luco and Cornell, 2007). Luco and Cornell (2007) pointed out that no single IM would be both efficient and sufficient for every seismic response problem. They also noted that "the only perfectly efficient and sufficient intensity measure is the demand measure of interest itself". Luco and Cornell (2007) proposed a structure-specific intensity measure that combines both the higher mode contributions and the inelastic structural response. It has been demonstrated that this advanced intensity measure is efficient and sufficient for both near-source and ordinary ground motions. Similarly, Tothong and Cornell (2007) introduced an alternative intensity measure based on inelastic spectral displacement (Sdi) for both ordinary and pulse-like records. It has been noted that this intensity measure is relatively efficient and sufficient with respect to the commonly used $Sa(T_1)$. Nevertheless, the applicability of the structure-dependent intensity measures is limited in risk-based structural response assessment procedures because the involved computations (e.g., seismic hazard curve, development of ground motion prediction model) must be structure-specific. Kalkan and Chopra (2011) proposed an inelastic scaling methodology that explicitly accounts for the structural strength. In this method, the earthquake records are scaled to match the inelastic deformation of an equivalent nonlinear SDOF system that may yield better prediction of the structural response. However, the accuracy of the structural response in the inelastic-based scaling methods depends on the proper choice of the target inelastic displacement. Haselton *et al.*

(2009) pointed out that if the inelastic target can be improved, these methods may provide precise results. Apart from the scalar intensity measures, several vector-valued intensity measures have been proposed with the aim of improving the performance of scalar intensity measures (Bazzurro and Cornell, 2002; Vamvatsikos, 2002; Conte *et al.*, 2003; Luco *et al.*, 2005). In general, the performance of IM improves with the inclusion of additional information about the ground motion characteristics and the structural properties. Since the spectral acceleration value at the fundamental period of the structure is a powerful predictor of the response of the structure, almost all vector-valued IMs uses $Sa(T_1)$ and the complementary predictor (PGA, PGV, ε, etc.). The use of a vector-valued IM may be appealing for prediction of structural response, however they are not widely used due to the computational complexities of the vector-valued PSHA.

2.4.2. Code-Based Scaling Methods

In code-based seismic design and assessment procedures, the earthquake records should be scaled such that their average response spectrum matches or exceeds the target design spectrum (e.g., UHS) within the period range of interest (e.g., Eurocode 8 (CEN, 2003); FEMA P-750 (BSSC, 2009)). The scaling over a period range preserves a consistency between the average spectral shape of scaled records and target spectrum that reduces the possible bias in structural response that might be introduced by scaling (Luco and Bazurro, 2007). The recommended criteria for the spectral mismatch is that the average record spectrum should not fall below a certain limits (e.g. 10%) of target spectrum at any spectral period over the period range of interest. However, no criteria for the upper bound are prescribed. It should be noted that the period interval is one of the critical issues for ground motion scaling. The specified period range accounts for the lengthening of the period of the structure due to inelastic behavior under strong earthquake shaking as well as the higher vibration modes. ASCE 7-10(ASCE/SEI 7-10, 2010) recommends $[0.2T_1\text{-}1.5T_1]$ as the period interval for the ground motion selection and scaling, where T_1 is the fundamental period of the structure. Eurocode 8 (CEN, 2003) and New Zealand Standard 1170.5 (NZS 1170.5, 2004) specify the period range of interest needs to be between $[0.2T_1\text{-}2T_1]$ and $[0.4T_1\text{-}1.3T_1]$, respectively. Beyer and Bommer

(2007) proposed a period range of $[T_{min} - \sqrt{\mu}\, T_1]$, where T_{min} is the period of the highest vibration mode that contributes significantly to the elastic response and μ is the displacement ductility demand of the structure. It is stated that the uncritical use of a period interval for ground motion selection and scaling may lead to large scatter in the structural response, and thus undermines the accuracy of the seismic response (Sextos *et al.*, 2011; Katsanos and Sextos, 2015).

The minimum number of records required to conduct a nonlinear response history analysis while achieving statistically reliable median structural response is one of the challenges faced by the engineers (Cimellaro *et al.*, 2009). In essence, the required number of records may depend on the objective of structural analyses and the desired level of accuracy in the estimated response. Many building codes require a limited number of ground motions to reduce the computational effort of a nonlinear response history analysis (e.g., ASCE, 2010). It is generally stated that the maximum response should be used if three records are used, while the average response may be used if seven or more records are used (e.g., CEN, 2003). As noted by Kircher (2005), this recommendation is chosen arbitrarily by code committee and has no scientific basis. IBC (2012) suggests that a minimum of seven ground motions should be employed in nonlinear response history analysis in order to prevent the dominance of the peaks and troughs of an individual record on the structural response. Recently, a minimum of eleven ground motions are proposed for nonlinear response history analysis to both obtain more reliable estimate of the mean structural response and to limit the computational effort (Haselton *et al.*, 2014). Shome *et al.* (1998) pointed out that the minimization of the variability in the structural response is equivalent to minimizing the required number of records needed to estimate the seismic demand with a given confidence level. If the records are selected purely to match the average response without attempting to control the deviation of the individual responses with respect to target spectrum, the resulting scatter in the structural response would be large that may affect the reliability of the structural performance. Araújo *et al.* (2015) showed that the use of minimum seven records would be adequate if the additional restriction on the spectral mismatch is adopted; otherwise the minimum number of records required to conduct nonlinear analysis is dependent on the structural response parameter to

be estimated (e.g., global and local deformation demands) and on the considered limit states.

To control each individual record mismatch with respect to target spectral accelerations, an average spectrum deviation (i.e., how far the mean spectrum of a record set deviates from the code spectrum) parameter (δ_i) is proposed by Iervolino *et al.* (2009). The compatibility between the target and individual spectrum is quantified by using the following equation:

$$\delta_i = \sqrt{\frac{1}{N}\sum_{i=1}^{N}\left(\frac{S\alpha_j(T_i) - S\alpha_{REF}(T_i)}{S\alpha_{REF}(T_i)}\right)^2} \qquad (2.5)$$

where $S\alpha_j(T_i)$ represents the spectral ordinate of the real spectrum j at the period T_i, $S\alpha_{REF}(T_i)$ is the value of the spectral ordinate of the target spectrum at the same period and N is the number of values used within a predefined period range. The above equation is then implemented into the REXELite online software tool (Iervolino *et al.*, 2011) that allows for searching input motions compatible with the target spectrum and implicit causal parameters. Alternative software packages for earthquake record selection can be found elsewhere (e.g., Wang *et al.*, 2015; Katsanos and Sextos, 2013; Corigliana *et al.*, 2012).

2.5. Common Ground Motion Scaling Methods

As noted previously, the selected accelerograms for nonlinear response history analysis should represent the level of the expected seismic motion at the site of interest. The records having similar implicit causal parameters (e.g., magnitude, source to site distance) are typically multiplied by a scale factor to match the target spectrum at a single period or over a period interval. One of the most common scaling approaches is to multiply the amplitude of each record by a constant scalar factor to match a target spectral acceleration at the fundamental period of the structure (Shome and Cornell, 1998; Iervolino and Cornell, 2005). The period of interest is typically chosen as the first-mode period of the structure with the premise that the fundamental period is the most critical

period in the prediction of structural response. In this approach, the scale factor for each ground motion can be computed by using the following equation:

$$SF_i = \frac{Sa_{t\,\arg et, T_1}}{Sa_{i, T_1}}$$
(2.6)

where SF_i is the scale factor applied to the $i^{\,th}$ records, and Sa_{i, T_1} is the spectral acceleration of the $i^{\,th}$ records at fundamental period of the structure, and $Sa_{t\,\arg et, T_1}$ is the spectral acceleration value of target spectrum. As noted before, this single period scaling ($Sa(T_1)$) method has proved to be particularly attractive to practitioners because it minimizes the required number of records needed to obtain more reliable performance estimate. Figure 2.6 shows a suite of 15 ground motions that are scaled to match target UHS (for 10% in 50 years) at the conditioning period $T_1=0.5s$. As seen in Figure 2.6, the spectral amplitude of each scaled record is equal to the target intensity level, whereas, at periods other than T_1, it introduces variability in spectral accelerations. Thus, the analyst should be aware that the extent of uncertainty in structural response depends on the level of higher mode contributions and/or inelastic behavior.

To match the record spectrum to the target spectrum over the period range, Beyer and Bommer (2007) proposed a scale factor (α) that minimizes the root-mean-square difference (D_{rms}) between the scaled geometric mean record spectrum (Sa_R) and the target spectrum (Sa_T). In this approach, the records which have the smallest root-mean-square difference are selected as the optimum recordings. The computation of D_{rms} can be performed by using Equation 2.7.

$$D_{rms} = \sqrt{\frac{1}{k - j + 1} \sum_{i=j}^{k} (\alpha Sa_R(T_i) - Sa_T(T_i))^2}$$
(2.7)

where T_j and T_k are the jth and k^{th} entries of the period vector for which the spectral accelerations are defined. The interval $[T_j \; T_k]$ defines the period range for which the spectral matching is desired.

Similarly, each ground motion can be scaled such that the record spectrum over the period range (e.g., $0.2T_1$-$2T_1$) of interest is equal to the average target spectrum over the same periods. In this approach, i.e. Period-Range scaling, scale factor (SF) can be calculated by taking the ratio of the average spectral ordinates in the specified range as given in Equation 2.8.

$$SF_i = \frac{\sum_{i=1}^{n} Sa_{t\arg et}(T_i)}{\sum_{i=1}^{n} Sa_{record}(T_i)} \tag{2.8}$$

where n represents the number of period points within the period range of interest, $Sa_{t\arg et}(T_i)$ and $Sa_{record}(T_i)$ are the target and record spectral acceleration value at i^{th} period, respectively. This type of scaling is illustrated in Figure 2.7. A structure's first-mode period is designated as T_1 in the figure and a suite of 15 ground motions are scaled to match UHS at the period range of interest $[0.2T_1$-$2T_1]$. In this case, the variability of each individual record is minimized over the period range of interest and some dispersion is preserved at the target spectral demand. It is important to note that the aforementioned period-range scaling procedures are mainly proposed to select ground motions compatible with the UHS, but they can be utilized for any desired target spectrum (e.g., scenario-based spectrum, CMS). A variety of methods for obtaining spectrum compatible ground motions, to be used in nonlinear response history analysis, are available in the literature (Naeim *et al.*, 2004; Reyes and Kalkan, 2012).
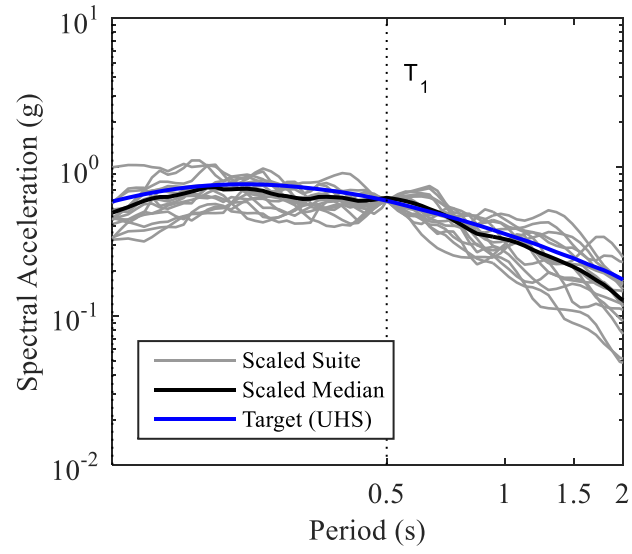
Figure 2.6. Response spectra for 15 ground motions scaled with single period, $Sa(T_1)$, scaling method.
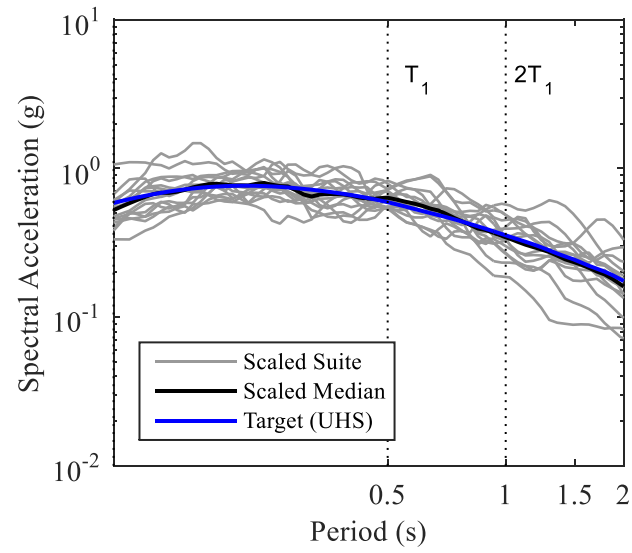
Figure 2.7. Response spectra for 15 ground motions scaled with Period-Range scaling method.

3. A PROPOSED GROUND MOTION SELECTION AND SCALING METHODOLOGY

3.1. Introduction

This chapter presents a new ground motion selection and scaling procedure that implicitly addresses the uncertainty in the target intensity measure with the level of dispersion preserved in the ground motion suite. This procedure aims to consider the uncertainties originating from PSHA by preserving the spectral variation at the target spectral demand. The candidate ground motion suits are formed based on dispersion statistics about the target spectral demand. The scaling stage is based on the minimization of the error between scaled median and the target spectra where the dispersion of the earthquake shaking is preserved along the specified period interval. The proposed procedure allows performing further modification on each scaled ground motion in order to match the target variance of the scenario-based spectrum. This method provides appropriate ground motion inputs for use in nonlinear response history analysis for code-based design as well as performance-based assessment of buildings. The bilinear single degree of freedom (SDOF) systems of varying periods and nonlinearity levels are used as case studies to evaluate the performance of the proposed methodology in predicting the nonlinear structural responses. Nonlinear response history analyses are conducted using different number of ground motions and the results of the proposed procedure are compared with those obtained by the most commonly used scaling method. The impact of different ground motion selection and scaling methodologies on structural response distribution is discussed at the end of this chapter.

3.2. Ground Motion Selection and Scaling

Numerous ground motion selection and scaling approaches are recently developed to have a close match between recorded ground-motion spectra and the target by means of different search and optimization algorithms (e.g., Jayaram *et al.*, 2011; Naeim *et al.*, 2004; Kottke and Rathje, 2008). Determination of ground motion sets of (k) accelerograms from a large database may require significant computer memory and execution time due to combinatorial nature of the problem. In the current study, an alternative algorithm is presented to ensemble ground-motion sets. The proposed method establishes the candidate ground motion suits based on dispersion statistics about the target intensity level. The algorithm reduces the computational complexity of the problem by using sort and sliding window approach as will be discussed later in subsequent sections. The ground motion selection stage imposes sets of criteria to obtain suitable candidate record subset. The optimum ground motion set is linearly scaled by using an optimization algorithm that minimizes the error between scaled median record spectrum and target spectrum. The scaling stage ensures that median of the scaled record spectrum provides a reasonable match to the target median in a previously defined period range (e.g., $0.2T_1$ and $2T_1$). Additionally, the method allows performing a further modification on each scaled ground motion in order to match the target variance of the scenario-based spectrum. The main steps of the proposed ground motion selection and scaling procedure are explained in more detail in the following sections.

3.2.1. Ground Motion Database and Spectral Measure Definition

The ground motion database utilized in this study includes 4493 accelerograms with two-horizontal components which are compiled from the Next Generation Attenuation (NGA) strong-motion database (Pacific Earthquake Engineering Research Center, PEER) and RESORCE (Akkar *et al.*, 2014). It should be noted that the detailed description of the ground motion library used in this study is already given in Chapter 1.

3.3. Main Steps of the Proposed Procedure

3.3.1. Record Selection Stage

Step 1: Ground motion parameters to obtain representative ground motion subset. The initial subset of ground motions are assembled for a particular earthquake scenario that is described by a target magnitude-distance pair and soil condition specific to the site of interest. The earthquake scenario is determined either through deterministic seismic hazard analysis (DSHA) or site-specific disaggregation of PSHA. The records having magnitudes within ±0.5 magnitude units about the target magnitude and distances within the 100km are extracted from the ground-motion library. It is noteworthy that the ground motions should be explicitly excluded from the database in order to exclude the near fault effects (i.e., pulse, fling). The site classes (ideally represented by V_{S30}; average shear-wave velocity of the upper 30m soil layer) of the extracted records should be consistent with the local site conditions of the site. The maximum usable period of each record (i.e., the period that includes relevant information for engineering application) should be greater than the maximum of the target spectral period interval. Note that these limits serve as an initial filter for identifying a proper suite of records to assemble the ground-motion bin to be used for the second stage of the record selection. If the number of records is insufficient for certain earthquake scenarios, they can be relaxed. However, this should be done with caution as improper relaxation of above criteria may yield unrealistic records that misrepresent the required conditions for the target earthquake scenario.

The final subset of candidate ground motions is determined from the consideration of spectral shape. The logarithmic differences (δ_i) between the spectral ordinates of the records and the target spectrum is calculated for logarithmically equally-spaced *n* periods along the specified period band using Equation (3.1). It is recommended to use at least 50 periods per log cycle of period (e.g., 100 periods between 0.1 s and 10 s) to prevent unexpected variation of the spectrum as well as to obtain better resolution in error computations. Here, the average dispersion of each individual record with respect to target spectrum is chosen as a proxy to account for the spectrum shape. The mean (μ_δ) and

standard deviation (σ_δ) of logarithmic differences for each record are calculated using Equations (3.2) and (3.3), respectively. The smaller standard deviations (σ_δ) indicate lesser deviations from the target spectrum. After sorting the standard deviations of the records in ascending order, the top half of the records with smaller σ_δ are chosen to form the final subset of candidate ground motions. Therefore, it is important to have sufficient number of recordings from the first step for selecting the final subset of records having spectral shapes as close as to the target spectral shape. The record selection exercises made during the evolution of this study suggest that the initial subset having at least 150 accelerograms would be sufficient to achieve this objective.

$$\delta_i = \ln Sa_i^{record} - \ln Sa_i^{t\arg et} \tag{3.1}$$

$$\mu_\delta = \frac{1}{n}\sum_{i=1}^{n}\delta_i = \frac{1}{n}\sum_{i=1}^{n}(\ln Sa_i^{record} - \ln Sa_i^{t\arg et}) \tag{3.2}$$

$$\sigma_\delta = \sqrt{\frac{1}{n-1}\sum_{i=1}^{n}(\delta_i - \mu_\delta)^2} \tag{3.3}$$

The final subset having N records are subjected to the sliding window procedure to assemble k ground-motion datasets from which the most proper ground-motion set for scaling is determined. The first step of the algorithm computes the logarithmic differences (Δ_i) between the spectral ordinates of N ground motions and the target spectrum at the fundamental period of the structure (T_1) by using Equation 3.4.

$$\Delta_i = \ln Sa_i(T_1) - \ln Sa(T_1)^{t\arg et} \tag{3.4}$$

To develop ground motion sets of k accelerograms from N records, Δ_i values are sorted in ascending order first, and then k ground motions are chosen under a constant window length over the sorted list. The constant window moves down by one element and

calculates the standard deviation at each time until reaching the (N-k+1) number of slides. Thus, each sliding window represents a ground-motion dataset associated with a standard deviation (σ_i). Note that the sorting algorithm leads to ground-motion datasets with standard deviation changing from minimum to maximum. As will be discussed later, the level of uncertainty at the target is addressed by dispersion of the ground motion set. Figure 3.1 illustrates the schematic representation of the sliding window approach.
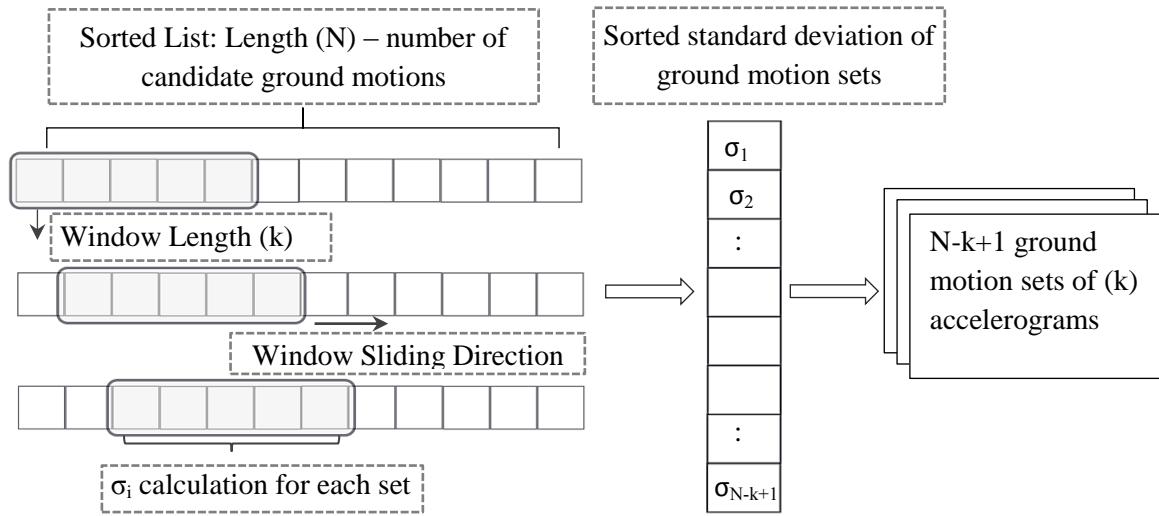
Figure 3.1. Schematic representation of the sort and sliding window approach to constitute ground motion sets of (k) accelerograms.

The optimum ground-motion dataset among the (N-k+1) sets is determined from the sum of the squared error (SSE) formula given in Equation (3.5). Goodness of fit between the spectral ordinates of target spectrum and the median and variances of each ground-motion dataset in the period range of interest (i.e., $0.2T_1$ to $2T_1$) is estimated using the following equation:

$$SSE = \sum_{i=1}^{n} \left[(\mu_{\ln Sa(T_i)} - \mu_{\ln Sa(T_i)}^{t\arg et})^2 + w(\sigma_{\ln Sa(T_i)} - \sigma_{\ln Sa(T_i)}^{t\arg et})^2 \right] \quad (3.5)$$

In Equation (3.5), the parameter w stands for the weighting factor determining the relative significance of the errors in the mean $\ln Sa$ of ground motion set ($\mu_{\ln Sa(T_i)}$) and the target (

$\mu_{\ln Sa(T_i)}^{t \arg et}$) and their corresponding standard deviation values ($\sigma_{\ln Sa(T_i)}$ and $\sigma_{\ln Sa(T_i)}^{t \arg et}$) at the period T_i. It is important to note that the scatter around the target spectral demand is determined by the standard deviation of the optimum ground motion suite at this stage. Although this procedure does not impose any restrictive bounds for the variation of the spectral accelerations, the excessive variation of spectral values may be controlled by assigning a larger value to w parameter (i.e., more significance on standard deviation) during the selection process. Finally, the set which has the lowest *SSE* score would be chosen as the optimum.

3.3.2. Record Scaling Stage

Step 2: Scaling of the optimum ground motion set to match target median and variance.
Scaling stage aims to obtain a satisfactory match between the median spectrum of the ground-motion set and the target spectrum for the period range of interest (e.g., $0.2T_1$ to $2T_1$). The scale factor (SF_1) is computed using an optimization algorithm which minimizes the difference between the median record spectrum ($Sa^{median}(T_i)$) and the target spectrum ($Sa^{t \arg et}(T_i)$) over the periods (T_i) at which the spectral values are defined. The objective function of the minimization problem can be given by

$$\min_{SF_1} \| \ln SF_1 \times Sa^{median}(T_i) - \ln Sa^{t \arg et}(T_i) \|_{0.2T_1 < T_i < 2T_1} \qquad (3.6)$$

where $\| . \|$ represents the Euclidean norm. Herein, an additional criterion is adopted to ensure that the scaled median of the spectral values do not fall below 90% of the target spectrum in the specified period interval. This is a condition required by the most contemporary seismic code provisions (Haselton *et al.*, 2014). Thus, the normalized differences (s_d) between the spectral values of the scaled median spectrum and the 90% of the target median are calculated in order to obtain the adjusting scale factor (SF_2). The computation of the SF_2 is given in Equation 3.7.

$$\text{If} \quad \min_{0.2T_1 < T_i < 2T_1} [SF_1 \times Sa^{median}(T_i) / Sa^{t\arg et}(T_i)] < 0.9 :$$

$$s_d = \frac{\max_{0.2T_1 < T_i < 2T_1} (0.9 \times Sa^{t\arg et} - SF_1 \times Sa^{median})}{(0.9 \times Sa^{t\arg et})}$$

$$(3.7)$$

$$SF_2 = (1 - s_d)^{-1}$$

Thus, the final scale factor of the ground motions to match target median is computed as $SF_{median} = SF_1 \times SF_2$. When the ground motions are multiplied by this median scale factor (SF_{median}) the variability within the ground motion suite is preserved along the period range of interest. It should be emphasized that this scaling procedure is adopted while selecting ground motions to match PSHA-based target spectrum such as Uniform Hazard Spectrum (UHS) or Conditional Mean Spectrum (CMS).

In the case of the scenario-based target spectrum, the target distribution of the spectral demand is mainly considered as target median ± standard deviation ($\sigma^{t\arg et}$) estimation of the ground motion prediction model. Therefore, each scaled ground motion needs to be further modified to control the variance of the ground motion suite. In order to capture the target probability distribution at the given period, the new spectral ordinate of each ground motion is defined by epsilon (ε) values. This parameter is assumed to be normally distributed and it corresponds to the number of standard deviations above or below the median. The location of ε corresponds to the center of equally divided portions in cumulative distribution function (CDF) where the corresponding values can be obtained using inverse CDF. It should be noted that similar approaches are also employed in previous studies (Kottke and Rathje, 2008; Huang *et al.*, 2011; Buratti *et al.*, 2011). For illustration, the computed ε values for a suite of five motions are shown in Figure 3.2. The distribution of the target spectral ordinates is developed with respect to the natural logarithm of the scaled median spectrum ($\ln S\tilde{a}^{median}(T_1)$) at the fundamental period (T_1). Thus, the match between scaled median and target spectra is preserved so that the applied scale factors will affect only the standard deviation of the ground motion set. The target

spectral ordinates ($\ln Sa^{t\arg et}(T_1)$) for the n number of ground motions at the target period are computed by using Equation (3.8).

$$\ln Sa^{t\arg et}(T_1) = \ln S\tilde{a}^{median}(T_1) + \varepsilon_n(\sigma^{t\arg et})$$ (3.8)

Equation (3.9) presents the computation of the individual scaling factor (SF_n) of each ground motion which is obtained by taking the ratio of the sorted logarithmic spectral values of the target and the ground motions ($\ln Sa_n(T_1)$) at the fundamental period.

$$SF_n = \frac{\ln Sa^{t\arg et}(T_1)}{\ln Sa_n(T_1)}$$ (3.9)

The final scale factor (SF_{final}) for each ground motion is obtained by using Equation (3.10). At the end of this stage, the scaled ground motion set provides a reasonable match to target median and variance of the scenario-based spectrum over the specified period interval.

$$SF_{final} = SF_{median} \times SF_n$$ (3.10)
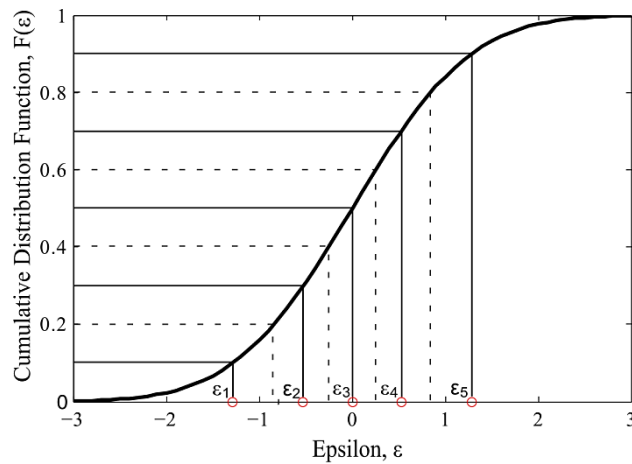
Figure 3.2. Determination of epsilon (ε) values for suites of five ground motions by dividing cumulative distribution function.

3.4. Application of the Proposed Procedure

3.4.1. Case Study Based on Matching Scenario-Based Spectrum

The performance of the proposed methodology is tested by using a suite of 15 ground motions to match both target median and variance. It should be noted that the geometric mean of two horizontal components (i.e., the square root of the product of the two horizontal components) is used in record selection and scaling stages to maintain consistency with the spectral measure definition used in ground motion prediction model. Scenario-based target spectrum is computed using the ground motion prediction model of Campbell and Bozorgnia (2008) for the most dominant event parameters of magnitude (M_w) 7.0, source to site distance (R_{jb}) 15 km, and shear wave velocity, Vs_{30}=360 m/s. The fundamental period of the structure is chosen as T_1=1.0s. Target variance is associated with median$\pm$ (n) sigma ($\sigma^{t \arg et}$) estimation of the selected ground motion prediction model (CB08). It should be noted that the target variance can be determined based on (n) varying number of standard deviation. The case study uses the one-sigma as a target variance. Figure 3.3a depicts the performance of the proposed procedure when the ground motions are scaled to match the target median. Note that when the ground motions are scaled to match the target median (i.e., median scaling), the target variance is set to zero in the ground motion selection stage (see Equation 3.5), and thus the scaled suite would result in lower dispersion at the target period. To capture the spectral distribution of the target intensity, scaled ground motions should be further modified with their specific scale factors to match target variance at the fundamental period (i.e., variance scaling). Figure 3.3b presents the case for matching both target median and variance (i.e., 16th and 84th percentiles of the target spectrum). It is important to note that the ground motions that are modified to match target variance at the fundamental period may produce excessive dispersion at other periods. However, the results of this study indicate that a satisfactory compatibility is obtained in terms of target variance match along the specified period interval (i.e., $0.2T_1$-$2T_1$). Figure 3.3c illustrates the standard deviations of the ground motions for the median scaling and variance scaling cases. As seen in Figure 3.3b and Figure 3.3c, the distribution of the spectral acceleration ordinates provides a good match with the target distribution. Table 3.1 lists the seismological characteristics of the selected

records and their corresponding scale factors. It is observed that the amplitudes of the scale factors are varied from 0.47 to 1.95. On the basis of these results, it can be concluded that the proposed procedure provides a representative suite of motions for scenario-based seismic assessment of structures.
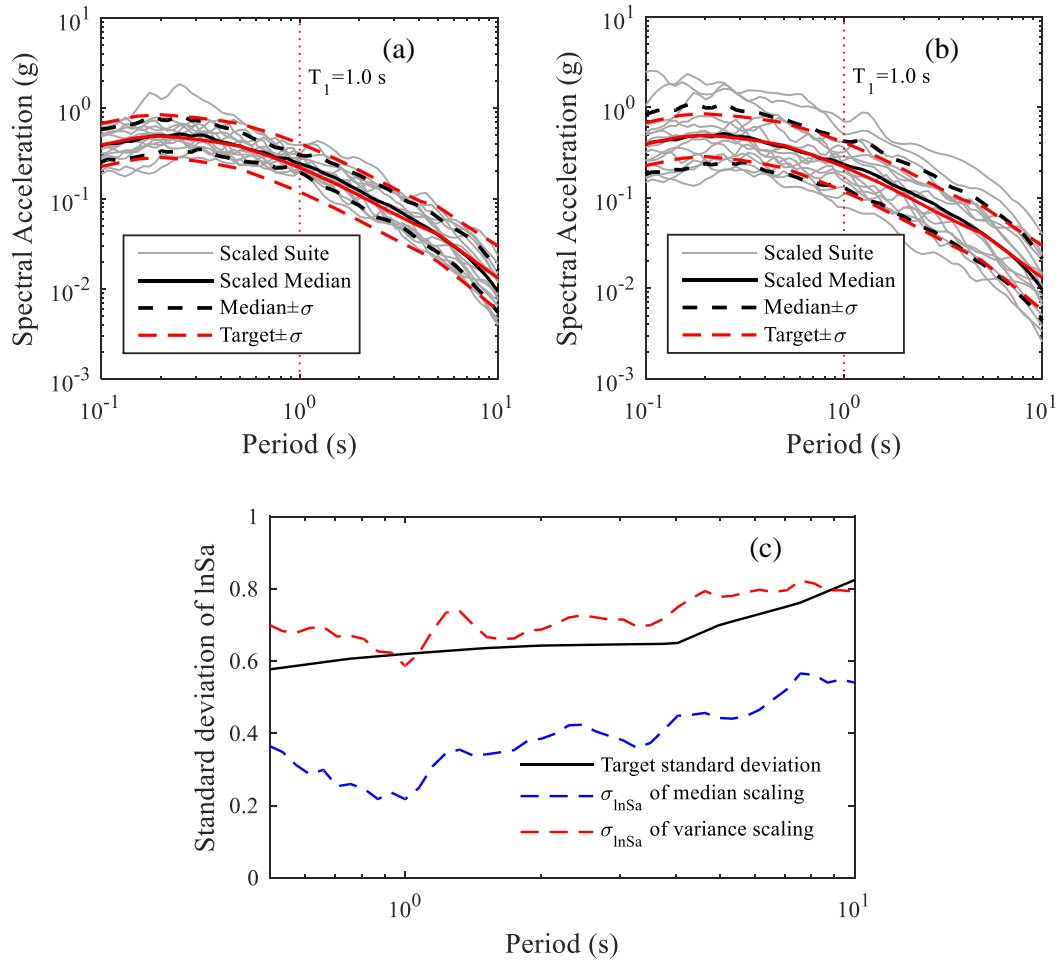
Figure 3.3. Performance of the proposed procedure for (a) matching the target median (CB08 median prediction), (b) matching the target median and variance (CB08 median±1sigma prediction), (c) Standard deviations of lnSa for the median scaling and variance scaling cases.

Table 3.1. Seismological properties of the selected records and their corresponding scale factors.

Record	NGA Sequence Number	Event (Year)	M_w	R_{jb}, km	Vs_{30}, m/s	Scale Factor (SF_{final})
1	183	Imperial Valley-06 (1979)	6.53	3.86	206.1	1.95
2	184	Imperial Valley-06 (1979)	6.53	5.09	202.3	1.44
3	728	Superstition Hills-02 (1987)	6.54	13.03	193.7	1.21
4	848	Landers (1992)	7.28	19.74	271.4	1.29
5	721	Superstition Hills-02 (1987)	6.54	18.20	192.1	1.16
6	161	Imperial Valley-06 (1979)	6.53	8.54	208.7	1.16
7	174	Imperial Valley-06 (1979)	6.53	12.45	196.3	1.11
8	735	Loma Prieta (1989)	6.93	41.68	415.3	1.04
9	1640	Manjil, Iran (1990)	7.37	93.30	274.5	0.95
10	830	Cape Mendocino (1992)	7.01	26.52	513.7	0.94
11	68	San Fernando (1971)	6.61	22.77	316.5	0.88
12	1056	Northridge-01 (1994)	6.69	85.75	308.6	0.82
13	881	Landers (1992)	7.28	17.32	345.4	0.72
14	175	Imperial Valley-06 (1979)	6.53	17.94	196.9	0.64
15	162	Imperial Valley-06 (1979)	6.53	10.45	231.2	0.47

3.4.2. Case Study Based on Matching PSHA-Based Spectrum

This section focuses on the application of the proposed methodology to select ground motions for matching PSHA-based target spectrum. In order to estimate the seismic hazard level of the given site, site-specific PSHA calculations are performed using EZ-FRISK Program (Risk Engineering, 2005). The seismic hazard curve is obtained for a site (40.99˚N, 29.09˚E) located in the city of Istanbul, with a shear wave velocity in the top 30 m of the soil, V_{S30}, of 450 m/s. The period of interest is chosen as T_1=1.0s. The mean value of the most contributing earthquake scenario parameters such as magnitude (M_w), source to site distance (R_{jb}; Joyner and Boore distance), and epsilon (ε) values are determined by disaggregation of the probabilistic seismic hazard for 475year mean return period (i.e., 10% probability of exceedance in 50 years). The target intensity level, $Sa(T_1)$, for a return period of 475 years is obtained as 0.30g. It is observed that the seismic hazard for the selected site is mostly dominated by the rupture at the North Anatolian Fault-Central Marmara Segment. The characteristic parameters of most contributing earthquake scenario are obtained as M_w =7.16, R_{jb} =21.2 km and ε (epsilon) =1.38. The target Conditional Mean Spectrum (CMS) is developed for the fundamental period of T_1=1.0s using the disaggregation information and the Campbell and Bozorgnia (2008) ground motion prediction model (GMPM). Since a single GMPM is used to derive the CMS, the target epsilon (ε*=1.44) is obtained by performing back calculation. The detailed computation of this spectrum can be found in Lin *et al.* (2013).

It is worth noting that this study does not attempt to match the full conditional distribution of the target CMS (i.e., Conditional Spectrum) because the aim of this method is to select ground motions to match target median (i.e., spectrum compatibility) while preserving natural peaks-to-troughs (i.e., inherent variability with frequency) of the unscaled ground motions along the period interval. As noted before, the uncertainty associated with the predicted level of intensity measure is taken into account by the dispersion statistics of the ground motion set. A suite of 20 ground motions are selected to match both the Conditional Mean Spectrum (CMS) and the Uniform Hazard Spectrum (UHS) for illustration. As noted before, the unscaled ground motions are scaled by a constant scale factor to obtain a reasonable match between scaled median spectrum and

target spectrum. Therefore, the shape of the scaled spectrum and the dispersion in the record set would be the same as the unscaled situation. The scale factors of record set are generally changed between 0.8 and 3.0 at varying intensity levels indicating that the proposed procedure avoids excessive modifications of the ground motions, and the potential structural response biases induced by a large scale factor are prevented. Figure 3.4a and Figure 3.4b illustrate the response spectrum of the ground motions that are selected and scaled to match the target UHS and CMS, respectively. Also shown on that plot are the median record spectrum, 16th and 84th percentiles of the scaled ground motions. Since the records are selected to have an appropriate spectral shape, the median scaled record spectrum matches reasonably well to the target spectra for the specified period interval (i.e., $0.2T_1$-$2T_1$). Unlike most code-based scaling techniques which artificially minimize the record-to record variability of the individual records over the specified period range, the proposed procedure controls the dispersion of the ground motion set at the target level and over the period range of interest. Figure 3.5 shows the standard deviation of logarithmic spectral accelerations of the ground motions that are selected based on matching target UHS and CMS. It is observed that the dispersion values are changed between 0.2 and 0.4 and they show approximately uniform trend along the period range of interest. It is important to note that the magnitude of elastic spectral dispersion may change as a function of number of records. For instance, the dispersion of the ground motions is generally minimized at the target period if the suits of 7-10 records are used, while dispersion values become more stabilized for suits of 15-40 ground motions at the period interval of $0.2T_1$-$2T_1$. The effect of level of spectral elastic dispersion on structural response will be discussed later in this chapter.
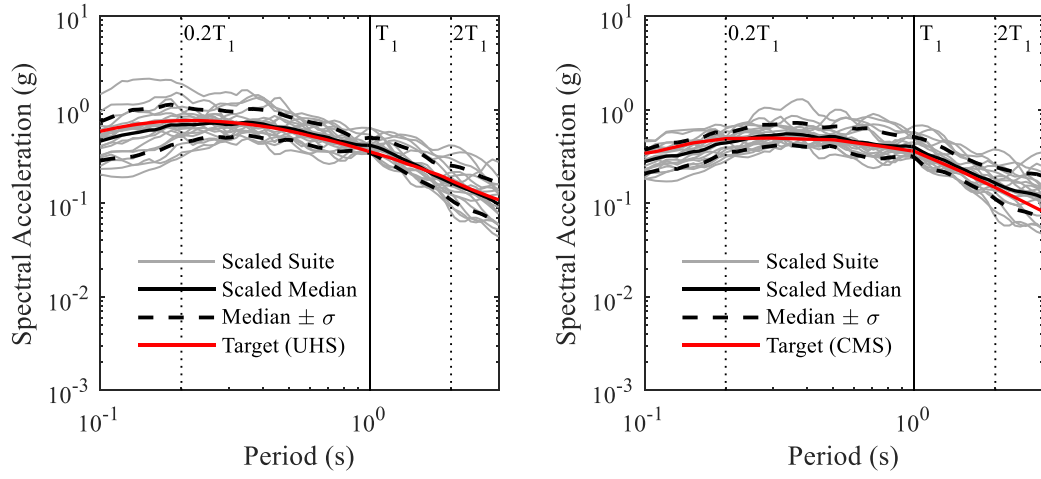
Figure 3.4. Comparisons of scaled median and target spectra for period of T_1=1.0s for suites of 20 of ground motions. The left panel shows the UHS and the right panel corresponds to CMS.

Figure 3.5. Standard deviations of the lnSa values of the ground motions that are selected to match UHS and CMS.

3.5. Probabilistic Seismic Demand Models for the Estimation of EDP|IM

This section gives brief overview of the probabilistic seismic demand models that are commonly used in structural response estimation. Depending on the approaches utilized for the ground motion selection, different estimation methods may be adopted to determine the probabilistic relationship between structural response and intensity measure (IM) for performance-based assessment of structures. These probabilistic models are then used to estimate the fragility curves that expresses the probability of failure for a given seismic intensity level. The two common approaches that are used to estimate the structural response (or engineering demand parameter, EDP) conditioned on a given ground motion intensity level are known as stripe and cloud analyses (Vamvatsikos and Cornell, 2004; Jalayer and Cornell, 2003; Iervolino and Cornell, 2005).

In the stripe analysis, statistical parameters of EDP|IM distribution is obtained through the nonlinear dynamic analysis of the structure subjected to a set of scaled records. The records are scaled to target $Sa(T_1)$ value with the assumption of zero dispersion in spectral demand, whereas some level of dispersion is preserved in the structural response due to randomness of the ground motions. This approach, hereinafter referred to as $Sa(T_1)$ scaling, provides stripe of response results at conditioning IM value. One can select and scale different sets of ground motions to successively increasing IM values or target hazard levels in order to assess the seismic performance of structure at multiple intensity levels (i.e., Multiple Stripe Analysis). In this method, the distribution of EDP at each IM value can be obtained by modeling the distribution of the demand through a statistical distribution. A common assumption is that EDP can be modeled as log-normally distributed random variables; and thus the distribution of the demand parameters may be fully described by its first and second moments (Shome *et al.*, 1998; Cornell *et al.*, 2002; Aslani and Miranda, 2005). The other probabilistic seismic demand model is known as cloud analysis. In its simplest form, the nonlinear dynamic analysis is performed under a set of unscaled ground motions (or scaled by a constant) of wide range of $Sa(T_1)$ intensity levels that result in cloud of structural response values. In this approach, the ground motions are often selected from a magnitude-distance bin for proper representation of the scenario event parameters. In this case, the estimations of structural response, i.e.

conditional median and standard deviation of EDP given IM, can be obtained from regression analysis which considers a linear relationship between the natural logarithms of the variables (Cornell *et al.*, 2002). Cloud analysis is more effective to establish probabilistic seismic demand model for large number of structures, such as those needed in loss assessment study, whereas multiple stripe analysis approach is generally used to quantify the seismic performance of the specific building by using site-specific ground motions. Detailed information and discussion on these methods can be found in Baker and Cornell (2006). These probabilistic seismic demand models can be used as a tool to compute probability of exceeding specified demand value in given intensity measure (i.e., fragility curve). The variability related to ground motion intensity is included with a fully probabilistic approach by integrating the structural response estimations with the occurrence rate of the intensity measure in order to compute seismic demand hazard curve (i.e., risk-based assessment).

Unlike the aforementioned procedures, the proposed method aims to select ground motions that would represent the spectral variation (or distribution) in the family of the hazard curves for a specified annual rate of exceedance. The ground motions are scaled to the specific hazard level with the consideration of dispersion in the spectral demand. Thus, the records have different range of spectral values (IM) at the target period that produce cloud points in the plane of EDP versus IM. In this case, the conditional distribution of EDP for a given IM can be computed by performing the linear regression analysis at each hazard level (which is similar to the cloud method approach). However, in order to incorporate the effect of spectral variation in the target intensity measure on the fragility curve derivation, a new probabilistic seismic demand model is required. In this study, a new statistical model is also proposed in order to take into account the uncertainties in both seismic demand (due to record-to record variability) and spectral demand on fragility curve computations. The utilized statistical model, namely Gaussian Mixture Model, provides joint occurrence probability of EDP-IM pair in a continuous scale at different seismic intensity levels. The main objective is to investigate the effect of spectral variation on the fragility curve derivation. Figure 3.6 shows the schematic presentations of the cloud analysis, stripe analysis and Gaussian Mixture model approaches. Further discussion on these different probabilistic seismic demand models can be found in Chapter 5.
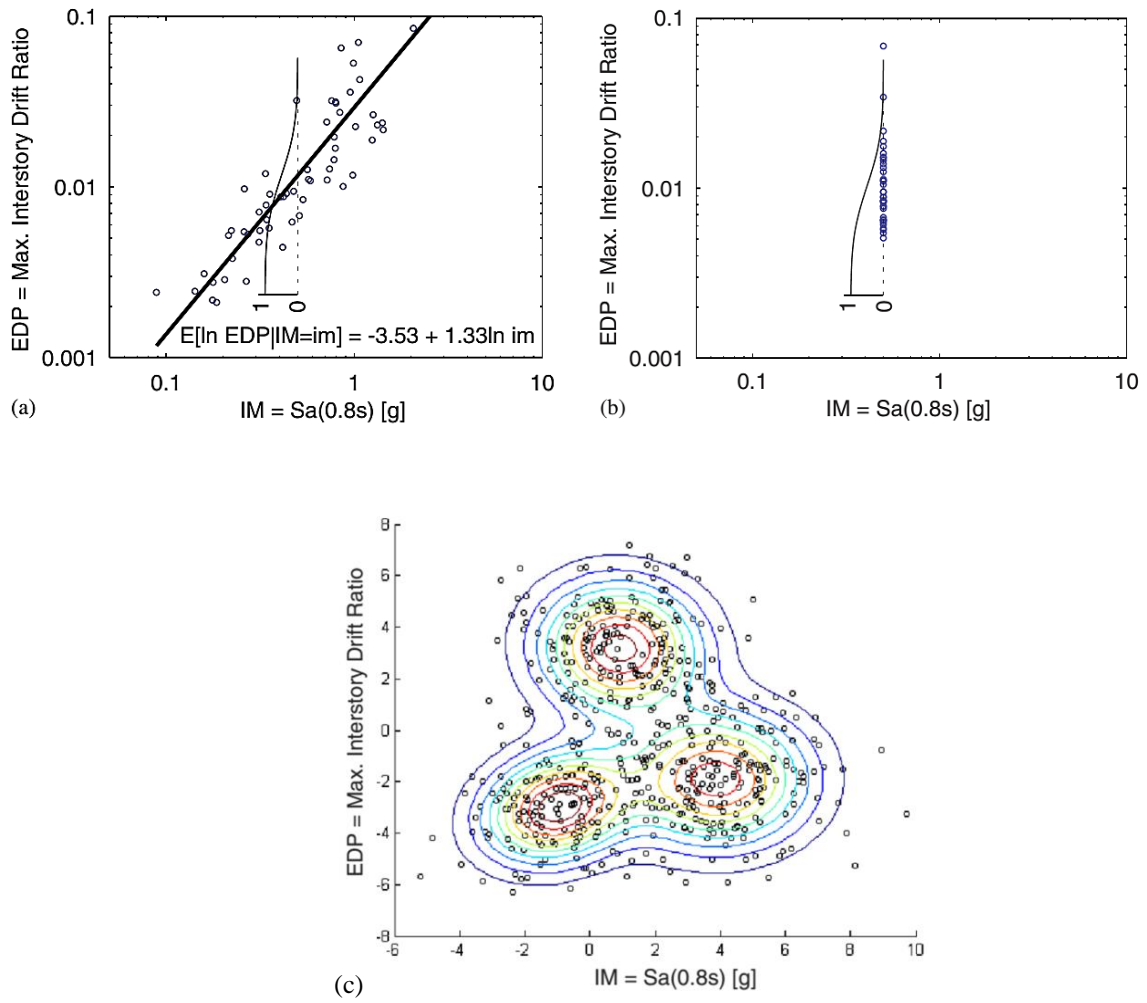
Figure 3.6. Schematic presentations of the (a) cloud analysis, (b) stripe analysis (Baker and Cornell, 2006), and (c) Gaussian Mixture model approaches.

3.6. Nonlinear Seismic Response of SDOF Structural Systems

The performance of the proposed approach in predicting the seismic demand is evaluated by comparing the seismic response analysis results of this study to those obtained using the $Sa(T_1)$ scaling method. These comparative studies would provide some insight into how different scaling procedures affect the outcome of the response history analysis. Nonlinear response history analyses are conducted using sets of records modified by both ground motion selection and scaling procedures for the selected scenario event. Site-specific PSHA calculations are performed for the same target site as mentioned previously in Section 3.4.2. The specified probabilistic hazard level is related to ground motions having 10% probability of exceedance in 50 years (i.e., return period of 475 years). The most contributing earthquake scenario parameters are determined by disaggregation of the probabilistic seismic hazard analysis for the considered intensity level at each period of interest. Target earthquake scenario parameters and target spectral ordinates ($Sa(T_1)$) are listed in Table 3.2. Note that the earthquake records are selected from a ground motion database that is constrained by the seismological parameters (e.g., magnitude, distance, site condition) of the target scenario event. The selected ground motions have a magnitude range of 6.7 to 7.7 and distance range of 10 to 100km. The records within 0-10 km distance ranges are explicitly excluded in order to avoid the near fault effects. The site classes of the ground motions are compatible with the NEHRP C and D site class definitions (i.e., 180 m/s $< Vs_{30} < 760$ m/s).

Table 3.2. Target earthquake scenario parameters (M_w, R_{jb}, ε) and target spectral ordinates ($Sa(T_1)$) at each period of interest.

Periods	M_w	R_{jb}, km	Vs_{30} (m/s)	ε	$Sa(T_1)$, g
T_1=0.5s	7.13	26.6	450	1.59	0.59
T_1=1.0s	7.16	21.2	450	1.44	0.36
T_1=2.0s	7.18	29.1	450	1.63	0.18

Target Conditional Mean Spectrum (CMS) is derived from the scenario earthquake parameters of site-specific PSHA and the Campbell and Bozorgnia (2008) ground motion prediction model at each structural period. The proposed methodology selects the ground motions to match both UHS and CMS. In order to make comparisons between two different ground motion scaling approaches, the earthquake records are also selected and scaled to match the Conditional Spectrum (CS) that takes into account both mean and variability of the response spectrum. This selection and scaling approach gives comparable results to those obtained by the point of comparison estimate of the median maximum drift (Haselton *et al.*, 2009), and is therefore used as a benchmark for evaluating performance of the proposed procedure in seismic response estimation. In this approach, the distribution of the ground motion suite is consistent with the multivariate normal distribution of logarithmic spectral acceleration (lnSa) of the Conditional Spectrum. The ground motions are modified with their specific scaling factor to match target at the fundamental period of the structure. The uncertainty at the target intensity level is considered as zero, whereas the spectral variability is included at other periods of this spectrum. It has been shown that the dispersion of the ground motion suit is consistent with the target variance of the Conditional Spectrum. Herein, this selection and scaling scheme is referred to as $Sa(T_1)$ scaling method.

For illustration, a suite of 40 scaled records of both methodologies are plotted along with their median and target spectra in Figure 3.7. The standard deviations of the lnSa values of the scaled ground motions from this study and the $Sa(T_1)$ scaling method are compared in Figure 3.8. It is seen that the dispersions of the ground motions at periods away from the conditioning one increase as a result of decreasing correlations of spectral accelerations, whereas dispersion statistics obtained from the proposed procedure follows approximately uniform trend along the period interval. The ground motion sets selected by the proposed method and the $Sa(T_1)$ scaling method are listed in Table 3.3 and Table 3.4, respectively.
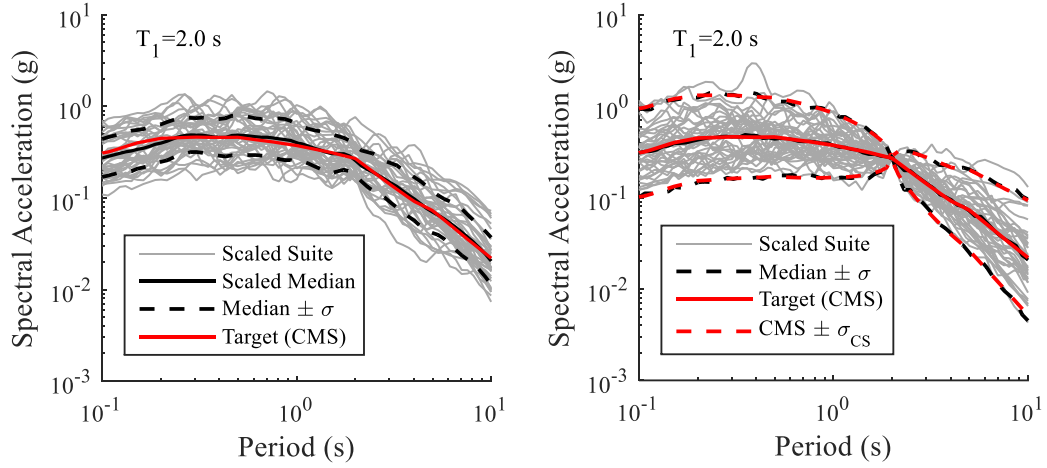
Figure 3.7. Comparisons of scaled median and target spectra for period of T_1=2.0 s for suites of 40 of ground motions. The left panel shows the re sults of this study and the right panel corresponds to the $Sa(T_1)$ scaling method.
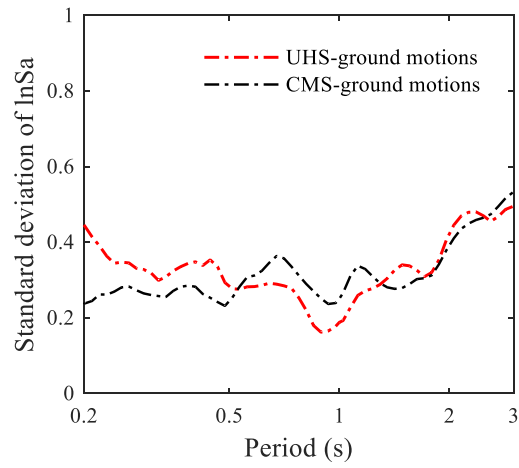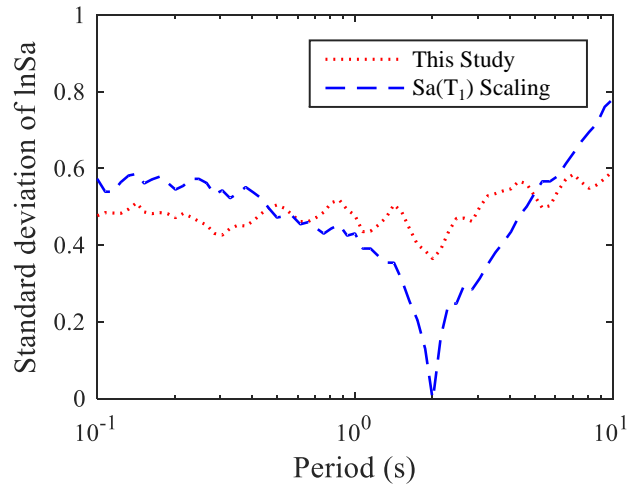

Figure 3.8. Standard deviations of the lnSa values of the scaled ground motions from this study and the $Sa(T_1)$ scaling method.

Table 3.3. The ground motion set selected by the proposed methodology.

Record number	NGA sequence number	Earthquake Name	Year	Station Name	M_w	R_{jb} (km)	Vs_{30} (m/s)
1	1158	Kocaeli, Turkey	1999	Duzce	7.51	13.6	276
2	1633	Manjil, Iran	1990	Abbar	7.37	12.6	724
3	-	Montenegro, Serbia	1979	Ulcinj-Hotel Olimpic	6.9	13.0	399
4	777	Loma Prieta	1989	Hollister City Hall	6.93	27.3	198
5	776	Loma Prieta	1989	Hollister - South & Pine	6.93	27.7	370
6	1077	Northridge-01	1994	Santa Monica City Hall	6.69	17.3	336
7	888	Landers	1992	San Bernardino	7.28	79.7	271
8	1166	Kocaeli, Turkey	1999	Iznik	7.51	30.7	274
9	757	Loma Prieta	1989	Dumbarton Bridge West	6.93	35.3	274
10	900	Landers	1992	Yermo Fire Station	7.28	23.6	353
11	-	Manjil, Iran	1990	Qazvin, Iran	7.3	49.0	435
12	1636	Manjil, Iran	1990	Qazvin	7.37	49.9	274
13	826	Cape Mendocino	1992	Eureka - Myrtle & West	7.01	40.2	338
14	1009	Northridge-01	1994	LA - Wadsworth VA	6.69	14.6	392
15	827	Cape Mendocino	1992	Fortuna - Fortuna Blvd	7.01	15.9	457
16	736	Loma Prieta	1989	APEEL 9	6.93	40.9	449
17	737	Loma Prieta	1989	Agnews State Hospital	6.93	24.3	239
18	731	Loma Prieta	1989	APEEL 10 – Skyline	6.93	41.7	392
19	1762	Hector Mine	1999	Amboy	7.13	41.8	271
20	1792	Hector Mine	1999	Indio - Riverside	7.13	74.0	207
21	832	Landers	1992	Amboy	7.28	69.2	271
22	985	Northridge-01	1994	LA - Baldwin Hills	6.69	23.5	297
23	740	Loma Prieta	1989	Anderson Dam	6.93	19.9	488
24	1113	Kobe, Japan	1995	OSAJ	6.90	21.4	256
25	1043	Northridge-01	1994	Neenach - Sacatara Ck	6.69	51.6	308
26	756	Loma Prieta	1989	Dublin - Fire Station	6.93	58.7	271
27	884	Landers	1992	Palm Springs Airport	7.28	36.2	207
28	138	Tabas, Iran	1978	Boshrooyeh	7.35	24.1	338
29	1057	Northridge-01	1994	Playa Del Rey – Saran	6.69	24.4	405
30	1640	Manjil, Iran	1990	Tonekabun	7.37	93.3	274
31	1637	Manjil, Iran	1990	Rudsar	7.37	63.9	274
32	1163	Kocaeli, Turkey	1999	Hava Alani	7.51	58.3	424
33	68	San Fernando	1971	LA - Hollywood	6.61	22.8	316
34	1155	Kocaeli, Turkey	1999	Bursa Tofas	7.51	60.4	274
35	1810	Hector Mine	1999	Mecca - CVWD Yard	7.13	91.9	345
36	812	Loma Prieta	1989	Woodside	6.93	33.9	454
37	1092	Northridge-01	1994	Ventura – Harbor	6.69	54.3	271
38	862	Landers	1992	Indio - Coachella Canal	7.28	54.3	345
39	1154	Kocaeli, Turkey	1999	Bursa Sivil	7.51	65.5	659
40	880	Landers	1992	Mission Creek Fault	7.28	26.9	345

Table 3.4. The ground motion set selected by the Sa(T_1) scaling methodology.

Record number	NGA sequence number	Earthquake Name	Year	Station Name	M_w	R_{jb} (km)	Vs_{30} (m/s)
1	1472	Chi-Chi, Taiwan	1999	TCU017	7.62	54.2	558
2	1538	Chi-Chi, Taiwan	1999	TCU112	7.62	27.5	215
3	1436	Chi-Chi, Taiwan	1999	TAP052	7.62	98.5	473
4	1554	Chi-Chi, Taiwan	1999	TCU145	7.62	35.3	215
5	884	Landers	1992	Palm Springs Airport	7.28	36.1	207
6	1144	Gulf of Aqaba	1995	Eilat	7.20	43.2	354
7	1216	Chi-Chi, Taiwan	1999	CHY059	7.62	73.2	191
8	880	Landers	1992	Mission Creek Fault	7.28	26.9	345
9	1487	Chi-Chi, Taiwan	1999	TCU047	7.62	35.0	520
10	1536	Chi-Chi, Taiwan	1999	TCU110	7.62	11.6	212
11	832	Landers	1992	Amboy	7.28	69.2	271
12	1598	Chi-Chi, Taiwan	1999	WTC	7.62	42.2	215
13	882	Landers	1992	North Palm Springs	7.28	26.8	345
14	1223	Chi-Chi, Taiwan	1999	CHY067	7.62	83.5	228
15	1539	Chi-Chi, Taiwan	1999	TCU113	7.62	31.0	230
16	827	Cape Mendocino	1992	Fortuna - Fortuna Blvd	7.01	15.9	457
17	1243	Chi-Chi, Taiwan	1999	CHY100	7.62	53.4	230
18	1338	Chi-Chi, Taiwan	1999	ILA050	7.62	63.8	473
19	1637	Manjil, Iran	1990	Rudsar	7.37	63.9	274
20	1208	Chi-Chi, Taiwan	1999	CHY046	7.62	24.1	442
21	1101	Kobe, Japan	1995	Amagasaki	6.90	11.3	256
22	1813	Hector Mine	1999	Morongo Valley	7.13	53.1	345
23	862	Landers	1992	Indio - Coachella Canal	7.28	54.2	345
24	1280	Chi-Chi, Taiwan	1999	HWA031	7.62	47.4	473
25	1113	Kobe, Japan	1995	OSAJ	6.90	21.3	256
26	1202	Chi-Chi, Taiwan	1999	CHY035	7.62	12.6	473
27	-	Manjil, Iran	1990	Qazvin, Iran	7.3	49.0	435
28	1541	Chi-Chi, Taiwan	1999	TCU116	7.62	12.4	493
29	1553	Chi-Chi, Taiwan	1999	TCU141	7.62	24.2	215
30	1209	Chi-Chi, Taiwan	1999	CHY047	7.62	24.1	272
31	796	Loma Prieta	1989	SF – Presidio	6.93	77.3	594
32	1482	Chi-Chi, Taiwan	1999	TCU039	7.62	19.9	540
33	14	Kern County	1952	Santa Barbara	7.36	81.3	515
34	755	Loma Prieta	1989	Coyote Lake Dam	6.93	19.9	597
35	1335	Chi-Chi, Taiwan	1999	ILA046	7.62	77.0	396
36	738	Loma Prieta	1989	Alameda Naval Air Stn	6.93	70.9	190
37	740	Loma Prieta	1989	Anderson Dam (L Abut)	6.93	19.9	488
38	1633	Manjil, Iran	1990	Abbar	7.37	12.5	724
39	1277	Chi-Chi, Taiwan	1999	HWA028	7.62	49.9	272
40	766	Loma Prieta	1989	Gilroy Array #2	6.93	10.3	270

The non-degrading bilinear single degree freedom (SDOF) systems with 3% post-yield stiffness hardening ratio and 5% damping ratio are considered as simplistic models of the complex multi-degree of freedom systems. The fundamental periods are chosen as T_1=0.5, 1.0, and 2.0 seconds. The yield displacements of the inelastic SDOF systems are determined by using the strength reduction factors (i.e., the ratio of elastic to yield strength of an SDOF system) of R=2 and R=6. The strength reduction factor of R=1 corresponds to elastic structural response for a record scaled to the specified target hazard level at the fundamental period of the structure. Note that R=2 and R=6 can be considered as mildly-inelastic (or nearly-elastic) and highly-inelastic responses at the target intensity level, respectively. The nonlinear response history analyses are conducted using sets of 7, 10, 15, 20, 30, and 40 records for the SDOF systems in order to investigate the effect of number of scaled ground motions on structural response estimations. The maximum inelastic displacements are used as a structural response parameter of interest. Figure 3.9-3.11 illustrate the elastic (Sd,e) and inelastic displacements (Sd,i) of both scaling methodologies together with their 16th and 84th percentiles (or median ± 1standard deviation) at fundamental periods of T_1=0.5, 1.0, and 2.0 seconds, respectively. The left panel represents the elastic spectral displacements (R=1). The middle and right panels compare the structural responses as a function of number of ground motions for the mildly-inelastic (R=2) and highly-inelastic cases (R=6), respectively.

As noted before, the ground motions selected by $Sa(T_1)$ scaling method produces zero dispersion in the elastic spectral displacement. The proposed method, on the other hand, introduces an additional uncertainty in target intensity measure to account for the scatter in the earthquake shaking. As seen in the left panel of the figures, the non-zero dispersion is preserved at the target hazard level in which the magnitude of the variability increases with the increasing number of ground motions. It should be noted that the level of elastic spectral dispersion preserved at the target intensity level is not significantly affected by the choice of target spectra. The analysis results show that the proposed method yields fairly similar structural response distribution (both median and standard deviation) in the elastic and mildly-inelastic behavior at each fundamental period for each ground motion set. The preserved dispersion within the ground motion suite is directly observed in the inelastic displacement variability, indicating that the deviation of the

spectral accelerations from the target level produces similar degree of deviation in the mildly-inelastic responses. In other words, the distribution of the structural response can be thought of as a linear function of the elastic spectral dispersion in the target median. In the short period range (T_1=0.5s) and at high nonlinearity level, the proposed method produces lower variability in the structural response compared to $Sa(T_1)$ scaling method for small number of ground motions (e.g., for 7-10 records). The median responses, on the other hand, are slightly higher than the $Sa(T_1)$ scaling method. This can be explained by the fact that the ground motions that are selected to match the CMS have larger variance at and near the T_1 compared to CS-based matched ground motions. Therefore, as the period of the structure lengthens due to nonlinearity, the structure becomes highly sensitive to the variation of spectral shape immediately adjacent to the spectral acceleration at the fundamental period. Moreover, the preserved dispersion within the ground motion suite shows high fluctuation trend due to the jaggedness of the spectral shape for shorter vibration periods. Thus, the extreme (or peaked) spectral shape of the single spectrum may impose higher spectral demand and offset the median estimations. The sensitivity of the central response to the local spectral shape or to the outliers can be minimized by using large number of ground motions that yield more stable (or uniform) standard deviation along the period interval. It is observed that the median responses are relatively insensitive to the choice of target spectra for mildly-inelastic behavior (R=2). It is demonstrated that the ground motions selected based on UHS produce larger median responses than the CMS and CS-matched ground motions at high level of nonlinearity. This result is expected because the UHS does not represent a single scenario earthquake and it includes higher spectral acceleration values at all periods which, in turn, leads to biased estimates (conservatively) of the median response. In the mid-period (T_1=1.0s) and long-period (T_1=2.0s) of vibrations, both scaling methods produce similar median estimations, and in general the results are not very sensitive to the number of ground motions. The discrepancies between two scaling methodologies are more pronounced if the analyses are conducted using suites of 7-10 ground motions. It is seen that the sensitivity of the median structural response to the number of ground motions is diminished for larger than 20 records for both methods. The results indicate that median responses do not differ considerably among different nonlinearity levels for long period structure (T_1=2.0s). These findings also validate the applicability of the equivalent-displacement rule in that region. It

is worth noting that the proposed method scales the ground motions to obtain a reasonable match between the scaled median record spectrum and target spectrum for a specified period interval. The scaled median spectrum of the ground motions (particularly for small number of records) slightly deviates from the target intensity level (i.e., $Sa(T_1)$) of the UHS that may lead to over-prediction in median structural response compared to the CMS and CS-based matched ground motions.

The uncertainties in the nonlinear structural response obtained from both methods are compared as a function of number of ground motions at each fundamental period as shown in Figure 3.12. In the case of the proposed method, the elastic spectral dispersion of the ground motions at the target level is also provided for comparison. It has been shown that the variability in the structural response is consistent with the elastic spectral dispersion values for mildly-inelastic behavior (R=2), and this consistency particularly becomes more evident for larger than 20 records. It is apparent that the dispersions in structural response are increased as the structure behaves highly-nonlinear (R=6). In the case of the $Sa(T_1)$ scaling approach, the dispersion in structural response is substantially reduced for nearly elastic behavior, whereas it increases by a factor of 2.0 as the level of nonlinearity is increased. These results indicate that the structure becomes sensitive to the frequency content of the ground motions at the lengthened effective period. The inflation in the standard deviation is more pronounced for the number of 7-10 records at longer period of vibration. It can be concluded that, in general, dispersion in structural response tends to be unstable for number of 7-10 records, whereas it becomes stable for more than 30 records for both methods. These results indicate that a large number of ground motions (in the order of 30+) are needed to have a stable dispersion in structural response for both methods.

It should be noted that if the median response is of primary interest, reduced variability in the structural response increases the accuracy in median estimation. In this case, standard error ($S.E.$) on the sample mean estimation can be used as a statistical measure to construct the confidence interval for the prediction. It can be computed as the ratio of variability in the structural response ($\sigma_{\ln Sdi}$) to square root of the number of

observations (N_{obs}) carried out (i.e., $\sigma_{\ln Sdi}\big/\sqrt{N_{obs}}$). Herein, the standard deviation of the sample response is assumed to be equivalent of the true standard deviation of the population and the error computations are performed for one-sigma confidence level (i.e., 64% confidence level). It is noteworthy that the minimum number of records required to obtain a reliable estimate depends partly on the approach used in ground motion selection and scaling methodology, and the desired level of precision in the response estimate. The results indicate that the $Sa(T_1)$ scaling method is effective in minimizing the dispersion in mildly-inelastic structural responses, and hence reducing the number of records required to obtain accurate median estimate. However, its effectiveness is influenced by the inelasticity level. For example, as the structure behaves highly nonlinear, using less than 15 records yields unstable error estimation for this approach. It is observed that the standard error estimations are changed between 10% and 20%. In the case of $Sa(T_1)$ scaling method, at least 15 records are needed to predict median response with less than 10% error, whereas the proposed methodology requires 20 records in order to predict the median demand with the same level of precision. As expected, the error estimations of both methodologies tend to decrease with increasing number of ground motions (in the order of 30+). On the contrary, a suite of 7 or 11 records required by most seismic building codes for use in nonlinear response history analysis leads to unstable response and yields approximately 15% error in median estimations.
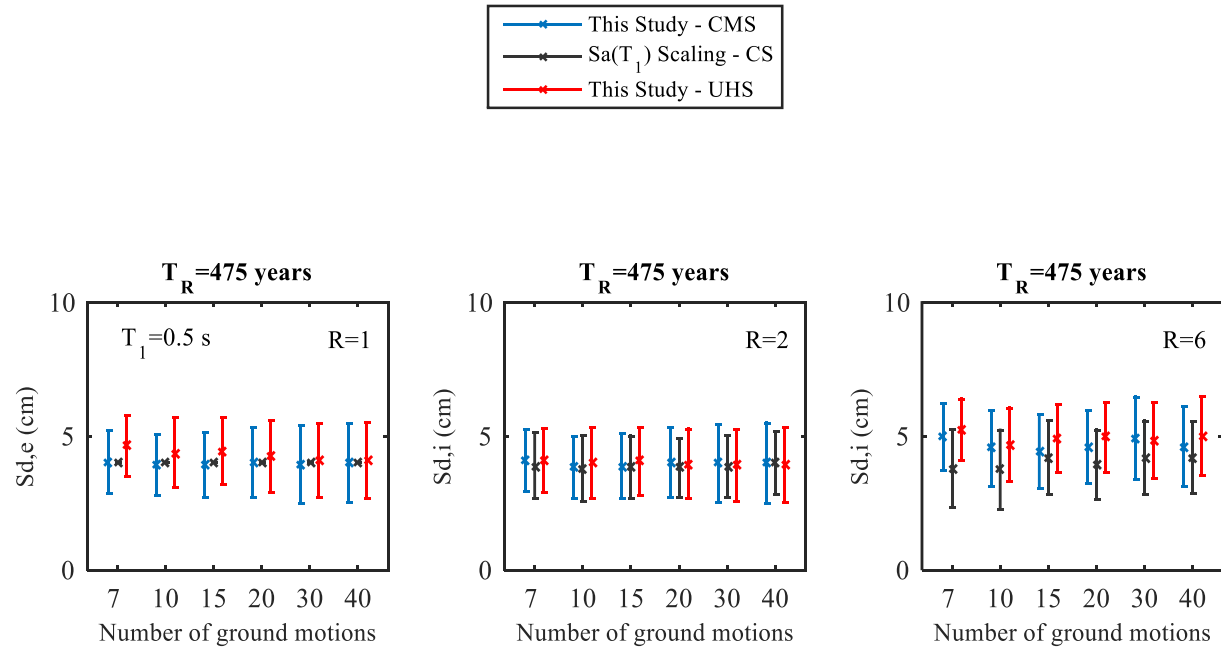
Figure 3.9. Elastic (Sd,e) and inelastic displacements (Sd,i) of this study (for target CMS and UHS), and the $Sa(T_1)$ scaling method (for target CS) together with their 16th and 84th percentiles (or median ± 1standard deviation) at the fundamental period of T_1=0.5s.
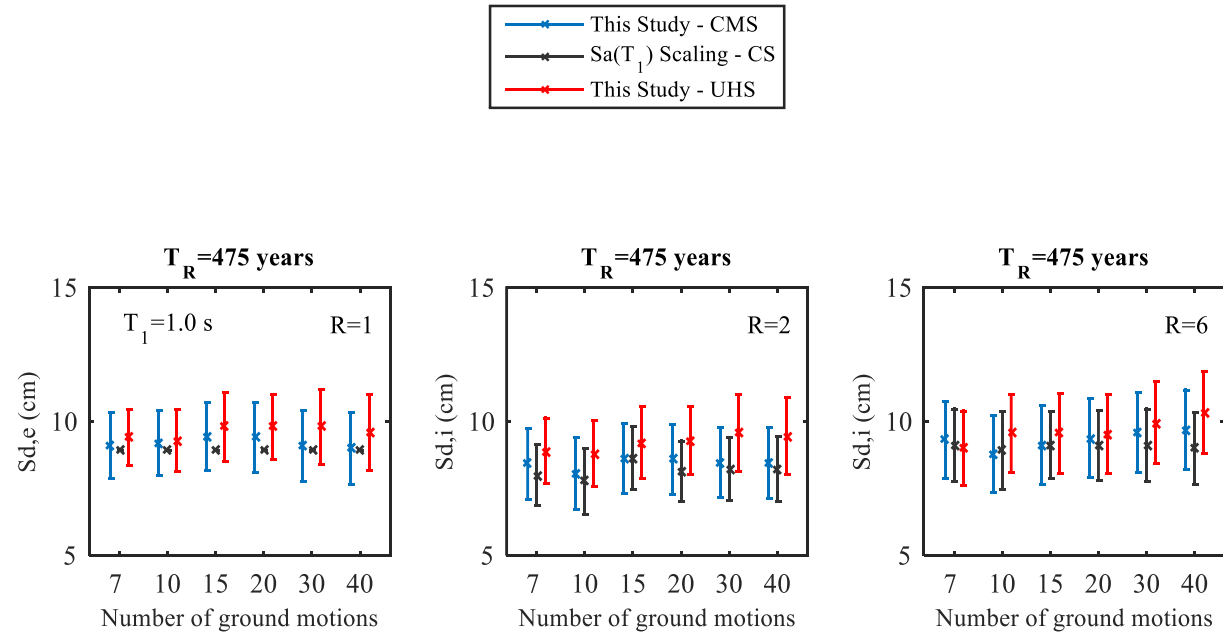
Figure 3.10. Elastic (Sd,e) and inelastic displacements (Sd,i) of this study (for target CMS and UHS), and the Sa(T_1) scaling method (for target CS) together with their 16th and 84th percentiles (or median ± 1standard deviation) at the fundamental period of T_1=1.0s.
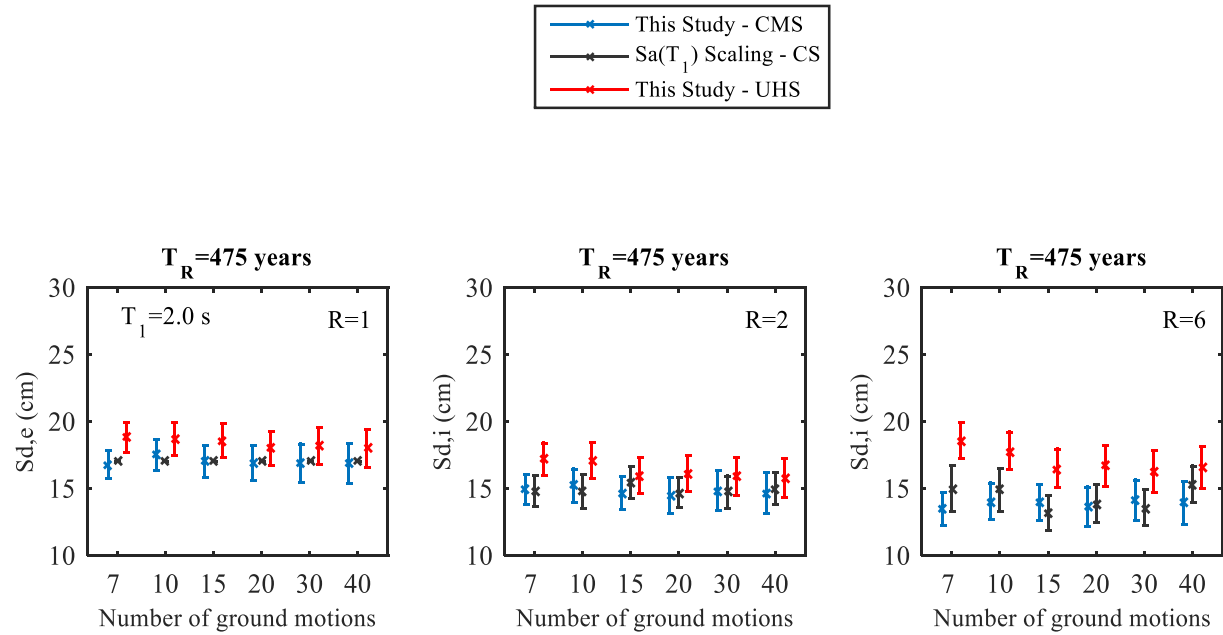
Figure 3.11. Elastic (Sd,e) and inelastic displacements (Sd,i) of this study (for target CMS and UHS), Sa(T_1) scaling method (for target CS) together with their 16th and 84th percentiles (or median ± 1standard deviation) at fundamental period of T_1=2.0s.
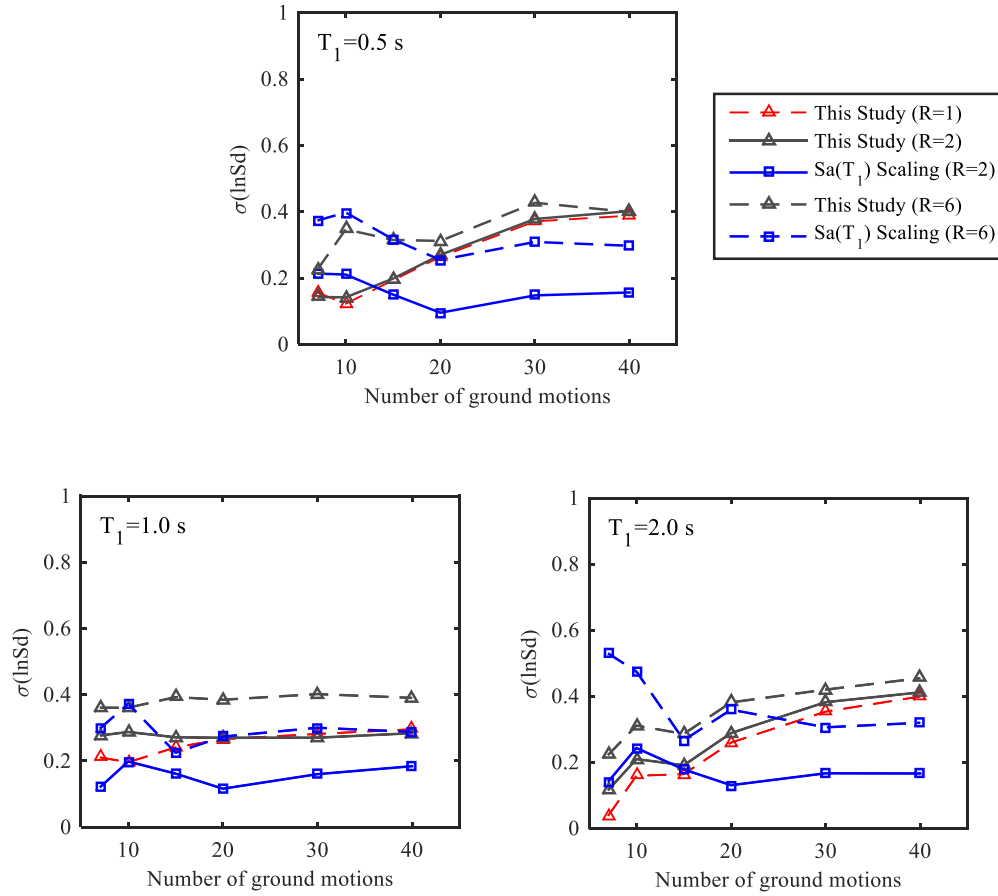
Figure 3.12. Comparisons of uncertainties in structural response of both methods as a function of number of ground motions at the fundamental periods of T_1=0.5, 1.0, and 2.0 seconds.

3.7. The Significance of the Difference between Two Means

The parametric hypothesis tests are performed in order to statistically quantify whether two different scaling methodologies produce same median structural responses. Note that Sa(T$_1$) scaling method is used as a benchmark to test the performance of the proposed method in predicting the unbiased median response. Note also that the biased estimate defined here as an estimate that does not agree with the expected response of the structure as obtained through the use of Sa(T$_1$) scaling method. Thus, the hypothesis that the proposed procedure produces same median estimations with the Sa(T$_1$) method. The Welch's t-test statistics can be employed to test the hypothesis that the means of the different samples are equal without making the assumption of the equal variances (Welch, 1947). If the mean of the two normally distributed random samples are assumed to be equal, the null hypothesis can be stated as $H_0 : \mu_1 = \mu_2$ or equivalently $H_0 = \mu_1 - \mu_2 = 0$. The two sample t-statistics can be generated using the in Equation 3.11.

$$t = \frac{\bar{X}_1 - \bar{X}_2}{\sqrt{\dfrac{s_1^2}{n_1} + \dfrac{s_2^2}{n_2}}}$$
(3.11)

Where $\bar{X}_i$, s_i^2, and n_i are the ith sample mean, sample variance and sample size, respectively. The t-statistics follows a t distribution with the estimated degree of freedoms (df):

$$df = \frac{\left(\dfrac{s_1^2}{n_1} + \dfrac{s_2^2}{n_2}\right)^2}{\dfrac{1}{n_1 - 1}\left(\dfrac{s_1^2}{n_1}\right)^2 + \dfrac{1}{n_2 - 1}\left(\dfrac{s_2^2}{n_2}\right)^2}$$
(3.12)

The null hypothesis is rejected when the observed value t falls in the critical region, or the p-value level is less than the predefined significance level (α). In this study, significance level is used as 0.05. The median inelastic displacements of each ground motion set at different periods and nonlinearity levels are compared across two scaling

methods. It should be noted that the proposed and the $Sa(T_1)$ scaling procedures match the ground motions based on target CMS and CS, respectively. Table 3.5 lists the hypothesis test results where the rejection cases in statistical test results (or the p-values lower than 0.05 significance level) are highlighted in bold. In the majority of cases, no significant differences are observed between the median responses of both scaling methodologies. These results indicate that the ground motions selected by the proposed methodology do not produce biased estimate in the central tendency of the structural response. However, the structural responses obtained from a suite of 40 ground motions are significantly different (i.e., rejection of H_0) for both short (T_1=0.5s) and mid-period (T_1=1.0s) systems, at high-inelasticity level. It is observed that the ground motions having large spectral amplitudes at target T_1 (i.e., due to spectral variability) impose higher demand than those of CS-based matched records, and lead to conservative bias and large scatter in seismic demand.

Furthermore, the structural response may be affected by the other characteristics of the ground motions such as magnitude (M_w) and source-to-site distance (R_{jb}). These seismological properties have an impact on the frequency content (or spectral shape) of a ground motion, and thus affect the structural response. It has been shown that when the ground motions are scaled to a common $Sa(T_1)$, the structural response becomes independent of magnitude and distance values (i.e., sufficiency of IM). Some researchers found that (Ruiz-Garcia and Miranda, 2005; Baker and Cornell, 2005) the source-to-site distance is statistically insignificant in structural response, while the earthquake magnitude can be significant, especially for short period of vibration. To examine the relationship between the structural response and the seismological parameters (M_w and R_{jb}), a standard linear regression of the natural logarithm of the inelastic displacements with the ground motion parameter of interest is employed. The regression model has the form $\ln EDP = \beta_0 + \beta x$, where EDP the engineering is demand parameter (i.e., inelastic displacements) and x corresponds to one of the selected seismological parameters (M_w and R_{jb}). In the regression model, β_0 and β represent the intercept parameter and the slope, respectively. A hypothesis test is conducted whether there is sufficient evidence that the slope of the regression line is different from zero. The null hypothesis states that the slope

β is equal to zero. If the p-value is less than the certain significance level (e.g., 5%), then the null hypothesis will be rejected.

Table 3.5. Welch test results (p-values) for comparing the median estimations of two scaling methods. The p-values lower than 0.05 significance level are highlighted in bold.

Nonlinearity level	R=2 (mildly-inelastic)						R=6 (highly-inelastic)					
Number of records	7	10	15	20	30	40	7	10	15	20	30	40
T_1=0.5s	0.08	0.89	0.67	0.41	0.69	0.79	0.06	0.23	0.65	0.10	0.10	**0.02**
T_1=1.0s	0.64	0.74	0.98	0.41	0.59	0.62	0.91	0.93	0.99	0.41	0.25	**0.03**
T_1=2.0s	0.77	0.78	0.44	0.88	0.91	0.09	0.63	0.75	0.59	0.88	0.69	0.29

Figure 3.13a and Figure 3.13b illustrate the dependency of the inelastic displacements (lnEDP) at the period of T=0.5s (i.e., rejection case) on magnitude (M_w) and distance (R_{jb}), respectively. Recall that the ground motions are selected over a magnitude and distance range of M_w (6.7-7.7), R_{jb} (10-100km), respectively, for the target scenario event which is characterized by values of M_w=7.13 and R_{jb}=27km. It is seen that no trend (i.e., zero slope) exists between the structural response and the magnitude, while there is a statistically significant negative correlation (ρ) between lnEDP and R_{jb} (p-value $\ll$ 0.0). It is interesting to note that the distance has a statistically significant effect in structural response estimate. The slope of the trend line gives some information about the distance bound that may be considered for the ground motion selection. As seen in Figure 3.11b, the ground motions at large distances (R_{jb}>50 km) produce lower structural responses, while the records within the 10-15km provide larger responses than the median. Therefore, using excessively wide bounds on distance parameter may yield inappropriate ground motions that misrepresent the required characteristics of the target rupture scenario.
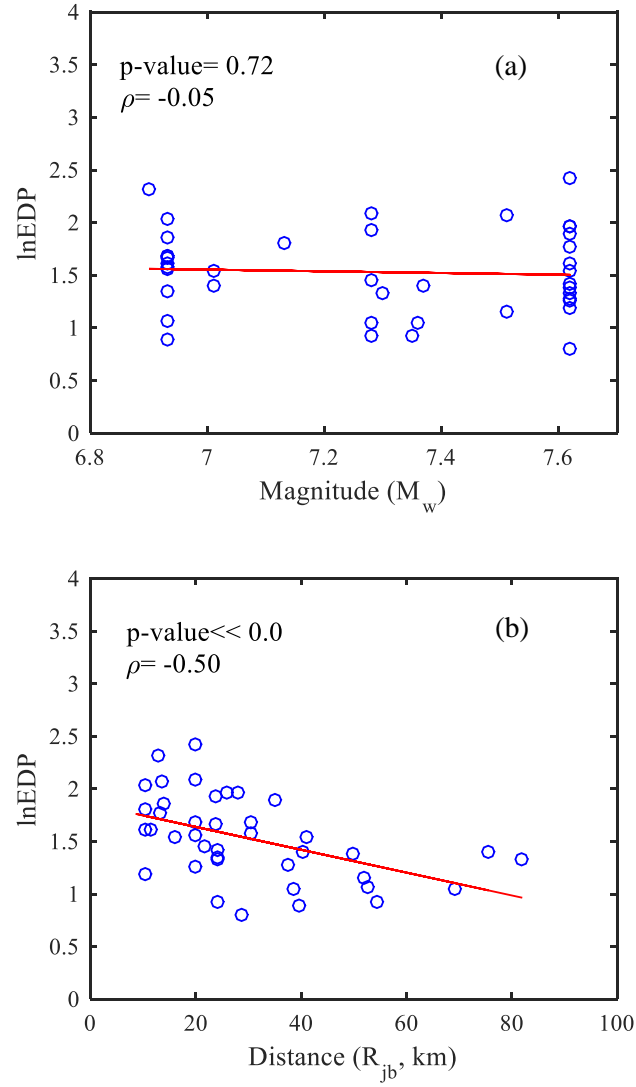
Figure 3.13. Dependency of the inelastic displacements (lnEDP) on (a) magnitude (M_w), and (b) distance (R_{jb}).

3.8. Estimation of the Structural Response for Period Interval

It is important to note that the structural response is not always dominated by the first-mode period of the structure due to the higher mode effects or the possible period elongation under earthquake loading. If the multiple periods are expected to contribute to the structural response, UHS should be used as a target spectrum. It is pointed out that the Conditional Spectrum concept has some limitations in predicting the structural response parameters when the response is dominated by the multiple modes. Moreover, questions remain regarding the identification of the single conditioning period before the structural design is finalized (Lin *et al.*, 2013). The UHS is widely adopted as target spectrum to define the seismic actions on the structures. The ground motions are selected to match this target spectrum over a period range of interest (e.g, $0.2T_1$-$2T_1$) in order to account for the variations in the structural period. The proposed procedure scales the ground motions to match target spectrum (UHS) over the period range $[0.2T_1$-$2T_1]$ that offers flexibility to estimate the structural response parameters of interest at periods other than the fundamental one.

This section illustrates the elastic and inelastic displacements of the SDOF system (T_1=0.5s) obtained from a suite of 10, 20, and 40 ground motions that are selected to match UHS. Figure 3.14 shows the elastic (R=1), the mildly-inelastic (R=2) and the highly-inelastic (R=6) structural responses together with their dispersion estimations. The analysis results are presented for the period interval of $[T_1$-$2T_1]$ as the higher modes do not contribute to the response of the SDOF systems. It is noted that the consideration of the spectral variability at target level provides benefits to implicitly account for the spectral shape at periods other than the fundamental one. In this scaling scheme, the distribution of the structural response becomes less sensitive to variation of the spectral ordinates away from the fundamental period. As seen in Figure 3.14, the proposed procedure preserves approximately uniform elastic spectral variability along the specified period interval that produces relatively constant level of uncertainty in the structural response. It is demonstrated that the variability in structural response increases as the nonlinearity increases. The results indicate that using a minimum of 20 ground motions produce stable median response with less than 10% error for the given cases.
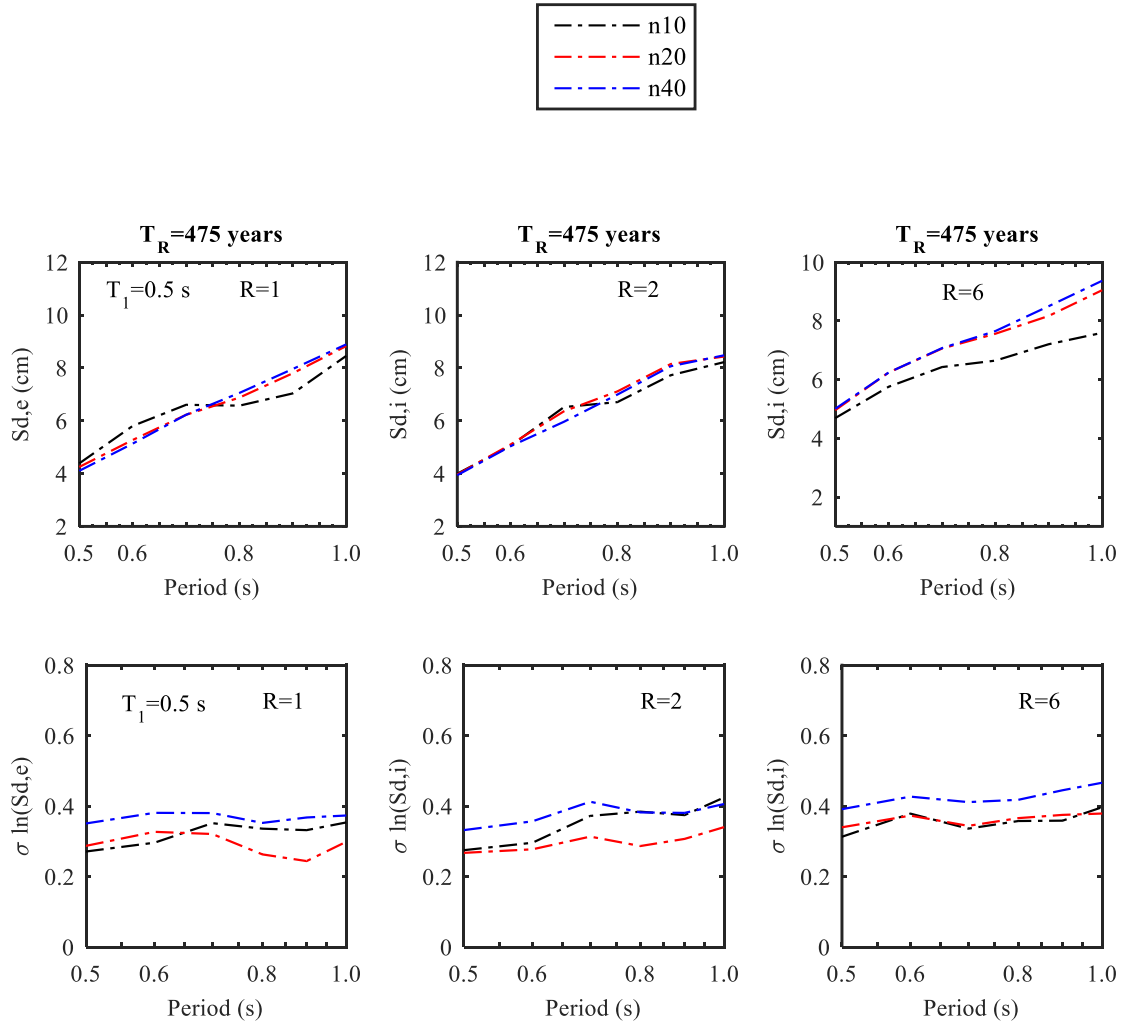
Figure 3.14. Median and dispersion statistics of the spectral displacements of SDOF system (T_1=0.5s) for the period interval of [T_1-2T_1]. n10, n20, and n40 represent a suite of 10, 20 and 40 ground motions, respectively.

4. SEISMIC DEMAND ESTIMATION OF A REINFORCED CONCRETE MOMENT FRAME BUILDING

4.1. Introduction

Within the context of performance based seismic assessment and design, one of the major tasks is the estimation of the probabilistic structural response due to future earthquakes at the given site. The accurate estimation of the seismic demand is the critical component in performance based earthquake engineering that directly affects the outcome of the earthquake risk and loss models. The two main challenges in predicting the seismic performance of the structure are understanding the sources of uncertainties due to ground motion characteristics and utilizing an appropriate approach for ground motion selection and scaling. In the previous chapter, a ground motion selection and scaling procedure is presented that addresses the uncertainty in spectral demand by preserving dispersion within ground motion suite. In this chapter, nonlinear dynamic analyses are conducted to estimate the seismic demand of a reinforced concrete building structure at specified seismic hazard levels. The reinforced concrete building having twelve stories and three bays is considered as a case study structure. The seismic response of the 12-story reinforced concrete frame structure is investigated by using the different ground motion selection and scaling approaches. The comparative studies are performed to examine how the probability distributions of engineering demand parameters (i.e., maximum interstory drift ratio, peak floor displacement, peak floor acceleration) are affected by different ground motion selection and scaling methodologies. This chapter begins with the general description of the building model, and then presents the details of the analytical modeling approach utilized in this study. The seismic performance of the model building is evaluated using different ground motion selection and scaling approaches at the end of this chapter.

4.2. Description of the Building

To evaluate the seismic performance of the moment resisting frame, a case study building is chosen that is assumed to be located in a high seismicity region in the city of İstanbul, Turkey. The twelve story reinforced concrete (RC) building represents the medium-rise residential construction which is designed according to Design Basis Earthquake level (i.e., 10% exceedance in 50 years) for the given site. The building is assumed to be located at a site in Zone I with Z3 (corresponding to very dense soil and soft rock with 400m/s<Vs_{30}<700m/s,) site classification. It is designed according to the governing provisions of the Turkish Earthquake Code (TEC, 2007), and the Turkish standards; TS 500-2000 (Turkish Standards Institute, 2000), TS 498 (Turkish Standards Institute, 1997) for high ductility level (R=8). The PROBINA Orion software (Prota, 2013) is used for the design of the building. The concrete and reinforcing steel for design are selected as C25 (concrete strength of 25MPa) and S420 (steel yield strength of 420 MPa), respectively. The columns dimensions are 60cm x 60cm for the first six stories and 50cm x 50cm in the other stories. The member dimensions of beams are 40cm x 60cm for the first six stories, 40cm x 50cm for the next four stories, and 40cm x 40cm in the last two stories. The building satisfies all the relevant capacity design and detailing requirements of the seismic code provisions (TEC, 2007). Figure 4.1 shows the elevation view of the three bay moment resisting frame structure. The first story building height is 4 m and the story heights of upper floors are 3 m. The building height is 37 m. The analytical modeling of the 2D frame structure will be discussed in subsequent sections.
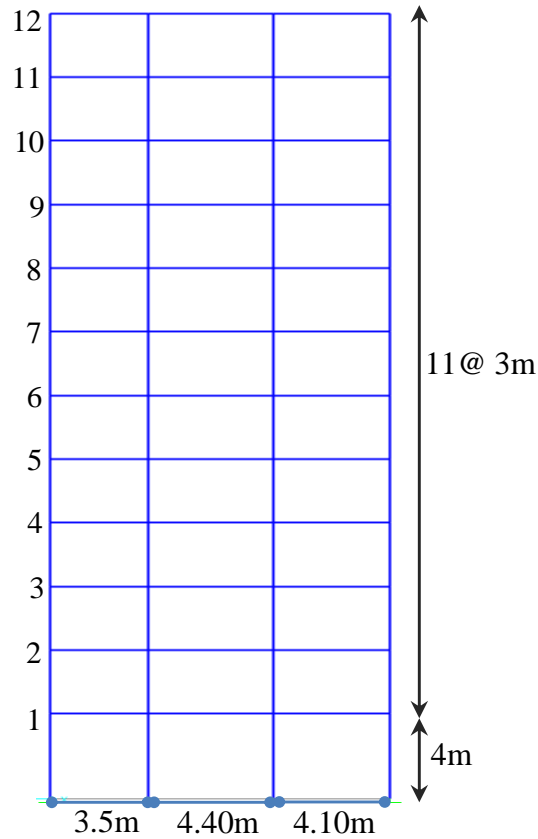
Figure 4.1. Elevation view of the 12-story reinforced concrete building frame model.

4.3. Analytical Modeling of the 12-Story RC Frame Structure

Despite its complexity, nonlinear dynamic analysis is the most rigorous approach to predict the inelastic behavior of structures due to ground shaking. To capture the nonlinear structural behavior properly an accurate analytical model should be developed. This can be achieved by understanding the sources of nonlinearities at various model levels (e.g., material, element-component) and applying rational analytical modeling assumptions. To characterize the nonlinear building behavior, the two-dimensional frame structure is modeled by using the PERFORM 3D (CSI, 2014) analysis program. PERFORM 3D is an enhanced nonlinear software for seismic analysis and performance based design. The response history analyses are performed in uniaxial direction for the 2D frame structure. The foundation flexibility due to soil-structure interaction is not considered in this study. Thus, the analytical model assumes fixed supports at the building foundation level and disregards soil-structure interaction. The RC frame model has a fundamental period of $T_1 =$

1.53s. The second and third mode periods are 0.55s and 0.30s, respectively. The eigenvalue analysis indicates that the first mode modal mass participation factor is 79% so that the system can be considered as first-mode dominant structure with noticeable level of higher-mode contributions. The effective modal mass percentages of the second and third modes are 14% and 3%, respectively. The following sections present the details of the analytical modeling assumptions of the model building.

4.3.1. Details of the Analytical Modeling Approach

The nonlinear model of the structure is developed using the deformation capacities and force-deformation relationships in PERFORM 3D. In general, the inelastic beam and column elements can be modeled in three ways: (1) lumped-plasticity beam-column elements (i.e., the linear elastic elements are connected at a point and the infinitesimal region around it by nonlinear springs and plastic hinge models) (2) fiber beam-column elements on a member cross section, (3) fiber (or distributed plasticity) throughout the member's length. Fiber section modeling provides significant advantages over lumped plasticity beam-column models. This model subdivides a cross-section into discretized fibers with a finite area and uniaxial force-deformation relationship of the material associated with the fiber. Unlike lumped-plasticity elements, fiber elements implicitly account for both neutral axis migration during lateral loading and the effect of axial load variation on element stiffness and strength. In other words, fiber section modeling is capable of representing the flexural behavior and its interaction with the axial force in beam-column elements. Disadvantages associated with fiber elements include increased detailed modeling and computation time compared to lumped-plasticity element modeling. Moreover, fiber strain values are highly sensitive to the selection of fiber sizes as well as the specified material stress-strain relationship. The lumped plasticity elements (or plastic hinges), on the other hand, are widely used because of its simplicity and less computational burden. For the beam-column element model, middle section is defined as linear elastic segment in which the plastic zones are located at both ends of the element. The nonlinear behavior is assumed to be concentrated at the center of plastic zone. Plastic hinge behavior can be represented by a moment-curvature relationship, moment-rotation relationship or

axial load-bending moment interaction. Generally, these relationships can be idealized as bilinearized functions with or without strain hardening.

In this study, the nonlinear behavior of beam members is represented by adopting the trilinear moment-curvature type hinge as they mainly suffer from flexural deformation. Figure 4.2 shows the trilinear moment-curvature hysteretic curve which typically defines the moment-deformation relationship with points Y, U, L and R to capture the main aspects of the behavior, namely the initial stiffness, strain hardening, ultimate strength and strength loss. Note that the curvature hinge requires a moment–curvature relationship and a tributary hinge length. The tributary length is mainly used to convert the moment-curvature relationship to an equivalent moment-rotation relationship (PERFORM 3D, 2006). The moment curvature analyses are performed by the section designer program XTRACT (Chadwell and Imbsen, 2002). The parameters of the moment curvature curve of the member are generated using cross-section properties, nonlinear material models and reinforcement details. For the column elements, the fiber model is employed in the elasto-plastic part of the members (i.e., specified hinge length) to account for the moment and axial force interaction. The remaining part (middle section between the plastic ends) of the member is described as elastic. In the fiber model, the force-deformation relationship at the cross-section level is derived according to the constitutive law of the constituent material. For RC members, three material models are defined: (1) unconfined concrete for the concrete cover, (2) confined concrete for concrete core, (3) steel material for longitudinal reinforcement bars. The stress-strain curve parameters of the materials are determined based on the governing provisions of the Turkish Earthquake Code (TEC, 2007). Note that the code provisions adopt the Mander concrete model (Mander *et al.*, 1988) to evaluate the stress-strain relationship of unconfined and confined concrete members. The reinforcement steel is modeled with a stress-strain relationship that exhibits an initial linear elastic portion, a yield plateau and a strain hardening branch. Figure 4.3 illustrates the representative element segments of the column member that are defined by fiber-cross sections. The layout of a fiber arrays is also shown in the same figure.
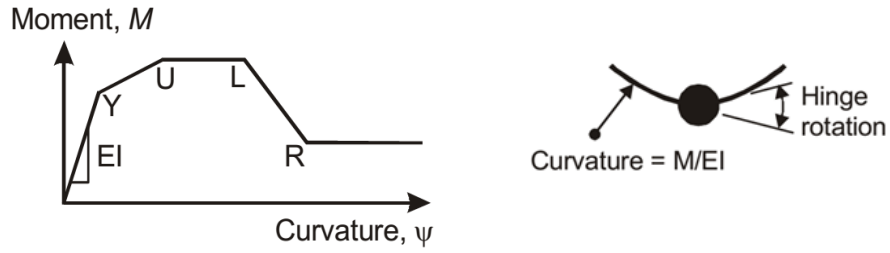
Figure 4.2. Moment-Curvature relationship of the inelastic beam and the equivalent hinge component (PERFORM 3D, 2006).
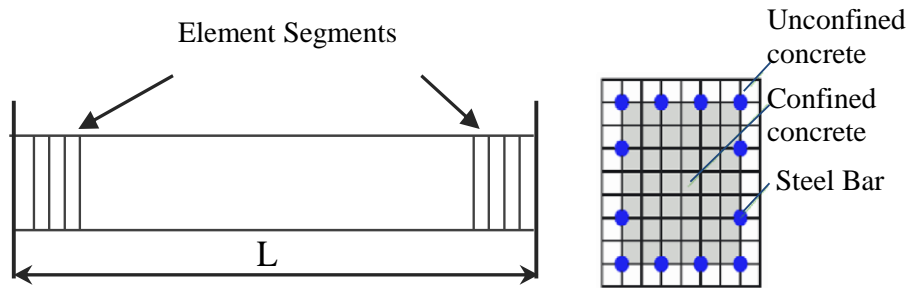
Figure 4.3. Element segments of a column member defined by fiber cross sections and the layout of fiber arrays.

4.3.2. Nonlinear Static Pushover Analysis

Nonlinear static (pushover) analysis is carried out to simulate the inelastic response of the structure under monotonically increasing lateral loads. According to code provisions (FEMA-356, 2000; Eurocode 8, (CEN, 2003)) the structure is subjected to monotonically increasing lateral forces with an invariant height-wise distribution until a prespecified target displacement is reached. In this study, the pushover analyses are performed using the first-mode proportional lateral load. Note that the detailed information about the commonly employed nonlinear static procedures can be found in Pinho *et al.* (2013). The lateral force at any story is calculated using Equation (4.1).

$$F_i = V_1 \left(\frac{w_j \phi_{i1}}{\sum_{j=1}^{n} w_j \phi_{j1}} \right) \tag{4.1}$$

where F_i is the lateral force at level i; V_1 is the first-mode base shear; w_j is lumped seismic weight at j^{th} level; and ϕ_{j1} is amplitude of the first mode at the jth level. The lateral loads are increased incrementally and the resulting base shear versus roof displacement of the structure is obtained. The ultimate base shear is divided by the total weight of the building to obtain the corresponding base shear coefficient and the roof displacements are normalized to estimate the roof drift ratio. Figure 4.4a illustrates response of the nonlinear static analysis (pushover) for the 12-story RC frame model building. It should be noted that the analyses are performed with the consideration of P-Delta effects in the structural model. A comparison is made between the structural responses with and without inclusion of the P-Delta effects. The pushover curve with P-Delta effect shows a pronounced loss in lateral strength for roof drift ratios greater than 1.5%. However, disregarding the P-Delta effects results in a positive post yield slope that may lead to deceptive results in nonlinear structural response. The distribution of story drift ratios at roof drift ratio of 2.5% is shown in Figure 4.4b. It is seen that the maximum story drift ratio reaches to approximately 4.5 % at the bottom stories for the 12-story model building.

(a)   (b)
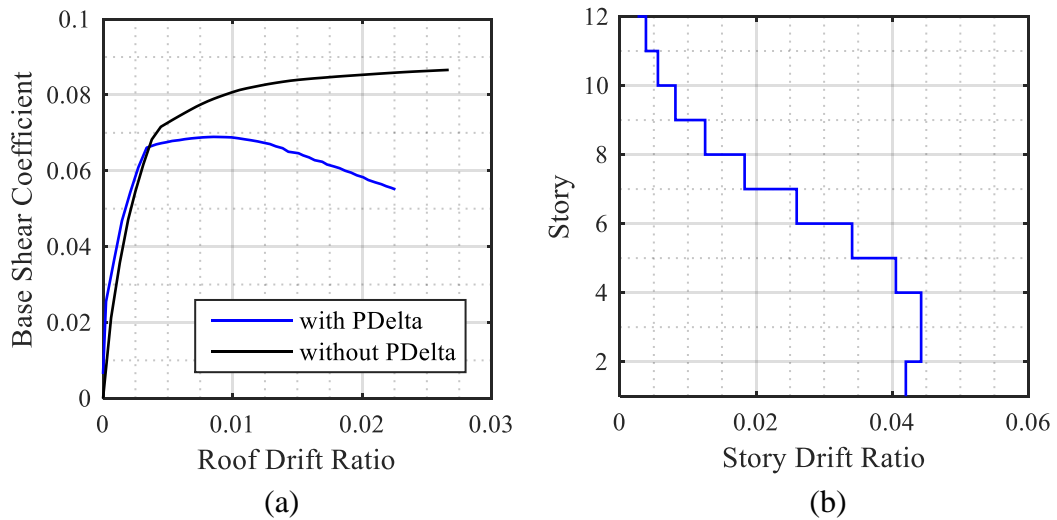
Figure 4.4. (a) Pushover curves of the model building with and without inclusion of the P-Delta effects, and (b) story drift ratios at a roof drift ratio of 0.025.

4.4. Seismic Demand Estimations

4.4.1. Site Hazard Characterization and Ground Motion Selection

To assess the seismic demand of the 12-story RC moment frame structure in terms of probability distributions of the structural response parameters, the ground motions are selected and scaled to match the target spectrum for different seismic hazard levels. To this end, the site-specific probabilistic seismic hazard analyses (PSHA) are performed for the selected intensity measure $Sa(T_1=1.5s)$ at three different seismic hazard levels. The target spectral amplitudes of the ground motions represent an earthquake with 20, 10 and 2% probability of exceedance in 50 years that correspond to the return periods of 225, 475, and 2475 years. The target earthquake scenario parameters are then determined from disaggregation of PSHA. The soil condition at the target site is considered as soft rock with $Vs_{30}= 450$ m/s (consistent with Z3 site class). The target moment magnitude (M_w), source-to-site distance (R_{jb}), epsilon values (ε) based on disaggregation results at each spectral amplitude (or specified exceedance rates) are listed in Table 4.1. The target spectral amplitudes of each hazard level are also given in the same table. The disaggregation results reveal that the hazard is mostly dominated by approximately the same magnitude-distance pair at the site of interest, the epsilon values, on the other hand, increase as the intensity level increases.

The ground motion database is first constrained based on parameters that represent the seismological properties (M_w, R_{jb}, and Vs_{30}) of the target earthquake scenario. The ground motions are initially selected from a bin with magnitude (M_w) bounds of ±0.5. Records with R_{jb} in the 10-100km range are utilized, so records that exhibit near fault characteristics (e.g., pulse, fling) are removed from the ground motion library. The site classes of the candidate records are selected based on wide range of Vs_{30} parameter (i.e., 180 m/s to 760 m/s). These constraints are utilized to remove records that should not be considered as candidates in the second stage of the ground motion selection. As noted previously, the final set of candidate records is selected based on spectral shape criteria by the proposed methodology. For each hazard level, a suite of 20 ground motion pairs selected and scaled to match the target spectrum. In order to assess the effect of different

scaling approaches on seismic demand predictions, the ground motions are also scaled using the $Sa(T_1)$ scaling method. Note that the proposed method select and scale ground motions such that response spectrum of the scaled median closely matches the target CMS. In the case of $Sa(T_1)$ scaling method, the ground motions are selected to match CS that represent the conditional mean and conditional standard deviation of the spectral acceleration along the period interval.

Table 4.1. Target earthquake scenario parameters (M_w, R_{jb}, ε) and corresponding target spectral ordinates at selected return periods.

Return Periods (T_R), [years]	Magnitude (M_w)	Distance (R_{jb}), [km]	Epsilon (ε)	$Sa_{target}(T_1)$, [g]
225	7.15	30	1.3	0.19
475	7.15	30	1.41	0.26
2475	7.22	25	2.19	0.40

4.4.2. Scale Factors Obtained from Different Ground Motion Selection and Scaling Approaches

Figure 4.5 and Figure 4.6 illustrate the scale factors for ground motions that are obtained from the proposed procedure and the $Sa(T_1)$ scaling method, respectively. Note that the seismic demand of the model building is assessed at three hazard levels (i.e., T_R= 225, 475, and 2475 years), however, as will be demonstrated in Chapter 5, the derivation of fragility curve is performed for a range of return periods (T_R) between 225 years and 10,000 years (corresponds to T_R= 225, 475, 975, 2475, 4975, and 10,000 years). Therefore, all scale factors are given here for the sake of completeness. As mentioned previously, in the case of the proposed procedure ground motions are scaled by a constant factor so that they are compatible with the target spectrum. The $Sa(T_1)$ scaling approach, on the other hand, modifies the ground motions individually to ensure that the ground motions are anchored to the same target level at the fundamental period of the structure.

As seen in Figure 4.5, the constant scale factors obtained from the proposed method are plotted with respect to the specified return periods in which the amplitudes of the scale factors vary in the range of 1.02-2.31. As noted before, it is desirable that the ground motions would have a scale factor closer to unity because it indicates that the small modifications are applied to the intensity of the record, and thus the characteristics of the original ground motion (in terms of frequency and duration) are well retained (Lamprey, 2007). Moreover, it is noteworthy that the excessive scaling may induce biased structural response particularly at high-intensity levels. Figure 4.6 depicts the cumulative distributions of the scale factors for the $Sa(T_1)$ scaling method. It is observed that more than 60% of the selected records have amplitude in the range of 0.3-3.0, which is recommended as scaling limits in some seismic design provisions (ASCE/SEI7-10, 2010; NZS1170.5, 2004). As seen in the figure, the amplitudes of the scale factors are increased with increasing hazard levels, particularly for return periods greater than 2475 years.
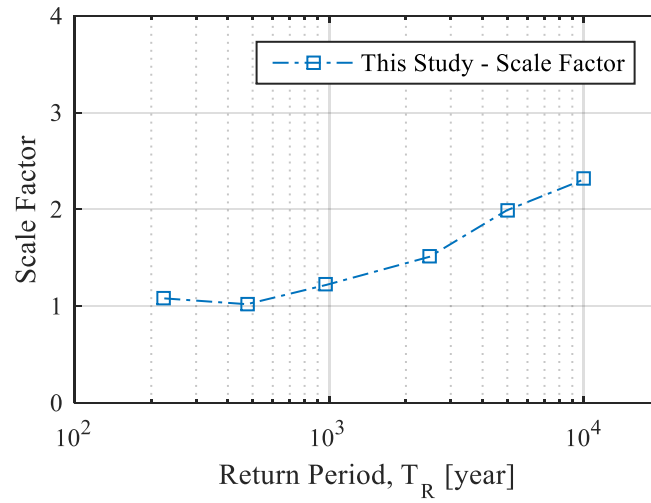
Figure 4.5. Scale factors that are obtained from the proposed ground motion selection and scaling approach at six different hazard levels.
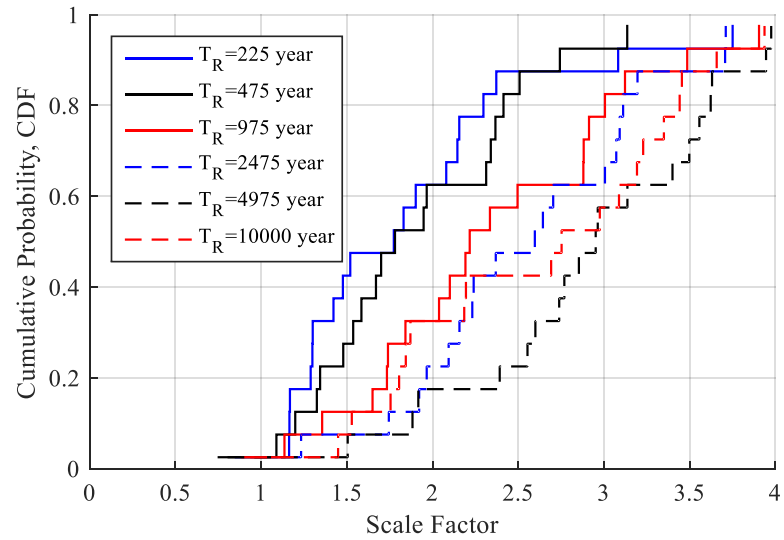
Figure 4.6. The cumulative distribution functions of the scale factors that are obtained from the $Sa(T_1)$ scaling method at six different hazard levels.

4.4.3. Ground Motion Selection and Scaling for Specified Hazard Levels

Nonlinear dynamic analyses are conducted by using a suite of 20 earthquake records that are selected and scaled to match the target spectra for the specified return periods using different ground motion selection and scaling approaches. The ground motions represent the 20/50, 10/50, and 2/50 hazard levels that correspond to the return periods of 225, 475, and 2475 years. Figure 4.7 and Figure 4.8 illustrate the response spectra of the ground motions that are selected and scaled to match the Conditional Mean Spectrum (CMS) using the proposed method for 475 and 2475 years hazard levels, respectively. Also shown on that plot are the median, 16th and 84th percentiles of the scaled ground motions. Figure 4.9 and Figure 4.10 show the response spectra of the ground motions that are selected and scaled based on the Conditional Spectrum (i.e., $Sa(T_1)$ scaling method) for 475 and 2475 years hazard levels, respectively. As seen from these figures, the median record spectra reasonably match the target CMS at the period interval of $[0.2T_1-2T_1]$ for both methods. In the case of the $Sa(T_1)$ scaling method, the ground motions are pinched at the target spectral demand, while the proposed method preserves the elastic spectral variability at that period. Figure 4.11a and Figure 4.11b present the logarithmic standard deviation of the elastic spectral accelerations of the records that are scaled to match the target spectra at 475 and 2475 years hazard levels, respectively. It is clearly seen that the standard deviation of the elastic record spectra obtained from both methods show different trend along the period interval. Note that the approximately uniform dispersion obtained from the proposed method reflects the natural variability of the unscaled ground motions, while the logarithmic standard deviation of the ground motions obtained from the $Sa(T_1)$ scaling method follows the target variance of the CMS (i.e., CS). Thus, two methods differ in the manner in which they define the uncertainty about the target median spectrum.
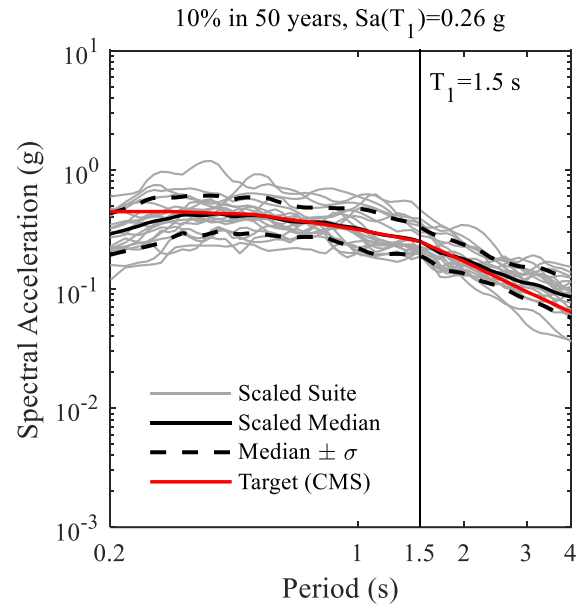
Figure 4.7. Response spectra of the ground motions that are scaled to match target spectrum (CMS) using the proposed method for the return period of T_R=475 years.
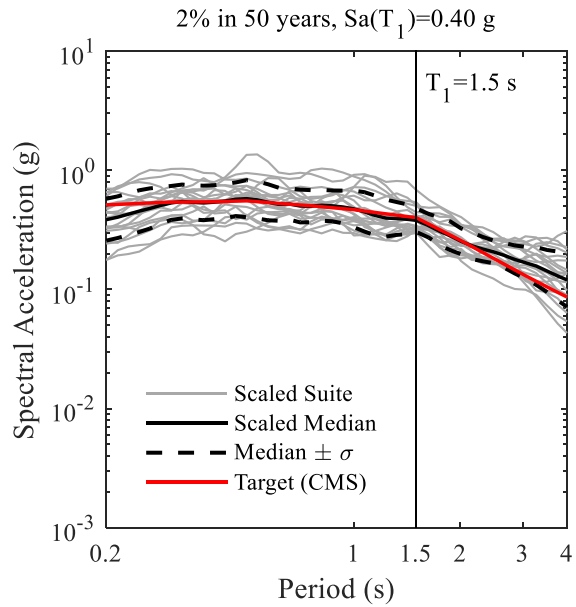
Figure 4.8. Response spectra of the ground motions that are scaled to match target spectra (CMS) using the proposed method for the return period of TR=2475 years.
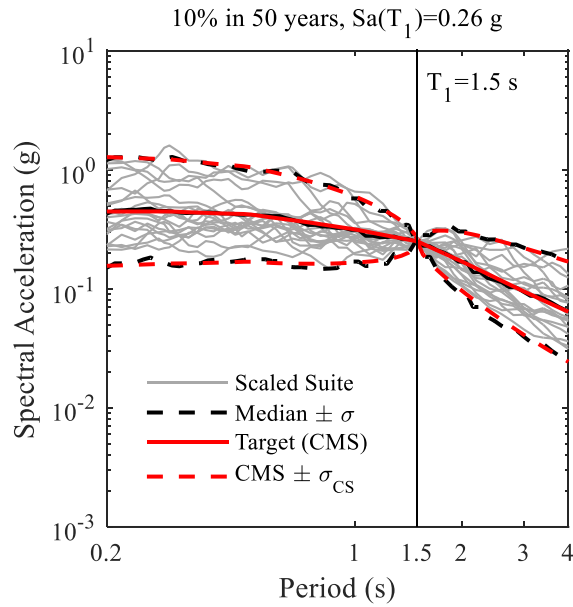
Figure 4.9. Response spectra of the ground motions that are scaled to match target spectra (CS) using the $Sa(T_1)$ scaling method for the return period of T_R=475 years.
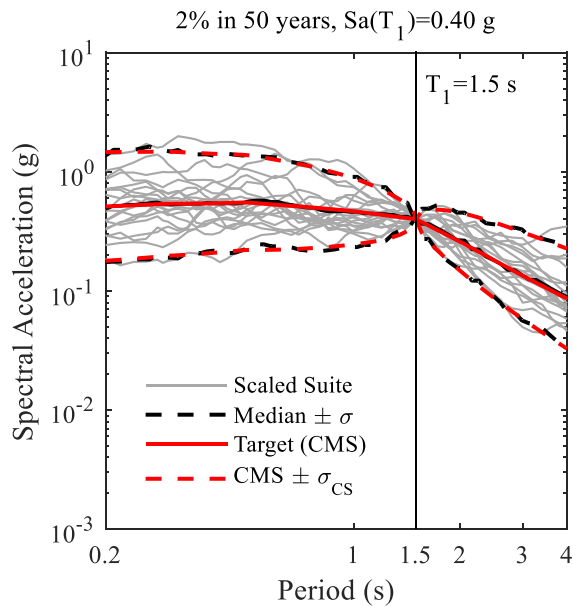
Figure 4.10. Response spectra of the ground motions that are scaled to match target spectra (CS) using the Sa(T1) scaling method for the return period of TR=2475 years.
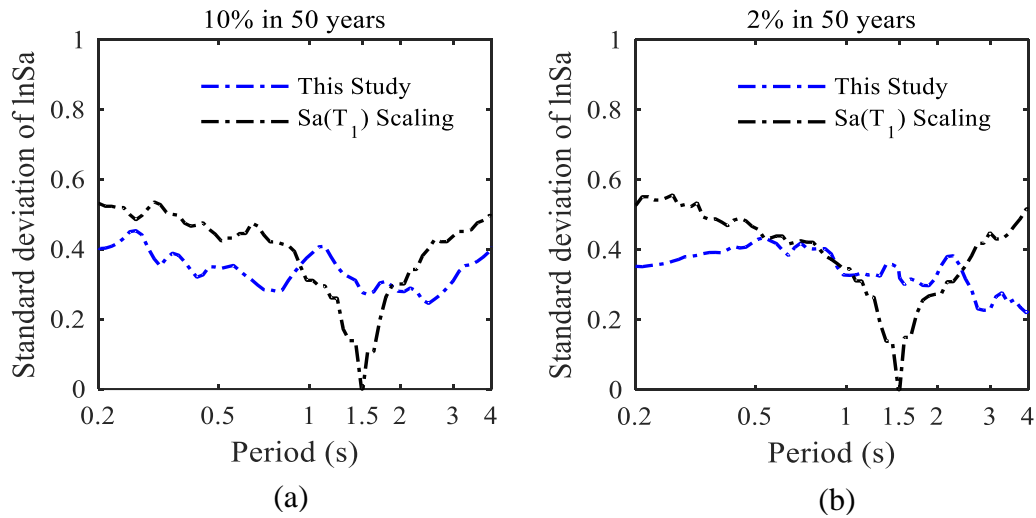
Figure 4.11. Comparisons of logarithmic standard deviations of the ground motions that are scaled by this study and the Sa(T1) scaling method for an earthquake with (a) 10%, and (b) 2% probability exceedance in 50 years.

4.4.4. Engineering Demand Parameters

This study adopts the maximum interstory drift ratio (MIDR) as a primary structural response parameter (or engineering demand parameter). Note that MIDR is widely utilized for design and performance assessment of structures. It can be defined as the relative lateral displacement between two consecutive floors normalized by the story height. It is closely related to plastic rotations and both global and local story collapse (Vamvatsikos and Cornell, 2002).

The other demand measures such as peak floor displacements and peak floor accelerations are also investigated. Peak floor displacement (PFD) relative to the base of the structure is typically used as a global damage measure for drift-sensitive structural and nonstructural elements. The peak floor acceleration (PFA), on the other hand, is used for the design and performance assessment of acceleration-sensitive nonstructural members that can be defined as the maximum absolute value of the acceleration history at each floor level where the peak ground acceleration is used at the ground level.

4.4.5. Heightwise Distribution of the Engineering Demand Parameters

This section compares the heightwise distribution patterns of the demand parameters such as interstory drift ratios, peak floor displacements and peak floor accelerations that are obtained by both scaling methods. The structural response parameters of the code-compliant building are evaluated by using the median and the logarithmic standard deviations (denoted here as dispersion) of the structural responses at three specified hazard levels. The left panel shows the results of this study and the right panel shows the $Sa(T_1)$ scaling method. Moreover, the correlations between the spectral accelerations and structural responses at each story of the building are computed for three different hazard levels so as to identify the sensitivity of the engineering demand parameters (EDPs) to the spectral acceleration values (IMs) at the specified the period interval (i.e., $0.2T_1$-$2T_1$). Note that the degree of the linear relationship between $\ln(IM)$ and $\ln(EDP)$ is measured by using the Pearson correlation coefficient (ρ). To evaluate the extent to which two variables covary, the following equation is used:

$$\rho = \frac{Cov(\ln(IM), \ln(EDP))}{\sigma_{\ln(IM)} . \sigma_{\ln(EDP)}} = \frac{E[(\ln(IM) - \mu_{\ln(IM)}).(\ln(EDP) - \mu_{\ln(EDP)})]}{\sigma_{\ln(IM)} . \sigma_{\ln(EDP)}} \qquad (4.2)$$

where $Cov(\ln(IM), \ln(EDP))$ refers to the covariance between random variable $\ln(IM)$ and $\ln(EDP)$; $E[\ln(IM)]$ refers to the expectation of random variable $\ln(IM)$; $\mu_{\ln(IM)}$ and $\sigma_{\ln(IM)}$ are the mean and standard deviation of random variable $\ln(IM)$. Note that if ρ is close to 1.0, it means the two variables correlate well and within a positive linear relationship, whereas 0.0 and -1.0 indicates no correlation and perfect negative correlation, respectively. The influence of the frequency content of earthquake ground motions on structural response is presented by the correlation coefficient contour plots. These plots make it easy to identify the higher mode effects and period elongation of the structure as well as to understand the differences between the ground motion suits obtained from two different scaling methodologies. Note that the correlation coefficients are computed at each story level over the height of the building.

Figure 4.12 shows the interstory drift ratio (IDR) profiles obtained from both scaling methodologies at three hazard levels. It is seen that the median demand values tend to increase with increasing intensity of earthquake shaking. Both scaling procedures provide fairly similar median responses at each hazard level. The IDR profile shows that the distribution of the drift demand is mostly concentrated at the bottom stories of the building. The largest responses of the structure are generally located around the 3rd or 4th story levels. For the 20/50 ground motion level, the maximum median drift is approximately predicted as 0.5% and the comparable dispersion statistics (in the order of 0.2) are obtained from both scaling methodologies. It is observed that the ground motion set selected by the proposed method results in slightly higher dispersion in the structural response than those of the $Sa(T_1)$ scaling method, because the proposed scaling procedure considers the spectral variation about the target median.

Since the structure is first-mode dominated, it is expected that the MIDR responses are highly correlated with the frequency content of the ground motions at the lengthened period. Figure 4.13-4.15 show the contour plots of the correlations between IDRs and spectral accelerations along the building height for the specified period interval (i.e., $0.2T_1$-$2T_1$). As seen from Figure 4.13a and Figure 4.13b, the correlation contour plots (at T_R=225 years) confirm that the structural responses at the lower stories show high degree of correlation (ρ =0.7) with the spectral values at periods longer than T_1. In the case of the $Sa(T_1)$ scaling method, the IDR values at upper stories (at T_R=225 years) also exhibit strong positive correlations with the spectral accelerations at the second (T_2=0.5s) and third modes (T_3= 0.33s) of the structure that lead to increased dispersions in upper stories (see Fig. 4.12 and Fig. 4.13). As seen in Figure 4.12, the maximum interstory drift ratios are obtained approximately as 0.7% and 1.5% at the 10/50 and 2/50 intensity levels, respectively. It is observed that the ground motions at 10/50 and 2/50 levels impose high seismic demands in which the interstory drift ratios of individual records reach or slightly exceed the value of 1.0% and 2.0% drifts, respectively. The ground motions selected by both scaling methods produce similar trend in median responses with different levels of precision (or uncertainty). In particular, an increase in the amplitude of the ground motions results in high level of dispersions due to large inelastic deformations in the structure. It is

seen that the presence of the scatter in the target spectral demand for the 10/50 hazard level propagates to a larger dispersion in the IDRs. As seen in Figure 4.14, the correlation contour plots at 10/50 hazard level show that the frequency content of the ground motions both at periods shorter and longer than T_1 contributes to the structural response. These results reveal that allowing the variation of spectral intensity in target spectral demand mobilizes multiple frequencies across the period band and produces inelastic action in all stories. Therefore, the observed interstory drift ratios are almost uniformly spread throughout the building (see Figure 4.12). The $Sa(T_1)$ scaling approach, on the other hand, does not take into account the variation in the elastic spectral demand that results in reduced dispersion in the prediction of the interstory drifts at 10/50 hazard level. In this case, increased in the intensity level increases the median estimations but does not significantly affect the level of the dispersion. However, the variability in the structural response is substantially increased by a factor of approximately 1.5 for the 2/50 hazard level. This is because of the fact that the effective (or lengthened) period of the structure falls into the range of $[1.5T_1\text{-}2T_1]$, where the large scatter (or dispersion) in elastic spectral accelerations is observed (see Figure 4.11b). It is clearly seen that the maximum interstory drift ratios and spectral values show a strong correlation at the period range of $[1.5T_1\text{-}2T_1]$. In this hazard level, both methods produce comparable dispersion (approximately 0.35) in the MIDR. Some discrepancies are observed at dispersion statistics of the upper story drifts because the ground motions that are selected by the proposed method show a high correlation with the spectral values of second and third modes of the structure, and thus the scatter in the upper story drifts is increased due to the higher mode effects.

This Study   **Sa(T$_1$) Scaling**
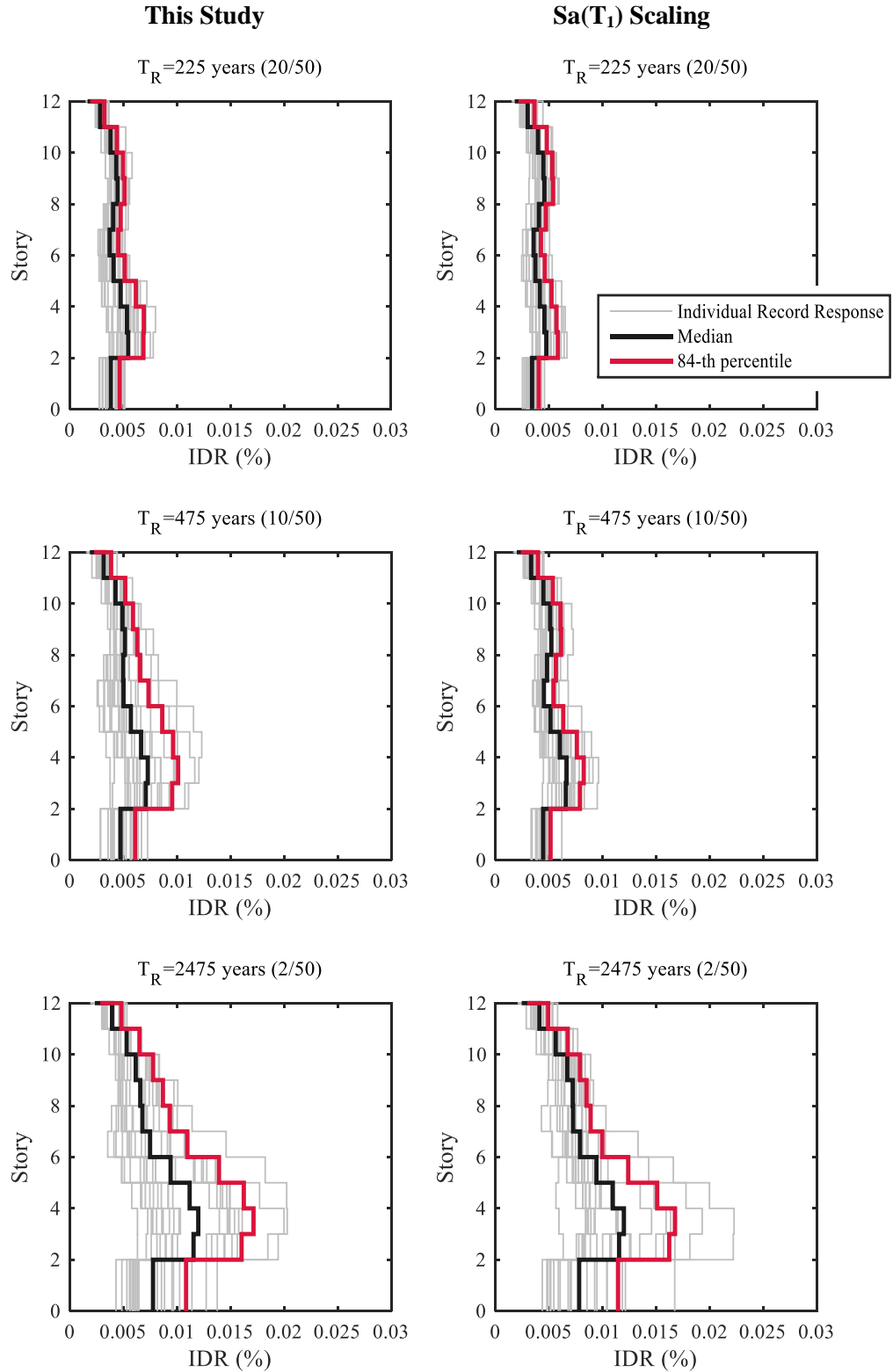
Figure 4.12. Heightwise distribution of the interstory drift ratios based on different scaling approaches at three different hazard levels.

Correlations between IDRs and Spectral Accelerations at T_R=225 years

(a)

Correlations between IDRs and Spectral Accelerations at T_R=225 years

(b)
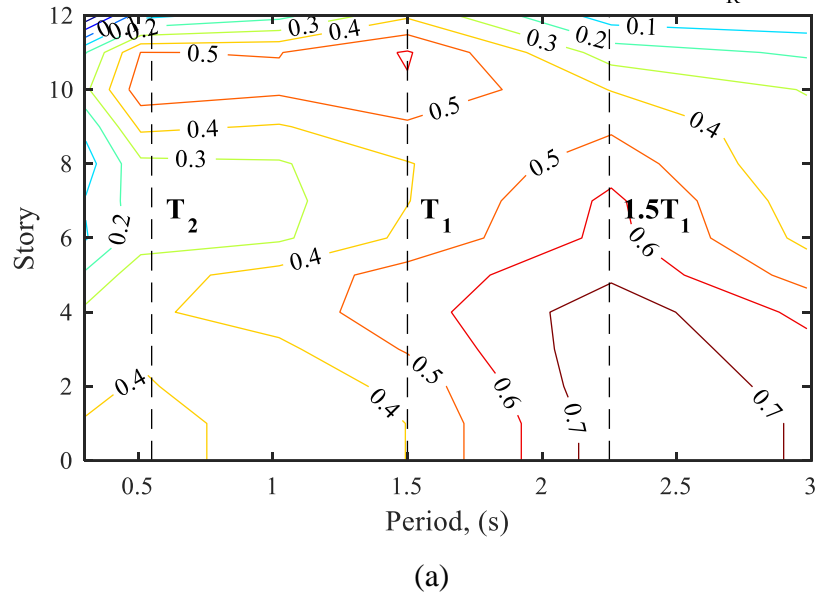
Figure 4.13. Contours of the correlation coefficients between IDRs and spectral accelerations along the building for the specified period interval (i.e., $0.2T_1$-$2T_1$) at T_R=225 years hazard level for (a) the proposed method, (b) the $Sa(T_1)$ scaling method. T_1, T_2 and $1.5T_1$ represent the first mode, second mode and lengthened periods of the structure, respectively.

Correlations between IDRs and Spectral Accelerations at T_R=475 years

(a)

Correlations between IDRs and Spectral Accelerations at T_R=475 years

(b)

Figure 4.14. Contours of the correlation coefficients between IDRs and spectral accelerations along the building for the specified period interval (i.e., $0.2T_1$-$2T_1$) at T_R=475 years hazard level for (a) the proposed method, (b) the $Sa(T_1)$ scaling method. T_1, T_2 and $1.5T_1$ represent the first mode, second mode and lengthened periods of the structure, respectively.

Correlations between IDRs and Spectral Accelerations at T_R=2475 years

(a)

Correlations between IDRs and Spectral Accelerations at T_R=2475 years

(b)

Figure 4.15. Contours of the correlation coefficients between IDRs and spectral accelerations along the building for the specified period interval (i.e., $0.2T_1$-$2T_1$) at T_R=2475 years hazard level for (a) the proposed method, (b) the $Sa(T_1)$ scaling method. T_1, T_2 and $1.5T_1$ represent the first mode, second mode and lengthened periods of the structure, respectively.

Figure 4.16 and Figure 4.17 illustrate the peak floor displacements (PFD) and peak floor acceleration (PFA) profiles obtained from both scaling methodologies at three hazard levels. As seen from the distribution of the peak floor displacements (PFD), both scaling approaches yield fairly similar median PFDs, whereas the level of dispersion depends on the nonlinearity levels as well as the spectral variability of the scaled ground motions in the specified period range, as discussed before. These results are compatible with the structural response behavior observed for the IDRs. This result is expected because an increase in the IDR responses would result in increased demands in PFDs due to strong correlation between two response parameters in most cases.

As seen in Figure 4.17, the PFA profiles show that the maximum responses are generally observed at upper stories of the model building, where the higher mode effects are dominant. It is seen that the PFAs show similar trend over the height at different intensity levels. Increase in the intensity level does not produce a proportional increase in the maximum responses because the nonlinear behavior limits the acceleration that the ground motions will impart to the structure. Figures 4.18-4.20 show the correlations between PFAs and spectral accelerations at three considered hazard levels. It is clearly seen that this response parameter shows a strong correlation with the higher vibration modes of the structure for both scaling methods. It has been observed that in some cases (see Figure 4.19), PFAs of the proposed method are also strongly correlated with the spectral ordinates at target T_1, indicating that the structural response is sensitive to the energy content of the ground motion set at different modes of vibration, whereas the ground motions from $Sa(T_1)$ method show weak correlations for the longer periods of vibration. Nevertheless, the analyses results indicate that both scaling procedures produce similar median and dispersion estimations of this response parameters at all hazard levels. It is apparent that, unlike the case of displacement response parameters (i.e., IDR and PFD), the PFA responses are less sensitive to the scatter in the target spectral demand. Thus, both scaling method produces comparable distribution of this structural response parameter.

Overall, comparative studies indicate that both scaling methods produce similar median responses of the selected engineering demand parameters (e.g., MIDR, PFD, and

PFA) at all specified hazard levels. These analysis results also validate the accuracy of the proposed procedure in predicting the median response of MDOF frame structure. It is observed that the distribution of the structural response can be sensitive to the ground motion bin utilized in different scaling methodologies as well as the differences in the frequency content of the ground motions. The proposed method produces relatively conservative dispersion in MIDR as it considers the uncertainties involved in the target spectral demand.

This Study **Sa(T₁) Scaling**
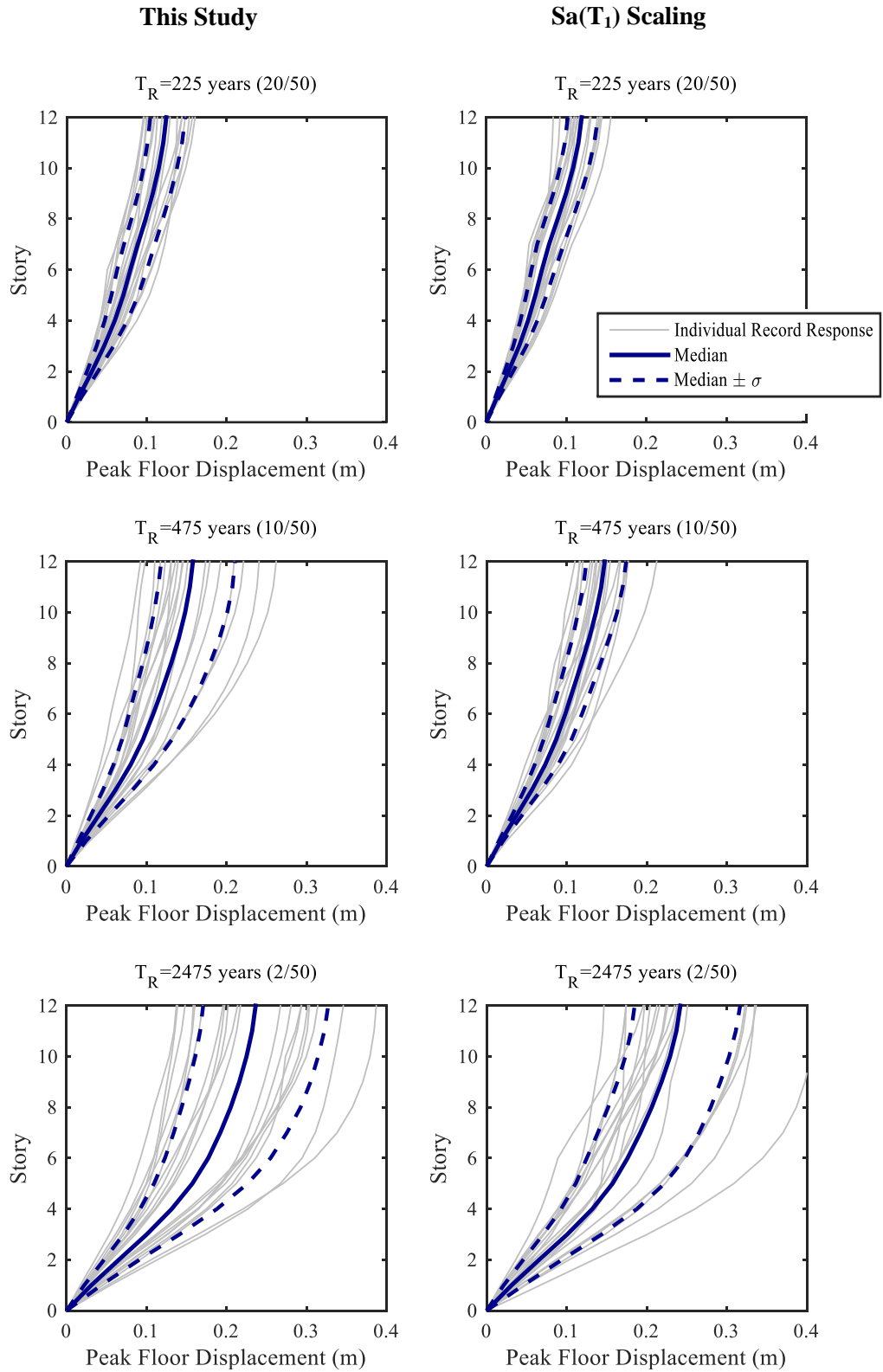
Figure 4.16. Heightwise distributions of the peak floor displacements based on different scaling approaches at three different hazard levels.

This Study **Sa(T₁) Scaling**
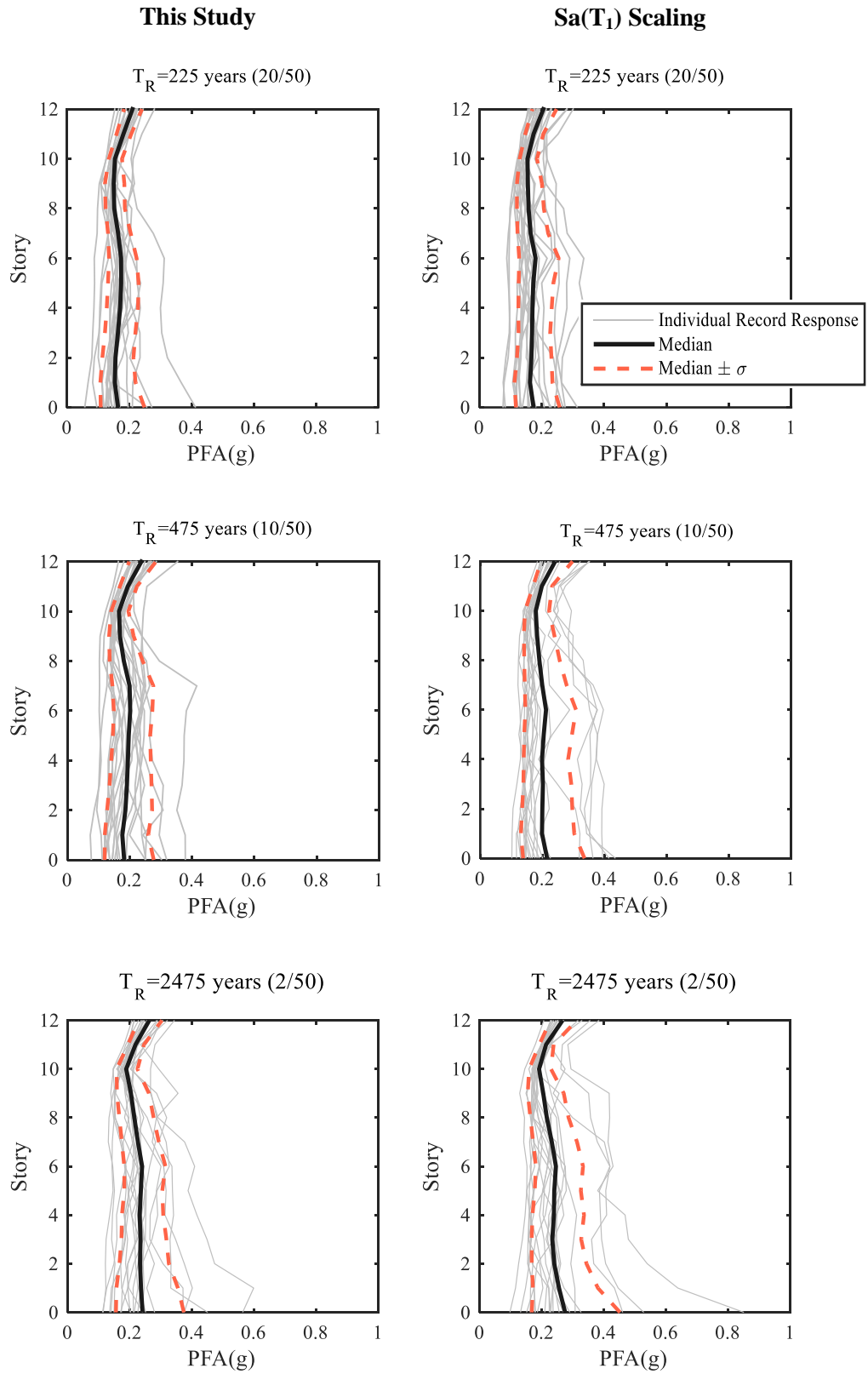
Figure 4.17. Heightwise distributions of the peak floor accelerations based on different scaling approaches at three different hazard levels.
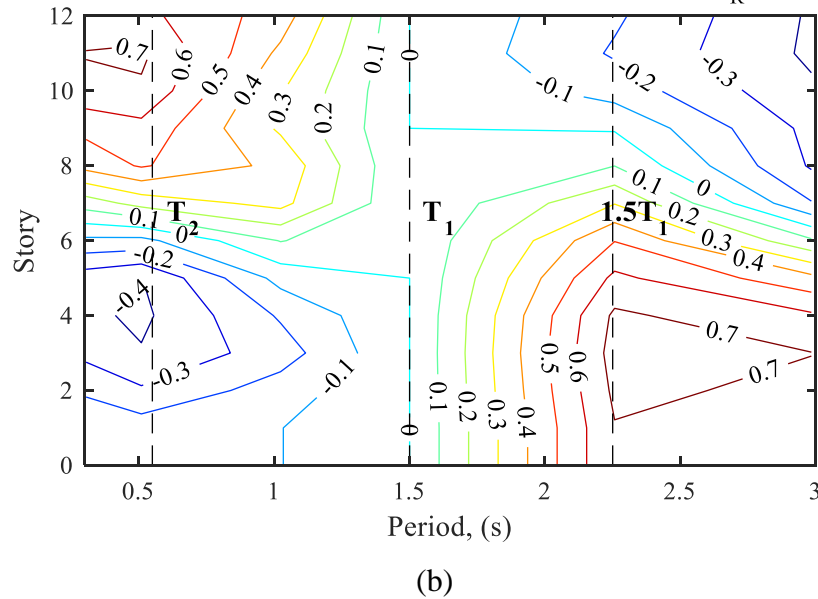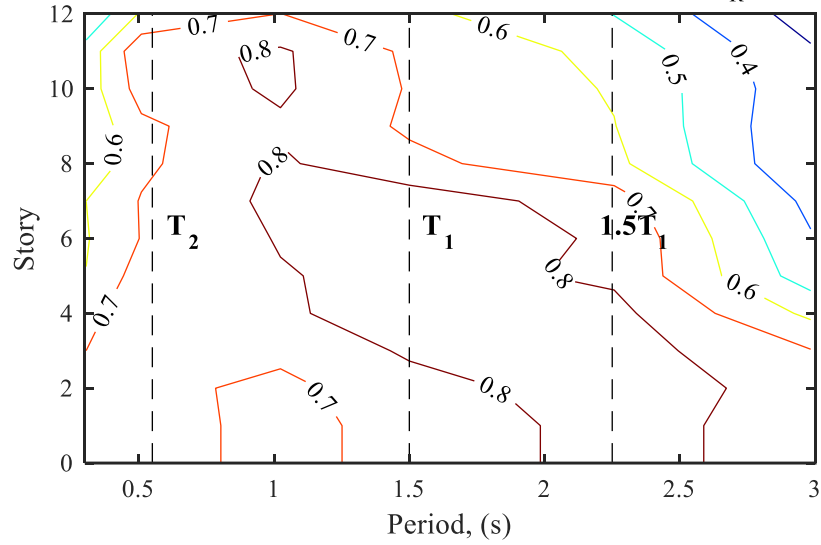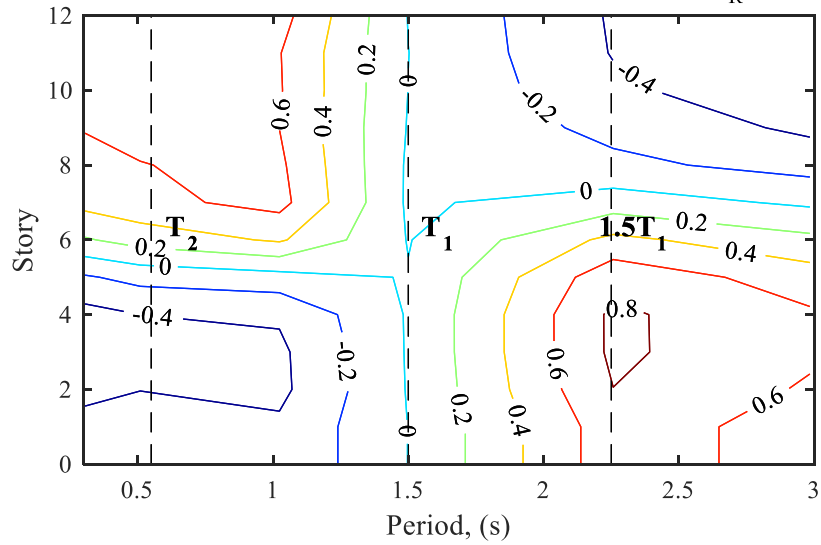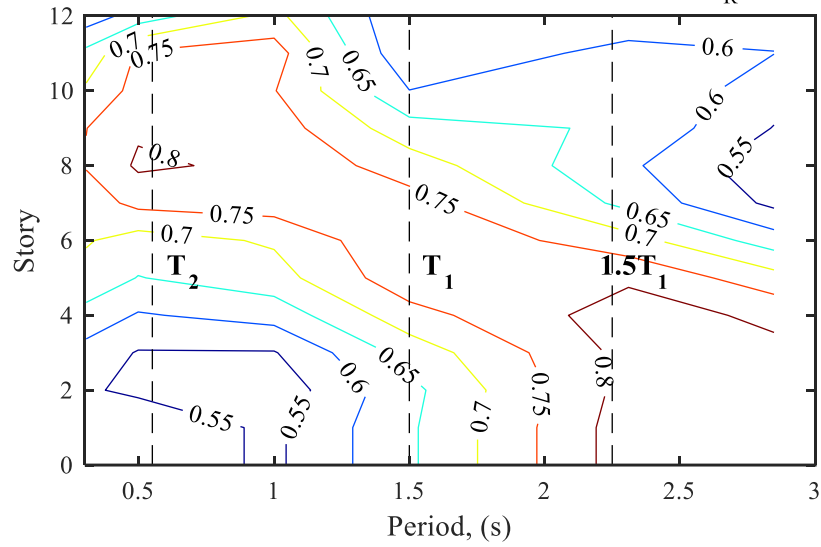
Correlations between PFAs and Spectral Accelerations at T_R=225 years
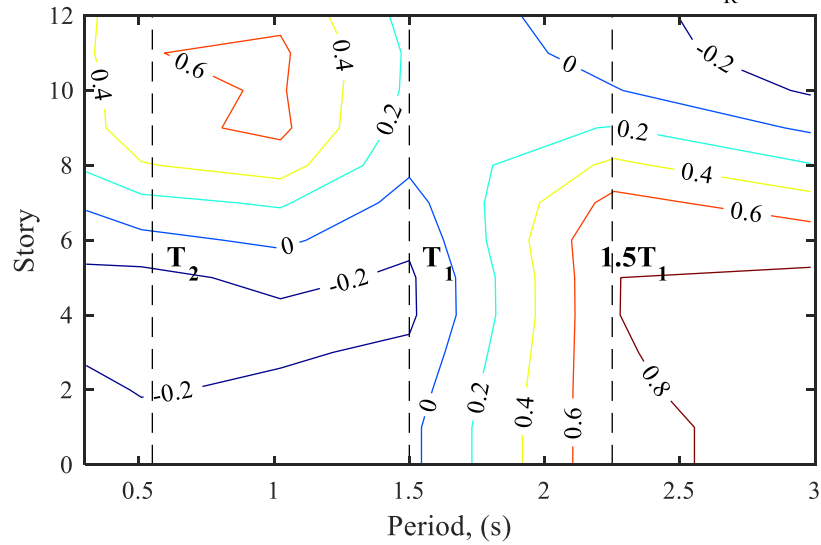

(a)
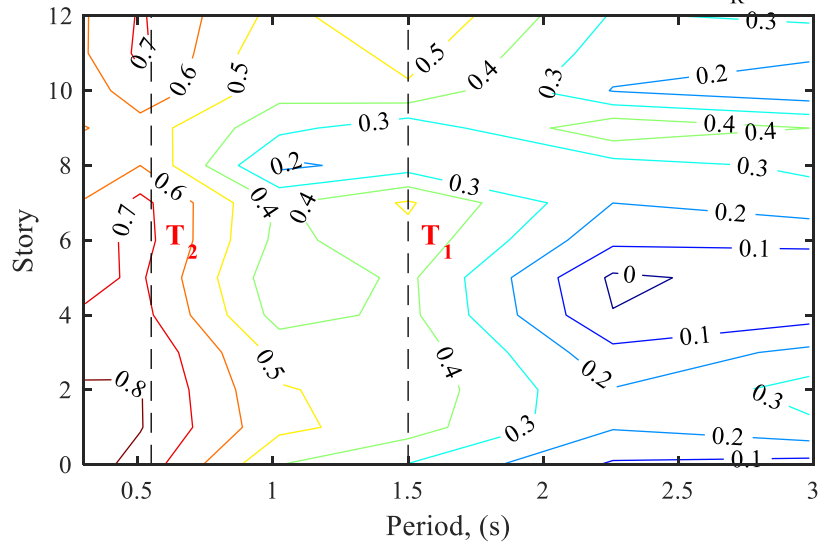
Correlations between PFAs and Spectral Accelerations at T_R=225 years

(b)

Figure 4.18. Contours of the correlation coefficients between PFAs and spectral accelerations along the building for the specified period interval (i.e., $0.2T_1$-$2T_1$) at T_R=225 years hazard level for (a) the proposed method, and (b) the $Sa(T_1)$ scaling method. T_1 and T_2 represent the first-mode period and second-mode period of the structure, respectively.

(a)
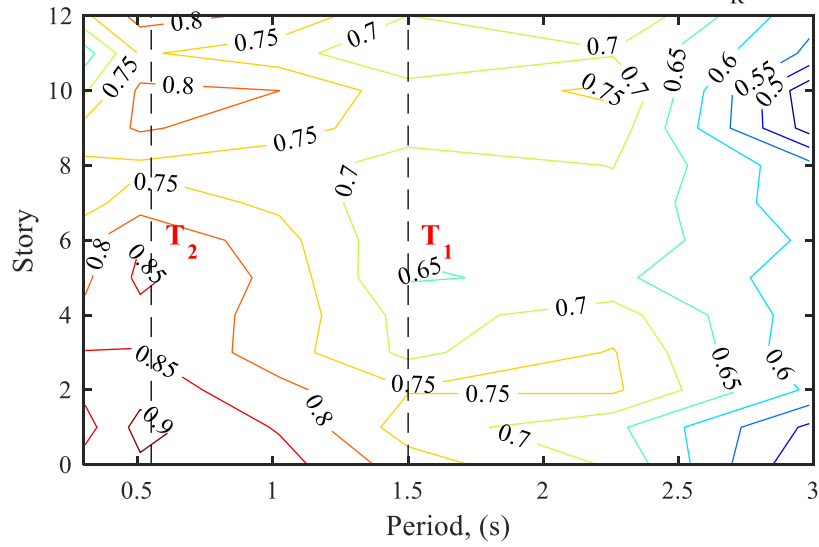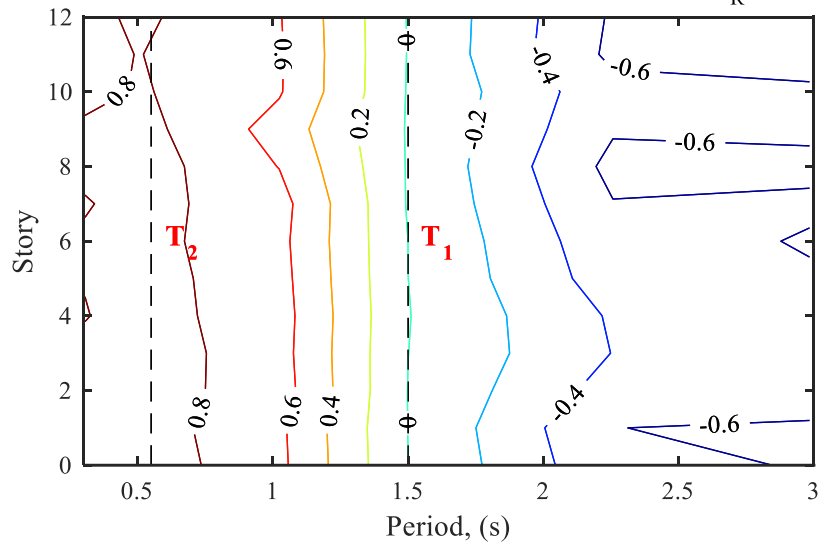
(b)

Figure 4.19. Contours of the correlation coefficients between PFAs and spectral accelerations along the building for the specified period interval (i.e., $0.2T_1$-$2T_1$) at T_R=475 years hazard level for (a) the proposed method, and (b) the $Sa(T_1)$ scaling method. T_1 and T_2 represent the first-mode period and second-mode period of the structure, respectively.

Correlations between PFAs and Spectral Accelerations at T_R=2475 years

(a)

Correlations between PFAs and Spectral Accelerations at T_R=2475 years

(b)

Figure 4.20. Contours of the correlation coefficients between PFAs and spectral accelerations along the building for the specified period interval (i.e., $0.2T_1$-$2T_1$) at T_R=2475years hazard level for (a) the proposed method, and (b) the $Sa(T_1)$ scaling method. T_1 and T_2 represent the first-mode period and second-mode period of the structure, respectively.

4.5. Probability of Drift Limit Exceedance

To understand the impact of the ground motion selection and scaling methodologies on the seismic performance assessment of structures, the exceedance probabilities of the MIDR estimations from two different scaling methodologies are evaluated at three seismic hazard levels (T_R=225, 475 and 2475 years). To compute the probability that the drift is exceeded to given damage state, the MIDRs of the structure are first sorted in ascending order, and then the empirical cumulative probabilities of non-exceedances are computed. The resulting curve is obtained by fitting the lognormal distribution to the response data. Figure 4.21 illustrates the fitted cumulative distribution functions (CDFs) for MIDR estimations obtained from two different scaling methodologies at the selected hazard levels. It is seen that the proposed method yields conservative non-exceedance probabilities than the $Sa(T_1)$ scaling method at T_R=225 and T_R=475 years hazard levels. As it is evident from the CDFs (at the value of 0.5), the proposed method provides slightly higher median values compared to $Sa(T_1)$ scaling method at these hazard levels. Additionally, the CDFs of the proposed method show heavier upper tail than those obtained by the $Sa(T_1)$ method, because the higher drifts obtained from the proposed method result in conservative dispersion in structural responses. However, as mentioned previously, both methods produce comparable median and dispersion statistics in structural response at T_R=2475 year hazard level, and thus approximately same non-exceedance probabilities are observed for this hazard level.

For reinforced concrete frame structures, FEMA 273/356 adopts three qualitative MIDR limits (1%, 2% and 4%) for the Immediate Occupancy (IO), Life Safety (LS), and Collapse Prevention (CP) performance levels, respectively. Similar limit states are defined in Turkish Earthquake Code (TEC, 2007) where the maximum MIDR limit in the regular buildings are given as 0.8% and 2.0% for IO and LS performance levels, while the MIDR values are limited to 3% to avoid collapse. It should be noted that the most code-complying reinforced concrete buildings will not reach the 3% drift limits (i.e., Collapse Prevention) under high earthquake shaking. Thus, this study evaluates the performance of the code-compliant model building based on the IO and LS limit states. The resulting exceedance probabilities of the drift values at the specified hazard levels are listed in Table 4.2.

The results show that the ground motions obtained from both methods do not exceed the Life Safety structural performance limits at T_R=225 years and T_R=475 years earthquake levels indicating that the structure satisfies the all relevant performance requirements of the building code. It is seen that the $Sa(T_1)$ scaling method yields lower exceedance probabilities than the proposed method for IO performance level. The probability that the interstory drift exceeds the IO level is 32% for the proposed procedure, while it is 17% for the $Sa(T_1)$ scaling case at T_R=475 years earthquake level. Since the proposed method propagates the variation in the earthquake shaking to the distribution of the structural response, it produces higher probability of exceedance than the $Sa(T_1)$ method at T_R=225 years and T_R=475 years hazard levels. Nonetheless, the results indicate that both methods present comparable results in terms of building performance prediction as the maximum difference between the probability of exceedance of the limit states obtained from the proposed method and $Sa(T_1)$ method is less than 15% at all cases. In this case, the approaches utilized in different ground motion selection and scaling methodologies do not introduce a significant change in the performance evaluation of the structure for the selected hazard levels. However, it is important to note that a more rigorous framework for performance evaluation should consider the full range of earthquake shaking (i.e., based on fragility curves). A more comprehensive discussion on the evaluation of the structural performance will be presented in Chapter 5.
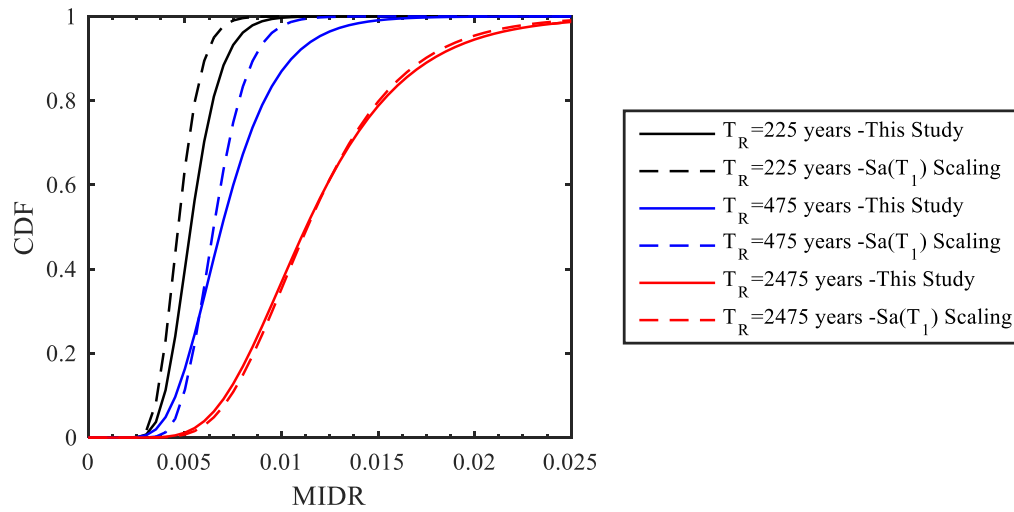
Figure 4.21. Cumulative distribution functions of the maximum interstory drift ratios (MIDRs) obtained from the results of this study and the $Sa(T_1)$ scaling method.

Table 4.2. Exceedance probabilities of the limit states for different ground motion selection and scaling approaches for three specified hazard levels.

Ground Motion Selection and Scaling Methods	Performance Levels	Return Periods		
		T_R=225years	T_R=475years	T_R=2475years
This Study	IO (%)	5.0	32.0	95.0
	LS (%)	0.0	0.0	6.0
$Sa(T_1)$ Scaling	IO (%)	0.0	18.0	85.0
	LS (%)	0.0	0.0	5.0

5. ANALYTICAL FRAGILITY CURVE ESTIMATION USING GAUSSIAN MIXTURE MODEL

5.1. Introduction

This chapter presents a novel approach for the estimation of the analytical fragility functions. The proposed method is based on a semi-parametric probability density estimation approach, namely Gaussian Mixture Model, which combines the multivariate probability distributions of the intensity measure (IM) and the engineering demand parameter (EDP) in a continuous 2-D scale. It enables to propagate the uncertainty of both ground motion intensity and the engineering demand parameter on fragility curve estimations. In this study, the spectral variation at the target intensity measure is captured by the earthquake records that are obtained from the proposed ground motion selection and scaling methodology. This chapter begins with the framework for seismic risk assessment and explains the concept of probabilistic seismic demand models that facilitate the development of fragility curves. Later, the theory of the Gaussian Mixture Model (GMM) and its specific implementation details are provided. It should be noted that this probabilistic approach is applied to 12-story RC model building for developing analytical fragility functions. To investigate the impact of uncertainties on fragility curve estimations, the results of the proposed approach are compared to those derived by using the conventional approach.

5.2. Background and Motivation

The most widely adopted probabilistic seismic risk assessment framework within the field of Performance Based Earthquake Engineering (PBEE) is formalized by the Pacific Earthquake Engineering Research (PEER) Center (Cornell and Krawinkler, 2000). The typical approach employed in the PEER framework consists of four main steps: seismic hazard analysis, structural response analysis, damage analysis, and loss analysis. The intermediate variables of these four steps are, respectively, intensity measure (IM), engineering demand parameter (EDP), damage measure (DM), and decision variable (DV). Figure 5.1 illustrates the PBEE model and its intermediate variables IM, EDP, DM and DV. In this model, for a given earthquake intensity measure, the structural demand model can be obtained by characterizing the relationship between IM and EDP. The damage model relates the EDPs to the measure of damages in the structure. The loss model defines the relationship between the damage values and the decision variables (i.e., death, financial loss and downtime).
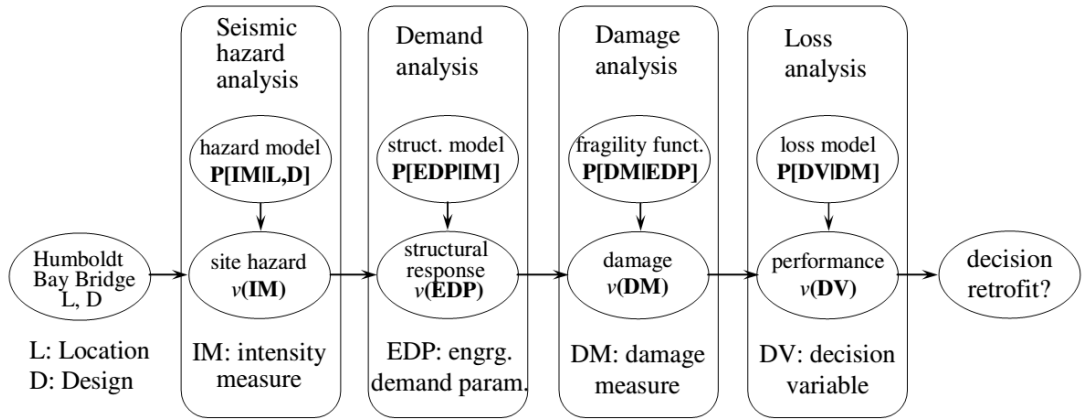
Figure 5.1. PEER PBEE methodology (Porter, 2003).

This formulation includes conditional probabilities in each intermediate model and accounts for all pertinent sources of uncertainties in order to rigorously assess the seismic risk of a structure. The mean annual frequency, $\lambda(DV)$, of a decision variable is computed using the triple integral as shown in Equation (5.1).

$$\lambda(DV) = \iiint G(DV \mid DM)\,dG(DM \mid EDP)\,dG(EDP \mid IM)\,d\lambda(IM) \qquad (5.1)$$

The fragility functions play a central role in a fully coupled seismic risk analysis that provides the link between seismic hazard and building loss estimation. Fragility curves describe the probability of exceedance of a specified damage or limit state of a structural component or system for a given ground motion intensity level. They have proven to be essential tool for quantifying and evaluating the seismic performance of structures under earthquake events. Existing fragility curve assessment methods can be classified into four groups of empirical, judgmental, analytical and hybrid, according to whether the damage data used in their generation is derived mainly from observed post-earthquake surveys, expert opinion, analytical simulations or combinations of these, respectively. A detailed review of the existing fragility functions can be found in Rossetto and Elnashai (2003). Among these methods, the most recent probabilistic seismic risk assessment approaches have relied on analytical procedures to describe the performance of the structure under different levels of seismic intensity. Nonlinear dynamic analysis is considered as the most reliable and rigorous approach to estimate the analytical fragility functions (Shinozuka *et al*., 2000). In this case, nonlinear dynamic analyses are conducted under a set of ground motions at various seismic intensity levels where the structural responses (i.e., engineering demand parameters) are recorded in order to build probabilistic seismic demand models. These models are then used to estimate the probability of the structure exceeding a given performance level (e.g., maximum interstory drift ratio, peak floor displacements, peak floor acceleration) for the selected seismic intensity level and consequently develop seismic demand fragility curve.

The proper selection of input motions for nonlinear response history analysis is one of the most critical steps for reliable seismic performance assessment. In the current seismic risk-based assessment approaches, the ground motions are typically selected based on a single intensity measure to characterize the earthquake shaking as well as the corresponding relationship between the structural response and probabilistic seismic hazard analysis (PSHA). It is noteworthy that the uncertainty and randomness in the ground motion intensity measure for a given annual probability of exceedance is captured explicitly by PSHA. A single hazard curve corresponding to an individual branch of the logic tree quantifies all ground motion variability (aleatory) of the corresponding model, whereas the distribution of the hazard curves for different values of ground motion

parameter is determined by the epistemic uncertainty (Abrahamson and Bommer, 2005; Bommer and Scherbaum, 2008). In the PEER PBEE framework, a suite of ground motions is typically anchored to a single intensity value of the selected fractile of the hazard curve (i.e., mean hazard curve) which is itself uncertain. However, for the fixed annual exceedance frequency (or return period), the natural choice would be to address the possible variations in earthquake intensity by using appropriate ground motion selection and scaling procedure. To this end, the proposed ground motion selection and scaling procedure addresses the epistemic uncertainty in the target intensity measure by preserving the inherent variability within the ground motion suite. In order to properly propagate the considered uncertainties in the system, a new probabilistic seismic demand model is developed. In the following sections, the most widely adopted probabilistic seismic demand models are discussed and then a new probability density estimation approach is introduced.

5.3. Probabilistic Seismic Demand Models

Following the Pacific Earthquake Engineering Research (PEER) framework, probabilistic seismic demand models relate intensity measures (IM) as the interface variable between seismic hazard and structural response. The structural response of interest is mainly quantified using Engineering Demand Parameter (EDP) that can be associated with the structural or nonstructural damage measures such as maximum interstory drift ratio and peak floor acceleration (Krawinkler *et al.*, 2003; Baker and Cornell, 2005). The intensity of the ground motion shaking can be represented by a scalar IM (e.g., peak ground acceleration, Sa (T_1), inelastic displacement etc.) or vector-valued IMs (e.g., {PGA, Mw}, {Sa (T1), ε}). The estimation of EDP|IM is obtained from the results of nonlinear dynamic analysis of the structure under a set of ground motions with specified intensity level. The conditional distribution of EDPs for a given intensity level is also known as fragility curve, which is defined as $P(EDP > y \mid IM = im)$ the probability of *EDP* exceeding demand value y given $IM = im$. The subsequent sections define the most widely used probabilistic seismic demand models that are used to derive relationship between EDP|IM, and hence generate the fragility curves.

5.3.1. Cloud and Stripe Analyses

As briefly mentioned in Chapter 3, the most common probabilistic seismic demand models are cloud and stripe analyses. In the cloud analysis, a set of unscaled ground motions are typically selected from a magnitude-distance bin that covered wide range of intensity level (i.e., $Sa(T_1)$) to represent the ground motion uncertainty. The selected ground motions can be modified by a constant if the intensity levels of the selected ground motions are not strong enough to cover the target intensity level (Baker and Cornell, 2006). This way, cloud responses are nearly centered on the target spectral acceleration which results in more reliable structural response estimation (Jalayer and Cornell, 2003). In this method, the ground motions used in nonlinear dynamic analysis produce structural responses with varying levels of spectral values (i.e., cloud response). In such cases, the estimations of structural response, i.e. conditional median and standard deviation of EDP given IM, can be calculated using least squares regression fits which consider a linear relationship between the natural logarithms of the variables (Cornell *et al.*, 2002). The expected demand of $\ln \mu_{EDP|IM=im}$ and estimated standard deviation or dispersion (σ_e) can be computed using Equation 5.2 and Equation 5.3, respectively.

$$\ln \mu_{EDP|IM=im} = \beta_0 + \beta_1 \ln im \tag{5.2}$$

$$\sigma_e = \sqrt{\frac{\sum_{i=1}^{n}(\ln EDP_i - \ln \mu_{EDP|IM})^2}{n-2}} \tag{5.3}$$

where β_0 and β_1 are parameters of linear regression; $\ln \mu_{EDP|IM=im}$ is the predicted value of the fitted line based on the record's $IM=im$; $\ln EDP_i$ is the natural logarithm of the EDP corresponding to the ith record and n is defined as the number of ground motion records. Figure 5.2 shows the schematic presentation of the cloud analysis approach. The probability that EDP exceeds y given $IM=im$ can be calculated using the normal complementary cumulative distribution function as given in Equation 5.4.

$$P(EDP > y \mid im) = 1 - \Phi\left(\frac{\ln(y) - \ln \mu_{EDP|IM=im}}{\sigma_e}\right) \tag{5.4}$$

where $P(EDP > y \mid im)$ is the complementary cumulative distribution function of EDP at given IM, and $\Phi(\cdot)$ is the cumulative distribution function of the standard Gaussian distribution.

In the case of stripe scaling method, each ground motion is scaled to the same target IM value with its specific scale factor in which the resulting demand estimations are aligned at the given intensity measure (IM). In this case, distribution of the data can be described by fitting a parametric function (i.e., lognormal distribution). Therefore, median and standard deviation of the structural response are estimated by taking mean (μ) and standard deviation (β) of the logarithmic EDP values, respectively. Note that the distribution of the EDP can be estimated at multiple IM values by repeating the analysis for a range of intensity levels (i.e., Multiple Stripe Analysis). Figure 5.3 shows the typical illustration of the stripe analysis approach. Unlike the cloud analysis, standard deviation of the structural response is not constant over the range of IM. The probability that *EDP* exceeds *y* given $IM = im$ can be calculated using the complementary cumulative distribution function as given in Equation 5.5.

$$P(EDP > y \mid im) = 1 - \Phi\left(\frac{\ln(y) - \mu}{\beta}\right) \tag{5.5}$$
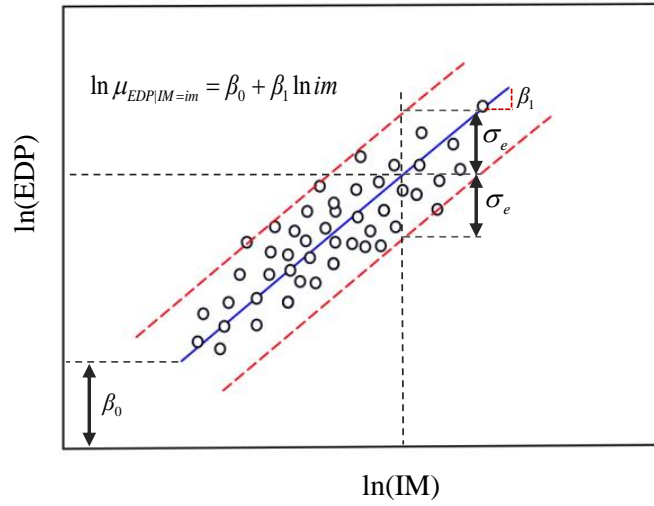
Figure 5.2. Schematic illustration of the probabilistic seismic demand model (Cloud analysis approach).
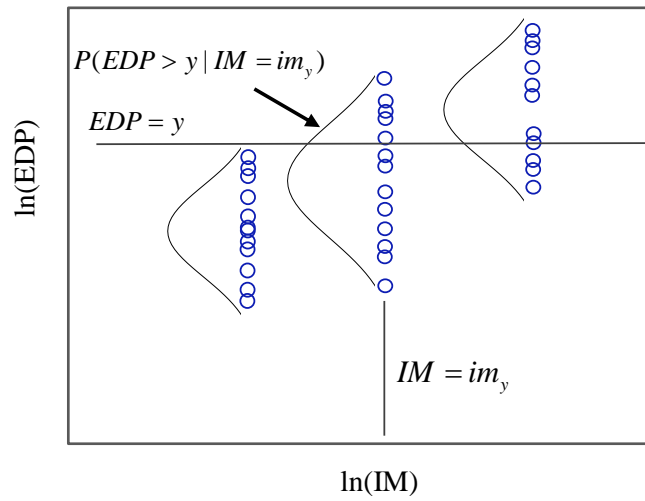
Figure 5.3. Schematic illustration of the probabilistic seismic demand model (Stripe analysis approach).

5.4. Gaussian Mixture Model

The performance assessment of structures requires development of seismic demand models that provide a link between the seismic hazard and the structural response. These probabilistic models are the key components for the derivation of fragility curves which express the probability of being or exceeding a damage state for a specified seismic intensity level. One of the main challenges in probabilistic seismic assessment procedures is the identification and propagation of uncertainties in a system that is essential to characterizing reliable seismic risk assessment. The uncertainties affecting the structural performance can be classified as aleatoric and epistemic. Aleatoric uncertainty refers to the inherent uncertainties that are random in nature and irreducible, whereas epistemic uncertainty results from lack of knowledge, prediction error or specification error that can be reduced by improving the state of knowledge. It is generally stated that natural uncertainty (or aleatoric) is a property of the system, whereas epistemic uncertainty is a property of the analyst (Cullen and Frey, 1999).

As stated before, one of the critical aspects of reliable seismic risk and loss assessment is to identify and incorporate the potential uncertainties through the seismic fragility analysis. The structural response can be affected by various sources of uncertainty such as material properties, modeling assumptions and earthquake-induced ground motion. Among all sources of uncertainty, the ground motion uncertainty (treated as aleatoric) is the major contributor to the overall uncertainty of mean fragility curve (Kwon and Elnashai, 2006; Ellingwood, 2007). It should be noted that the present study does not assess the effect of the modelling uncertainties (i.e., epistemic uncertainty due to the structural design and modelling assumptions) on the derivation of fragility curve. As noted previously, the current probabilistic seismic demand models do not consider the uncertainty in the intensity measure while relating the earthquake shaking to the demand parameters. Thus, the potential scatter in the earthquake intensity is generally disregarded in seismic response distribution where the dispersion of the fragility curve reflects the uncertainty in the demand (i.e., due to record-to record variability). To address this issue, the proposed ground motion selection and scaling approach accounts for the uncertainty in target intensity measure (i.e. the epistemic uncertainty from PSHA). To incorporate the

uncertainties in both target intensity measure and the structural response on fragility curve computations, a new probability density estimation method is required. In this study, a new probabilistic model, namely Gaussian Mixture Model, is presented so as to define the relationship between EDP and IM that will be subsequently used to estimate the fragility curve. The following sections briefly review the probability density estimation approaches and provide a background of the Gaussian Mixture Model with the concept of Expectation Maximization algorithm. Then, the statistical and computational framework will be further explored for fragility curve development.

5.4.1. Theoretical Background

Probability density estimation is the main step in statistics to characterize the behavior of a given dataset (i.e., random variables) and to form a statistical model that connects the data and the parameters. The density estimation problem can be defined as follows: Given a set of N points in d-dimensional vectors $\{x1,.....,xN\}$, estimate the probability density function (PDF) that approximates the true probability distribution from which data is drawn. This problem can be solved using parametric, non-parametric and semi-parametric approaches. In the parametric approach, the data is assumed to be drawn from a specific density model (e.g., Gaussian or normal distribution), and thus the problem reduces to the estimation of the values of the parameters (i.e., mean and standard deviation of the sample points). However, such assumptions may provide a false representation of the true density in some cases. In contrast, non-parametric methods do not make such strict assumptions about the form of the distribution in order to "let the data speak for themselves". It should be noted that the nonparametric approaches such as histogram, kernel method, orthogonal series estimators and other smoothing procedures have several drawbacks, including the choice of bandwidth or smoothing parameter and the curse of dimensionality, i.e., the exponentially increasing sample size is required as the number of dimensions increases (Silverman, 1986). The third approach, semi-parametric models combine the advantages of both parametric and non-parametric methods by allowing general class of functions to construct flexible models. This method does not assume any particular shape of the probability density function, however unlike the non-parametric methods, the complexity of the model is fixed in advance, and thus the number of

parameters does not increase with the size of the data set (Archambeau *et al.*, 2003). Gaussian Mixture Model is a powerful semi-parametric approach for density estimation in a wide variety of situations (Fraley and Raftery, 2002). This approach builds the model by treating the data as a linear combination of multiple probability density functions to describe the complete data. It has been widely used in the fields of statistical data analysis; signal processing, pattern recognition and machine learning (e.g. modeling, clustering and classification).

It should be noted that the GMM has a strong capability to describe the real data and it can be considered as an approximation of the actual world. In this model, the clusters in an n-dimensional dataset with k observations are obtained from different populations. The clustering problem can be transformed to a parameter estimation problem because the underlying population can be modeled as a mixture of K component densities. The multivariate Gaussian mixture model can be formulated as a simple weighted linear combination of Gaussian probability densities that provides a richer class of density models than a single Gaussian. Like k-means clustering, Gaussian mixture modeling uses an iterative algorithm that converges to a local optimum for model parameter estimation. The GMM method uses soft clustering, and therefore each point has a probability of belonging to each cluster as opposed to k-means which assumes that each point belongs to only one cluster (i.e., hard assignment). Furthermore, Gaussian Mixture Modeling may be more appropriate than k-means clustering when clusters have different sizes and correlation within them. Figure 5.4a and Figure 5.4b show the 2D and 3D representation of the Gaussian Mixture Model, respectively.
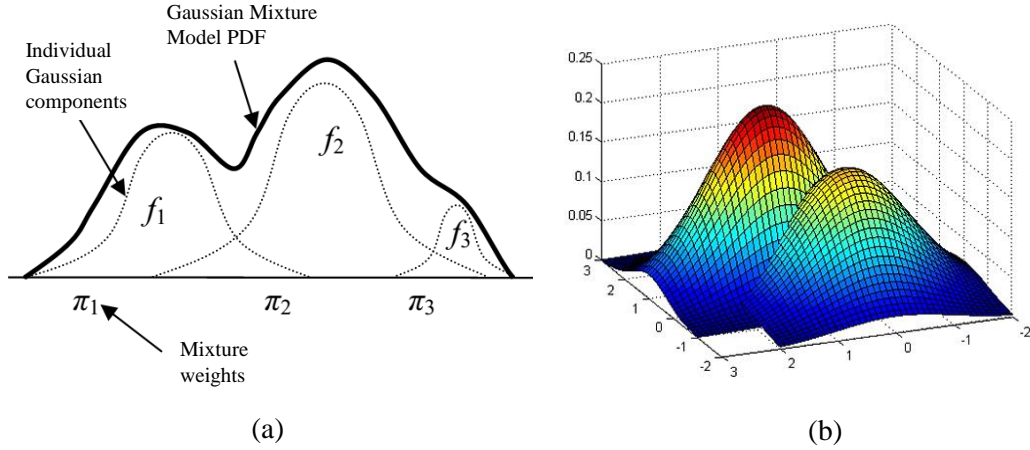
Figure 5.4. Illustration of the (a) 2D, and (b) 3D probability density functions of the Gaussian Mixture Model.

Assuming the data x_{ij} $(i = 1,....n,\ j = 1,...m)$ comes from a mixture of K probability distributions, each corresponding to different cluster, then the mixture model can be defined as follows:

$$p(x \mid \theta) = \sum_{k=1}^{K} \pi_k p_k(x \mid \mu_k, \Sigma_k) \tag{5.6}$$

where $p_k(x \mid \mu_k, \Sigma_k)$ denotes the conditional probability density of the kth component given mean vector μ_k and covariance matrix Σ_k. The K Gaussians are aggregated using the mixing proportions π_k of the kth component that must satisfy the constraints $0 \leq \pi_k \leq 1$ and $\sum_{k=1}^{K} \pi_k = 1$. The model parameters of the Gaussian mixture model can be summarized by the parameter vector $\theta = \{\pi_k, \mu_k, \Sigma_k\}$ where $k = 1,....,K$. Note that the probability density function (PDF) of the each component follows a normal distribution which is given in Equation 5.7.

$$p_k(x \mid \mu_k, \Sigma_k) = \mathrm{N}(\mu_k, \Sigma_k)(x) = \frac{1}{(2\pi)^{(d/2)} \det(\Sigma_k)^{1/2}} \exp\left\{-\frac{1}{2}(x - \mu_k)^T \Sigma_k^{-1}(x - \mu_k)\right\} \tag{5.7}$$

Note that the estimation of the parameters for a single multivariate Gaussian distribution is straightforward, whereas in order to find the values of (μ_k, Σ_k) of GMM, the log-likelihood function with respect to the parameters as given in Equation 5.8 should be maximized.

$$\log p(X \mid \theta) = \log p(X \mid \pi, \mu, \Sigma) = \sum_{n=1}^{N} \log \left\{ \sum_{k=1}^{K} \pi_k p_k(x_n \mid \mu_k, \Sigma_k) \right\} \qquad (5.8)$$

where N is a set of given observations $(x_1, x_2, ..., x_N)$. The optimization of this maximum likelihood function however is very complicated problem, because the presence of the inside summation over k prevents the logarithm function from acting directly on the Gaussian. The closed form solution (i.e., setting the derivatives of the log likelihood to be zero) is usually analytically intractable, because the likelihood of a Gaussian mixture model is non-convex. To solve this numerical optimization, the Expectation-Maximization (EM) algorithm is used as a powerful method for finding maximum likelihood estimates for models with missing or latent (unobserved) variables. The latent variable is represented by a set of observations $Z = \{z_1, z_2, ..., z_i\}$ where $z_i \in \{1, ..., K\}$ indicates which mixture component generated the observation x_i. The latent variables are indicator variables that are marginally distributed according to the mixing coefficients π_k. The values of latent variables are:

$$I_k(z_i) = \begin{cases} 1, & z_i = k; \text{ if } x_i \text{ comes from component } k \\ 0, & z_i \neq k; \text{ otherwise} \end{cases}$$

The dependence relationship of the observations x on z is shown in Figure 5.5.
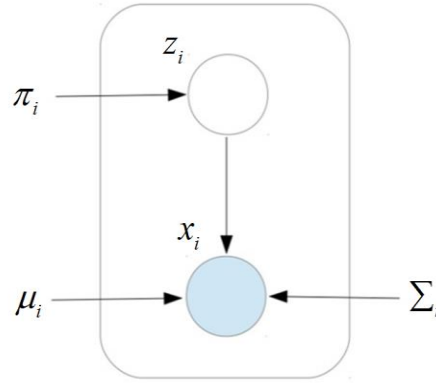
Figure 5.5. Graphical representation of a Gaussian mixture model for a set of data points x_i with corresponding hidden variables z_i .

Given a Gaussian mixture model, the main objective is to maximize the likelihood function with respect to parameters, the mixing proportions π_k , the mean vector μ_k and the covariance matrix Σ_k for the kth population which are given as:

$$\pi_k = \frac{1}{N} \sum_{i=1}^{N} I_k(z_i)$$

$$\mu_k = \frac{1}{\pi_k N} \sum_{i=1}^{N} x_i I_k(z_i)$$

$$\Sigma_k = \frac{1}{\pi_k N} \sum_{i=1}^{N} [(x_i - \mu_k)'(x_i - \mu_k)] I_k(z_i)$$

Note that each iteration of the EM algorithm consists of two processes: The E-step, and the M-step. This iterative technique alternates between E-step (Expectation) and M-step (Maximization). In the expectation, or E-step, the missing data are estimated given the observed data and current estimate of the model parameters. The procedure calculates the posterior probabilities that each data point is generated by the k-th mixture component. In the M-step, the likelihood function is maximized under the assumption that the missing data are known and re-calculates the means and covariances of the each mixture

component (Dempster *et al.*, 1977). In other words, it assigns a probability of each data using the component density function and adjusts according to the overall model. The details for this algorithm can be found in the literature (Bishop, 1995; McLachlan and Peel, 2004). Note that the task starts from an initial parameter estimates and then it proceeds iteratively in two steps as outlined below.

EM Algorithm Steps:

1. Initialize the means μ_k, covariances Σ_k, and mixing coefficients π_k, and calculate the initial value of the log likelihood. The standard approach initializes with the components given mean and covariance matrices and sets all mixture weights equal.

2. **E-step**. Estimate the posterior probability, γ_{ik}, of the ith observation belonging to the k-th mixture component using the current parameter values. The posterior probability, γ_{ik} represents the expected contribution of the k-th mixture to the total likelihood associated with observation x_i. It is computed by using Bayes Theorem,

$$\gamma_{ik} = \frac{\pi_k p_k(x_i \mid \mu_k, \Sigma_k)}{\sum_{k=1}^{K} \pi_k p_k(x_i \mid \mu_k, \Sigma_k)}$$

3. **M-step.** Given the known expectation, maximum likelihood methods can be used to obtain the next iteration of the model. In this case, the parameter estimates of π_k, μ_k and Σ_k is updated using the estimated posterior probabilities so that the expected likelihood is maximized. Thus, the means and covariances are evaluated by weighting each observation by the degree in which it belongs to the component.

$$\pi_k^{new} = \frac{1}{n}\sum_{i=1}^{n} \gamma_{ik}$$

$$\mu_k^{new} = \frac{1}{n\pi_k^{new}}\sum_{i=1}^{n} x_i \gamma_{ik}$$

$$\Sigma_k^{new} = \frac{1}{n\pi_k^{new}}\sum_{i=1}^{n} \gamma_{ik}(x_i - \mu_k^{new})'(x_i - \mu_k^{new})$$

4. Repeat steps 2 to 3 until GMM log likelihood, $\log p(X \mid \theta)$ of entire data set does not change appreciably, or number of iteration limit is reached. Algorithm generally reaches to convergence when the relative increase in log likelihood is smaller than the pre-specified tolerance limit (e.g. ~5x10^{-4}). It should be noted that the convergence is typically achieved before 200 iterations.

5.4.2. Application of the GMM

This section presents the application of the Gaussian Mixture Model approach to determine the probabilistic relationship between the engineering demand parameter (EDP) and the intensity measure (IM). The first step is to assemble ground motion suites that are representative of the different seismic hazard levels at the site of interest. To this end, the site-specific PSHA calculations are performed for the target site as mentioned in Chapter 4. The seismic hazard curve is obtained using the EZ-FRISK software (Risk Engineering, 2005). Figure 5.6 shows the hazard curve of the target site for $Sa(T_1=1.5s)$. The data is plotted on a logarithmic scale on the x and y axes. The present study considers six target intensity levels to select and scale the earthquake records. These target intensity levels correspond to a set of return periods (T_R) that ranges from 225 years to 10000 years (i.e., T_R= 225, 475, 975, 2475, 4975, and 10000 years).
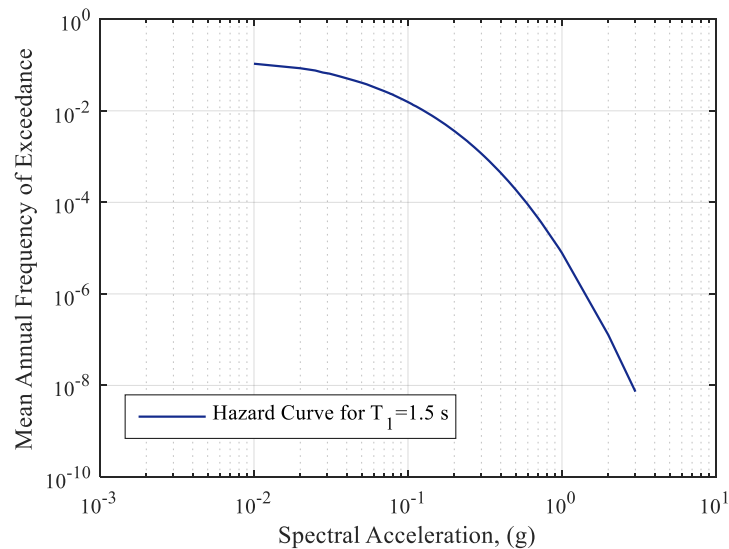
Figure 5.6. $Sa(T_1=1.5s)$ hazard curve for the selected target site.

It should be noted that the disaggregation information of the probabilistic seismic hazard analysis is used to identify the dominant earthquake scenario parameters at the target hazard levels for the period of interest. Table 5.1 lists the target earthquake scenario parameters and target spectral ordinates. As one can infer from Table 5.1, the most contributing scenario events have magnitudes between 7.15 and 7.25, and these events are approximately 25-30 km away from the target site. Note that the magnitude-distance pair

and site class information of the target scenario events are used to constrain the ground motion database at the record selection stage. It is seen that the scenario events have approximately same magnitude-distance pairs, and thus the candidate records are selected from similar magnitude and distance bins. As noted before, the epsilon values correspond to the normalized difference, in terms of number of standard deviations, between the target $Sa(T_1)$ level (obtained from PSHA) and the median response predicted by a ground motion prediction equation for a given magnitude-distance pair. As seen in the Table 5.1, target mean epsilon values change between the 1.30 and 2.77 and they increase as the return period increases. It is found that the maximum $Sa(T_1, 5\%)$ level is 0.62g for return period of 10000 years. The target CMS is derived from the magnitude, distance and epsilon values that are obtained through the disaggregation of the PSHA, and then a suite of 20 ground motions are selected and scaled to match the CMS for each of the six hazard levels. As shown in previous chapters, a suite of 20 ground motions are adequate to capture the structural response.

Table 5.1. Target earthquake scenario parameters (M_w, R_{jb}, ε) and corresponding target spectral ordinates for the selected return periods.

Return Periods (T_R), [years]	Magnitude, M_w	Distance, R_{jb}, [km]	Epsilon, ε	Sa_{target} , [g]
225	7.15	30	1.30	0.19
475	7.15	30	1.41	0.26
975	7.20	26	1.84	0.31
2475	7.22	25	2.19	0.40
4975	7.23	25	2.59	0.53
10000	7.24	24	2.77	0.62

The next step is to conduct the nonlinear response history analysis for a chosen intensity levels and then record the structural responses of the 12-story RC model building (i.e., maximum interstory drift ratio) in order to form the database. To this end, the nonlinear response history analyses are performed using the records that are selected and scaled by the proposed ground motion selection and scaling methodology. This database

results in clusters of (EDP, IM) in 2D-plane where each cluster belongs to the specific seismic hazard level. The statistical dependence is modeled by using joint probability distributions. It should be noted that the output variables of each cluster represent different characteristics, and thus Gaussian Mixture Model identifies the complex system using the combination of these clusters. It is noteworthy that consideration of uncertainty in target intensity measure for the proposed ground motion selection and scaling procedure motivates the introduction of the new fragility model. This statistical model is developed to consider the uncertainties in both the target spectral demand and structural response.

The joint probabilistic modelling of EDP and IM is examined by using the multivariate Gaussian PDF. Thus, the uncertainties of both demand and intensity measure and their correlation information are considered. The uncertainty of each random variable is determined from the standard deviation of the assumed Gaussian PDF. The marginal distributions of the demand and intensity measure are described by fitting a parametric function to data. Previous studies show that the structural response (e.g., MIDR) can be modeled as lognormal distribution (Shome and Cornell, 1998; Buratti *et al.*, 2011). In this study, the probabilistic distribution of the maximum interstory drift values is assumed to follow a lognormal distribution. Furthermore, it is assumed that the uncertainty over the intensity measure follow the lognormal distribution. Note that the uncertainty in the intensity measure corresponds to the spectral variability of the ground motion set at the fundamental period of the structure which is preserved by the proposed ground motion selection and scaling methodology. To assess the normality of a univariate distribution of the spectral accelerations, the normal quantile-quantile plot (QQ-plot) is used. Figure 5.7 shows the QQ-plots for the scaled records at six different intensity levels. It should be noted that the QQ-plot compares the distributions and checks the assumption of normality. The quantiles of the logarithmic spectral accelerations of the scaled records at the fundamental period of the structure are plotted on the Y-axis and the quantiles of the standard normal distribution (i.e., theoretical quantiles) on the X-axis. If the distribution of the data provides a good fit with the straight line on QQ-plot, then the lognormal assumption for the intensity measure can be validated. It is clearly seen that almost all points follow the straight line with slight deviations at the tails. The standard normal distributions of the logarithms of spectral values provide a good fit to the theoretical

standard normal distribution within ± 2 standard deviation (σ) range. From these observations, the data is sufficiently linear to accept normality. To further validate the lognormal assumption for the intensity measure, Kolmogorov-Smirnov test is conducted at the 5% significance level. The null hypothesis is that the lognormal distribution provides the correct statistical model for the observed data. The statistical test results show that the null hypothesis is not rejected. On the basis of these results, it can be concluded that the normality assumption for the logarithmic values of the spectral accelerations is acceptable for its implementation to the Gaussian Mixture Model.
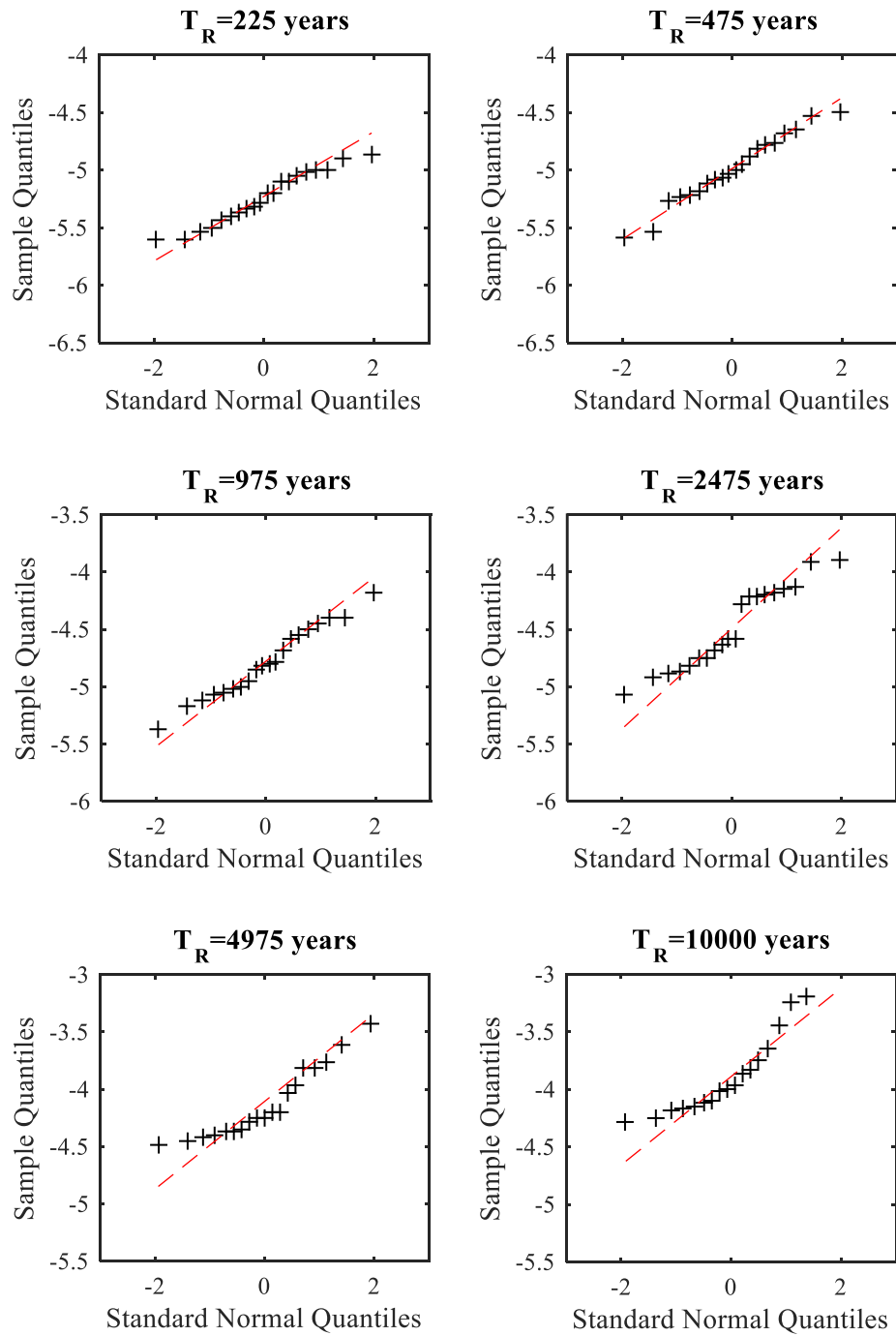
Figure 5.7. Quantile-quantile plots of the $\ln(Sa(T_1))$ for 20 real earthquake data at six different return periods.

5.4.3. Constructing Gaussian Mixture Model

As mentioned previously, in GMM method, each cluster corresponds to one Gaussian mixture component (e.g., multivariate Gaussian distribution) which is formed based on mean vectors, covariance matrices and mixture weights. This method is simple and computationally effective but it requires number of components to be specified in advance and is sensitive to initialization parameters, especially for high dimensional data. It may be difficult to determine optimum number of components and the initial parameters if no prior information of the problem is available. In this case, k-means clustering algorithm can be utilized for clustering data as well as initializing the component parameters. In the present work, the six clusters are formed based on the bivariate normal mixture with mean vectors and covariance matrices of the logarithmic values of the MIDR and $Sa(T_1)$. In other words, each cluster corresponds to the joint distribution of the MIDR and $Sa(T_1)$ at specified hazard levels. The multivariate random distribution of the observed data is used to generate 1000 simulation points. The scatter plot of the clusters is shown in Figure 5.8. It is seen that the clusters are partially or totally overlapped over the range of intensity measure. In this case, GMM offers a powerful approach to describe the true nature of the underlying data and reconstruct the overall probability distribution of the given model.

To fit the GMM to the simulated data, the Expectation-Maximization (EM) algorithm is initialized with the true mean and covariance matrices. Note that the full diagonal covariance matrices are used in order to consider the correlation between the predictors. Note also that uniform prior probability (i.e., mixing weight) is used so that all components are assumed to be equally probable. In this study, MATLAB's Statistical Toolbox is used to implement the EM algorithm and Gaussian Mixture Model. It is noted that the EM algorithm iteratively computes the parameters of the GMM to increase the likelihood of the estimations. As mentioned previously, the probability of each point is estimated in the E-step of the EM, and then M-step modifies the parameters based on the hidden variables to maximize the likelihood of the overall data with minimum level of computational cost. It should be noted that the detailed steps of the algorithm are already given in Theoretical Background section. Table 5.2 lists the true parameter and the

estimated parameters of each six cluster. The results indicate that EM algorithm captures the original observed statistics by using 1000 simulated sample while constructing the GMM. It generates a reasonable approximation to the true probability density functions. Figure 5.9 shows the contour plots and true density estimation of the GMM. As seen from figure, overlapping components are merged to form the single cluster which in turn results in two distinct peaks in the mixture model.
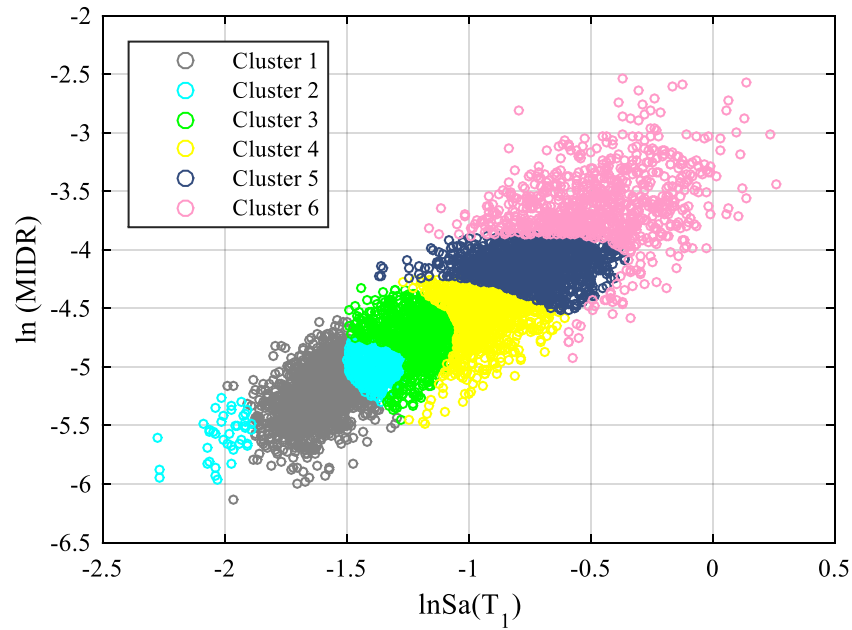
Figure 5.8. The scatter plot of the simulated samples of ln(MIDR) and lnSa(T_1) at each hazard level.

Table 5.2. True and estimated parameters for the samples. Each cluster (i.e., $\ln Sa(T_1)$, $\ln(MIDR)$) is parameterized by its mixing proportion (π_i), its mean (μ_i), and covariance matrices (Σ_i).

Clusters	Parameter	True value	Estimated value
Cluster 1	π_1	0.1667	0.1667
	μ_1	$[-1.6094\ -5.240]$	$[-1.6146\ -5.2474]$
	Σ_1	$\begin{bmatrix} 0.009 & 0.0096 \\ 0.0096 & 0.0540 \end{bmatrix}$	$\begin{bmatrix} 0.0180 & 0.010 \\ 0.010 & 0.0689 \end{bmatrix}$
Cluster 2	π_2	0.1667	0.1667
	μ_2	$[-1.3867\ -4.9762]$	$[-1.3850\ -4.9738]$
	Σ_2	$\begin{bmatrix} 0.076 & 0.0738 \\ 0.0738 & 0.1083 \end{bmatrix}$	$\begin{bmatrix} 0.0793 & 0.0750 \\ 0.0750 & 0.1088 \end{bmatrix}$
Cluster 3	π_3	0.1667	0.1667
	μ_3	$[-1.2110\ -4.7795]$	$[-1.2196\ -4.7794]$
	Σ_3	$\begin{bmatrix} 0.0609 & 0.0573 \\ 0.0573 & 0.0980 \end{bmatrix}$	$\begin{bmatrix} 0.0660 & 0.0620 \\ 0.0620 & 0.1102 \end{bmatrix}$
Cluster 4	π_4	0.1667	0.1667
	μ_4	$[-0.9678\ -4.4830]$	$[-0.9604\ -4.4865]$
	Σ_4	$\begin{bmatrix} 0.0535 & 0.0555 \\ 0.0555 & 0.1283 \end{bmatrix}$	$\begin{bmatrix} 0.0583 & 0.0588 \\ 0.0588 & 0.1336 \end{bmatrix}$
Cluster 5	π_5	0.1667	0.1667
	μ_5	$[-0.7269\ -4.1289]$	$[-0.7418\ -4.1436]$
	Σ_5	$\begin{bmatrix} 0.0628 & 0.0490 \\ 0.0490 & 0.0961 \end{bmatrix}$	$\begin{bmatrix} 0.0642 & 0.0477 \\ 0.0477 & 0.0938 \end{bmatrix}$
Cluster 6	π_6	0.1667	0.1667
	μ_6	$[-0.5723\ -3.8351]$	$[-0.5714\ -3.8268]$
	Σ_6	$\begin{bmatrix} 0.0693 & 0.0622 \\ 0.0622 & 0.1712 \end{bmatrix}$	$\begin{bmatrix} 0.0689 & 0.0635 \\ 0.0635 & 0.1773 \end{bmatrix}$
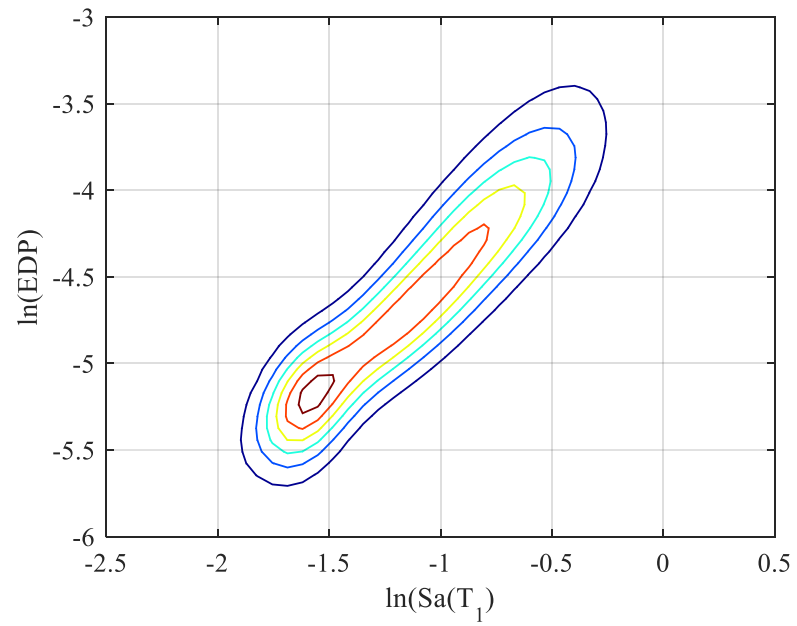
(a)
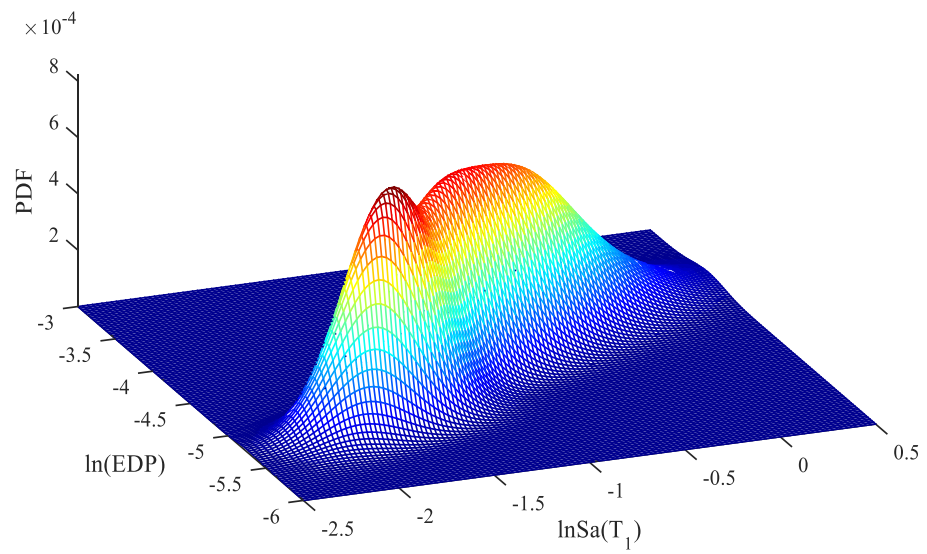
(b)

Figure 5.9. (a) The contour plots, and (b) true density estimation of the Gaussian Mixture Model.

5.5. Comparisons of Fragility Curve Estimations

In this section, site-specific seismic performance assessment of the 12-story model building is examined through the fragility curves that are generated for different damage (or performance) limit states. These fragility curves provide a more comprehensive evaluation for the seismic damage capabilities at different levels of earthquake shaking. As noted before, in the case of the proposed ground motion scaling methodology, the nonlinear response history analysis results in output variables that follow multimodal probability distributions. In this case, the combined contribution of structural response uncertainty and the intensity measure uncertainty on fragility curve computation is incorporated by the GMM probabilistic framework. To assess the impact of different fragility curve models on seismic damage estimations, another set of nonlinear response history analyses are conducted for the considered hazard levels by using ground-motion records that are selected based on $Sa(T_1)$ scaling method (i.e., CS-based ground motions). In this approach, the probabilistic seismic demand model is generated by the Multiple Stripe Analysis method that establishes two-parameter lognormal relationship between the demand and ground motion intensity. It can be regarded as conventional approach for the fragility curve development in which the ground motions are scaled to common intensity level (see Section 5.3). As mentioned previously, the Gaussian Mixture Model considers the joint distribution of intensity ($Sa(T_1)$) and demand (MIDR) parameters. If the joint distribution of two random variables $f(EDP, IM)$ is known, then the conditional probability distribution of the EDP given the IM ($f(EDP \mid IM = im)$) can be evaluated using the global joint and marginal ($f(IM)$) density estimations of GMM (i.e., Bayes theorem) as given in Equation 5.9.

$$f(EDP \mid IM = im) = \frac{f(EDP, IM)}{f(IM)} \tag{5.9}$$

To derive the fragility functions, i.e. the conditional probability of exceeding an EDP level edp at a given $IM = im$ ($P(EDP \geq edp \mid IM = im)$), the following equation can be used:

$$P(EDP \geq edp \mid IM = im) = \int_{edp}^{+\infty} f(EDP = x \mid IM = im)dx \qquad (5.10)$$

Figure 5.10 shows the median seismic fragilities of the model building across three damage limit states. These figures also include the fragility curves based on the conventional approach (i.e., $Sa(T_1)$ scaling) for comparison. The damage states correspond to three widely adopted performance levels (immediate occupancy, life safety, and collapse prevention) in the performance-based earthquake engineering (e.g., FEMA 273/356). In this study, MIDR limits of 0.8%, 2% and 3% are adopted for the Immediate Occupancy (IO), Life Safety (LS), and Collapse Prevention (CP) performance levels, respectively. It is assumed that structures will have no or slight damage at IO limit level, whereas at LS and CP limit states structures may experience significant and severe damage, respectively.

The parametric function is fitted to discrete points resulting from conditional cumulative distribution functions (CDF) of GMM in order to compare the results with the $Sa(T_1)$ scaling approach in a consistent manner. It should be noted that the approaches such as method of moments (MM), maximum likelihood estimation (MLE) and sum of squared error (SSE) can be adopted in order to fit lognormal CDF to the observed fractions. The detailed discussions about these models can be found in elsewhere (Porter *et al.*, 2007; Baker, 2015). In this study, the lognormal distribution is fitted by minimizing sum of squared errors (SSE) between the estimated and the observed probabilities. The results of the GMM and the $Sa(T_1)$ approach is evaluated by comparing the median and standard deviation (respectively θ and β) estimation of the fitted fragility curves. Table 5.3 presents the median and dispersion statistics of both approaches in terms of three limit states. As discussed in the previous chapter, when the seismic performance of the structure is evaluated based on a single hazard level (e.g., 2% in 50 years) both scaling methodologies provide approximately same performance prediction for the model building. However, these analysis results are based on lognormal distribution assumption for the structural response (i.e., unconditional representation), and thus the performance evaluation represents the demand uncertainty for both scaling approaches. In this section, the conditional fragility curve is derived by using GMM approach that implicitly considers

the uncertainties in both structural response and intensity measure. Therefore, the impact of different ground motion scaling approaches on seismic performance evaluation will be examined further at various earthquake hazard levels in this section. As depicted in Figure 5.10, the discrepancies between two methods are observed in median and dispersion predictions. It is apparent that the combined contribution of the uncertainty in intensity measure and structural response results in left-shift in median as well as decrease in dispersion statistics compared to $Sa(T_1)$ scaling case. The left-shift in median indicates an increase in the vulnerability of the structure while the slope of the curves is governed by the dispersions. Note that as the dispersion increases, the slope of the curve decreases. It is interesting to note that the preserving additional uncertainty in the intensity measure does not increase the dispersion of the fragility curve.As seen from Figure 5.10, the differences between median predictions of both methods increase for higher limit states. The median response of the fragilities is almost same for IO limit state, whereas the discrepancies are observed for CP limit state (approximately 20%). As one can infer from Table 5.3, the level of uncertainty increases for large drift limit states in both methods, due to the high nonlinear behavior. The dispersion estimation of both methods is fairly similar for CP limit state, whereas 25% differences in dispersion values are observed at IO and LS limit states. In the case of the GMM approach, it is observed that the model building has more than 50% probability of exceeding IO performance level when subjected to earthquake with spectral acceleration of 0.34g. The 50% probabilities of exceeding LS and CP performance levels are obtained under the earthquake intensity levels of 0.58g and 1.11g, respectively. The corresponding median spectral accelerations obtained from $Sa(T_1)$ scaling approach are 0.36g, 0.69g, and 1.36g for the IO, LS, and CP limit states, respectively. These results suggest that ignoring the spectral variation in the intensity measure would yield non-conservative median estimations when the system behaves highly nonlinear at high excitation levels. Furthermore, it results in underestimation in the probabilities of exceedances given the occurrence of the earthquake ground motion, particularly for high Sa levels. This underestimation occurs because $Sa(T_1)$ scaling approach reflects only the demand uncertainty in the fragility curve. In other words, conditional probability density function is computed based on the ground motions that are scaled to common intensity level, and therefore the deterministic approach is assumed while relating the structural response to given intensity measure. However, the ground motion amplitudes may vary for

a given seismic hazard level due to the epistemic uncertainties in PSHA, and therefore it should be considered in seismic risk assessment problems.

(a) Immediate Occupancy

(b) Life Safety

(c) Collapse Prevention
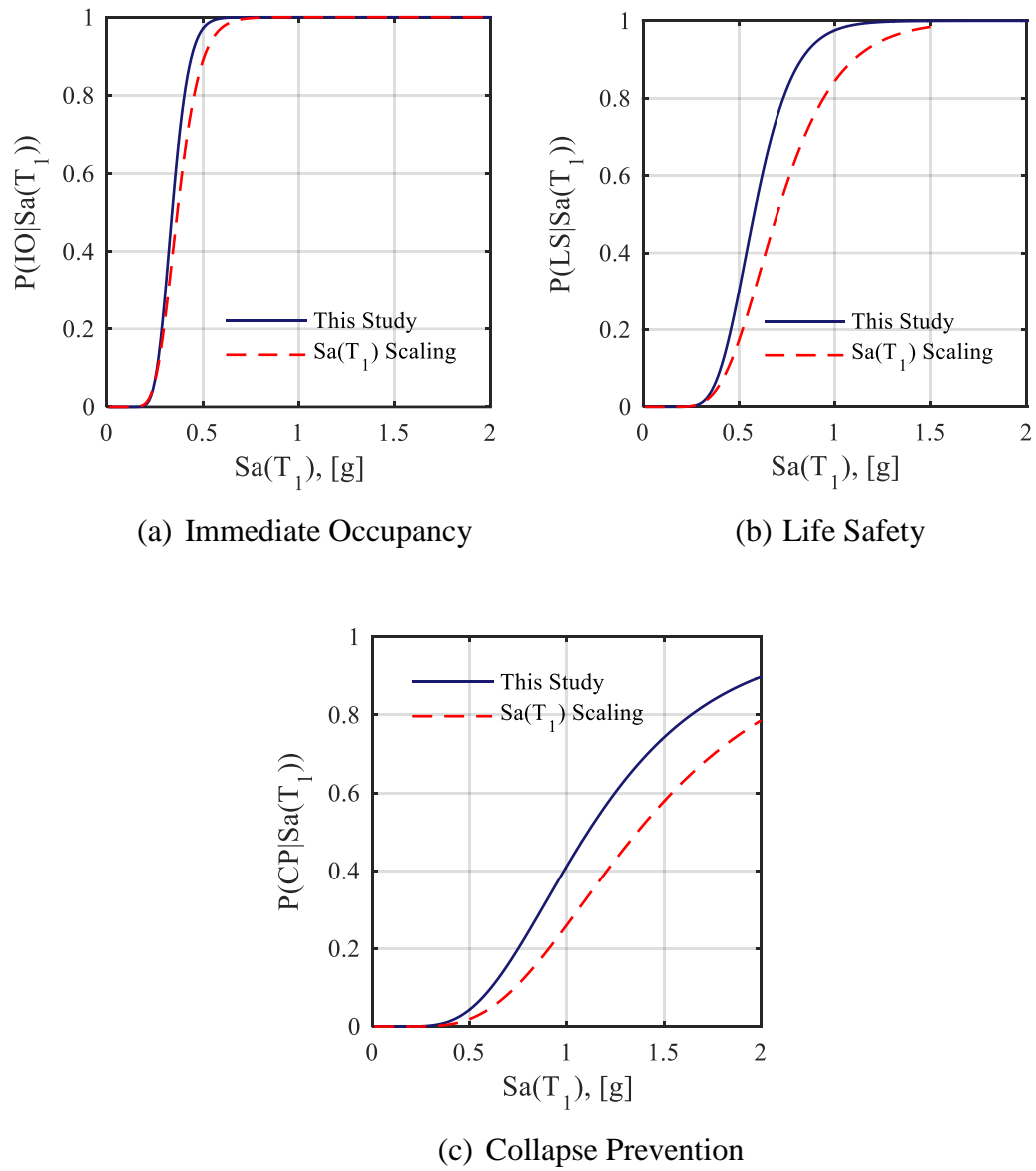
Figure 5.10. Fragility curves for (a) immediate occupancy (IO), (b) life safety (LS), and (c) collapse prevention (CP) for 12-story model building that are obtained from the proposed methodology and the $Sa(T_1)$ scaling approach.

Table 5.3. Log-normal distribution parameters of fragility curves that are obtained from the proposed GMM method and the $Sa(T_1)$ scaling method.

Limit States	Immediate Occupancy (IO)		Life Safety (LS)		Collapse Prevention (CP)	
Fragility curve parameters	θ	β	θ	β	θ	β
This Study (GMM)	0.34	0.20	0.58	0.28	1.11	0.46
$Sa(T_1)$ Scaling	0.36	0.25	0.69	0.35	1.36	0.48

As noted before, the propagation of the uncertainty in the intensity measure has an impact for large drift limits and high intensity levels. However, the lower tail of the fragilities is relatively less sensitive to the source of uncertainties utilized in different approaches which is more critical for the risk quantification. Given the seismic fragility curves, the vulnerability of the model building can be evaluated for a given earthquake scenario. For example, the maximum considered earthquake (MCE) (i.e., 2% probability of exceedance in 50 years or 2475 years return period) corresponds to spectral value of $Sa(T_1=1.5s)= 0.40g$. For this hazard level, the proposed approach predicts the conditional probabilities of slight, significant and severe damage as 79%, 37% and 6%, respectively, whereas $Sa(T_1)$ scaling approach yields conditional probabilities of slight, significant and severe damage as 64%, 23% and 3%, respectively. The results show that $Sa(T_1)$ scaling approach tends to underestimate the exceedance probabilities of IO and LS by as much as 15% while the difference between probability of exceedances of the CP performance level obtained from the proposed approach and the $Sa(T_1)$ scaling method is about 3%. Both methods estimate a high probability of exceeding the IO limit state, suggesting that the model building will have slight damage for the 2% in 50 years ground motions.

Finally, comparing the results for the fragility curves obtained from the proposed approach and the conventional approach show that the neglecting the uncertainty in intensity measure may yield non-conservative median estimations and lead to underestimation of the limit state exceedance probabilities at high earthquake intensity

levels. Furthermore, it is noted that the median response of seismic fragilities for life safety and collapse prevention performance levels are more sensitive to the uncertainty considered in the intensity measure. The findings of this study suggest that ignoring the uncertainties in intensity measure may significantly affect the outcomes of the risk calculations and decision variables in performance assessment process. In this context, the present study proposes a proper ground motion selection and scaling methodology to account for the uncertainty in the intensity measure as well as introduces a probabilistic framework to treat the uncertainties prudently in the system.

6. SUMMARY AND CONCLUSIONS

6.1. Summary

The main objective of this dissertation is to develop a ground motion selection and scaling methodology that takes into account the uncertainty in the spectral demand (i.e., epistemic uncertainty in PSHA) for a given earthquake event. The uncertainty in the intensity measure is considered implicitly by allowing the spectral variation within the ground motion suite. In this approach, the selection and scaling of ground motions are typically treated as two separate stages. In the selection stage, the records having similar seismological characteristics with target scenario event are extracted from large ground motion database. The final subset of ground motions is assembled by considering the spectral shape parameter of the individual record. The candidate record sets are constructed based on dispersion statistics about the target spectral demand. This is achieved by using the sort and sliding window approach. The optimum ground motion set is determined based on the goodness of fit measure between the spectral ordinates of target spectrum and the median and variances of ground motion set in the period range of interest. The scaling stage results in satisfactory match between the median record spectrum and the target spectrum within the specified period interval. The algorithm is further extended to scale ground motions for matching the target intensity distribution of the scenario-based spectrum.

The applications of the proposed methodology to select ground motions for matching PSHA-based target spectrum and scenario-based spectrum are presented in Chapter 3. Nonlinear response history analyses of different inelastic (SDOF) systems are conducted by using different number of ground motions. The performance of the proposed approach in predicting the structural response is evaluated by comparing the response predictions of this study to those obtained using the $Sa(T_1)$ scaling method. The effect of different ground motion selection and scaling methodologies on the seismic response of 12-story reinforced concrete model building has been investigated in Chapter 4. The

comparative studies are performed to examine the sensitivity of the structural response to different ground motion selection and scaling approaches. A new probabilistic framework, Gaussian Mixture Model, is introduced to consider the sources of uncertainties related to earthquake intensity and structural response for seismic risk assessment procedures. A theoretical background of the Gaussian Mixture Model with the concept of Expectation Maximization algorithm is provided in Chapter 5. The proposed approach is utilized to determine the probabilistic relationship between the engineering demand parameter (EDP) and the intensity measure (IM). To assess the impact of different fragility curve approaches on seismic damage estimations, the results of this study are compared with the conventional approach.

6.2. Conclusions

The major findings of this study are summarized as follows:

i.   The proposed ground motion selection and scaling methodology preserves the dispersion in the spectral demand and recognizes a wide range of periods. It provides a suite of motions whose median spectrum closely matches the target spectrum over the specified period interval. The possible scatter in the intensity measure is addressed by the spectral variability within the record set. The results from this study show that the proposed method produces unbiased estimate of the median demand and captures the dispersion of the structural response parameters. The consideration of the spectral variations about the target median may lead to relatively conservative estimates for the dispersion in structural response. This methodology can be used as a reliable tool for selecting and scaling ground motions for performance-based earthquake engineering.

ii.   The case studies in this dissertation show that the proposed procedure prevents excessive amplitude-scaling of the ground motion set. The scale factors of the record sets are generally changed between 0.8 and 3.0 at varying levels of seismic hazard, indicating that the proposed method avoids potential bias resulting from scaling the ground motions.

iii. It is demonstrated that the median responses obtained from the proposed method are not sensitive to the choice of target spectra (CMS and UHS) for mildly-inelastic behavior. The use of UHS typically overestimates the median responses, particularly in highly inelastic case. The structural response becomes sensitive to the spectral amplitudes and local spectral shape of the individual record for less than 15 earthquake records in the short-period range (T_1=0.5s). The sensitivity of the central response to the local spectral shape may be minimized by utilizing a large number of ground motions. It is demonstrated that a suite of 20 ground motions can adequately capture the distribution of the structural response.

iv. The $Sa(T_1)$ scaling method (Conditional Spectrum-based selection) is used as a benchmark to evaluate the performance of the proposed procedure for structural response estimation. This scaling method assumes zero dispersion at the target spectral demand and produces unbiased estimate of the median response. It reduces the dispersion in the structural response for elastic and mildly-inelastic systems, however, the response becomes sensitive to the spectral shape and scatter at periods longer than the fundamental period (when period elongates due to inelastic deformation) and at periods shorter than the fundamental period (higher modes contribution to the structural response). The case studies show that this scaling approach may provide stable median response for more than 15 earthquake records.

v. The presence of bias in the estimation of structural response is checked relative to the $Sa(T_1)$ scaling method. The results indicate that the ground motions selected by the proposed methodology produce unbiased estimate of the median response (SDOF systems) in most cases. It is demonstrated that both scaling methods result in similar median estimates of engineering demand parameters (including Maximum Interstory Drift Ratio, Peak Floor Displacement, Peak Floor Acceleration) for multi-degree-of-freedom (MDOF) model at different seismic hazard levels. The level of dispersion in the engineering demand parameters (EDPs) is influenced by the frequency content at periods longer than the fundamental period and at periods of higher modes. This is confirmed by

examining the correlations between the spectral accelerations and structural responses (Chapter 4).

vi. In the case of the proposed procedure, the presence of the variability at the target spectral demand yields conservative dispersion in the maximum interstory drift ratio (MIDR) at moderate intensity level. Both scaling methods produce comparable distribution of this response parameter at high intensity level. It is demonstrated that the peak floor acceleration (PFA) responses are less sensitive to the scatter in the target spectral demand.

vii. The Gaussian Mixture Model probabilistic approach is introduced to incorporate the uncertainties in both intensity measure and structural response on fragility curve computations. The results reveal that neglecting the variation in the intensity measure may yield non-conservative median fragility curve estimations and also may lead to underestimation of the limit state exceedance probabilities at high intensity levels.

6.3. Limitations and Future Work

The ground motions used in this study are selected based on the results from probabilistic seismic hazard analysis. The further studies can be conducted to evaluate the performance of the proposed ground motion selection and scaling methodology for scenario-based assessment procedures. This study investigates the seismic response of 12-story RC frame building. In the future, studies should be performed on the structures with different fundamental periods. Different systems such as structural walls and steel frame buildings can be examined to further test the performance of the proposed methodology. The effects of uncertainties on fragility curve estimations are investigated for a suite of 20 ground motions. The sensitivity of fragility curves to the different numbers of ground motions can be investigated as a future research.

REFERENCES

Abrahamson, N. A. and J. J. Bommer, 2005, "Probability and Uncertainty in Seismic Hazard Analysis", *Earthquake Spectra*, Vol. 21, No. 2, pp. 603-607.

Abrahamson, N. A., 2015, *Treatment of Epistemic Uncertainty Seismic Hazard for Critical Facilities: Issues and Proposed Solutions*, In Presentation made to the 2015 COSMOS Annual Meeting.

Akkar, S., M. A. Sandıkkaya, M. Şenyurt, A. A. Sisi, B. Ö. Ay, P. Traversa, J. Douglas, F. Cotton, L. Luzi, B. Hernandez, S. Godey, 2014, **"**Reference Database for Seismic Ground-Motion in Europe (RESORCE)", *Bulletin of Earthquake Engineering*, Vol. 12, No. 1, pp. 311-339.

Al Atik, L. and N. A. Abrahamson, 2010, "An Improved Method for Nonstationary Spectral Matching", *Earthquake Spectra*, Vol. 26, No. 3, pp. 601-617.

American Society of Civil Engineers (ASCE), 2006, *ASCE 7–05, Minimum Design Loads for Buildings and Other Structures*, Reston, VA.

American Society of Civil Engineers (ASCE), 2010, *ASCE/SEI-7-10 Minimum Design Loads for Buildings*, Reston, VA.

Ancheta, T. D., R. B. Darragh, J. P. Stewart, E. Seyhan, W. J. Silva, B. S.-J. Chiou, K. E. Wooddell, R. W. Graves, A. R. Kottke, D. M. Boore, T. Kishida and J. L. Donahue, 2014, "NGA-West2 Database", *Earthquake Spectra,* Vol. 30, No. 3, pp. 989–1005.

Araújo, M., L. Macedo, M. Marques and J. M. Castro, 2015, "Code-based Record Selection Methods for Seismic Performance Assessment of Buildings", *Earthquake Engineering and Structural Dynamics*, doi: 10.1002/eqe.2620.

Archambeau, C. and M. Verleysen, 2003, "Fully Nonparametric Probability Density Function Estimation with Finite Gaussian Mixture Models", *Proceedings of the 7th ICPAR Conference,* pp. 81-84.

Aslani, H. and E. Miranda, 2005, "Probability-based Seismic Response Analysis", *Engineering Structures*, Vol. 27, No. 8, pp. 1151-1163.

Ay, B. Ö. and S. Akkar, 2012, "A Procedure on Ground Motion Selection and Scaling for Nonlinear Response of Simple Structural Systems", *Earthquake Engineering and Structural Dynamics*, Vol. 41, No. 12, pp. 1693-1707.

Baker, J. W. and C. A. Cornell, 2005, "A Vector-Valued Ground Motion Intensity Measure Consisting of Spectral Acceleration and Epsilon", *Earthquake Engineering and Structural Dynamics*, Vol. 34, No. 10, pp. 1193-1217.

Baker, J. W. and C. A. Cornell, 2006, *Vector-Valued Ground Motion Intensity Measures for Probabilistic Seismic Demand Analysis*, Pacific Earthquake Engineering Research Center, College of Engineering, University of California, Berkeley.

Baker, J. W., 2011, "Conditional Mean Spectrum: Tool for Ground-Motion Selection", *Journal of Structural Engineering (ASCE),* Vol. 137, No. 3, pp. 322–331.

Baker, J. W., 2015, "Efficient Analytical Fragility Function Fitting Using Dynamic Structural Analysis", *Earthquake Spectra*, Vol. 31, No. 1, pp. 579-599.

Bazzurro, P. and C. A. Cornell, 2002, "Vector-Valued Probabilistic Seismic Hazard Analysis (VPSHA)", *Proceedings of the 7th US National Conference on Earthquake Engineering*.

Bazzurro, P. and N. Luco, 2005, "Accounting for Uncertainty and Correlation in Earthquake Loss Estimation", *Proceedings of the 9th International Conference on Structural Safety and Reliability (ICOSSAR)*, Rome, Italy.

Beyer, K. and J. J. Bommer, 2007, "Selection and Scaling of Real Accelerograms for Bi-Directional Loading: A Review of Current Practice and Code Provisions", *Journal of Earthquake Engineering*, Vol. 11, pp. 13-45.

Bishop, C. M., 1995, *Neural networks for pattern recognition*, Oxford University Press.

Bommer, J. J., S. G. Scott and S. K. Sarma, 2000, "Hazard-Consistent Earthquake Scenarios", *Soil Dynamics and Earthquake Engineering*, Vol. 19, No. 4, pp. 219-231.

Bommer, J. J., A. S. Elnashai and A. G. Weir, 2000, "Compatible Acceleration and Displacement Spectra for Seismic Design Codes", *Proceedings of the 12th World Conference on Earthquake Engineering.*

Bommer, J. J. and S. G. Scott, 2000, "The Feasibility of Using Real Accelerograms for Seismic Design", in A. Elnashai (ed.), *Implications of Recent Earthquakes On Seismic Risk*, Publisher: Imperial College, pp. 115-126.

Bommer, J. J. and A. B. Acevedo, 2004, "The Use of Real Earthquake Accelerograms As Input to Dynamic Analysis", *Journal of Earthquake Engineering*, Vol. 8, pp. 43-91.

Bommer, J. J. and N. A. Abrahamson, 2006, "Why Do Modern Probabilistic Seismic-Hazard Analyses Often Lead to Increased Hazard Estimates?", *Bulletin of the Seismological Society of America*, Vol. 96, No. 6, pp. 1967-1977.

Bommer, J. J. and F. Scherbaum, 2008, "The Use and Misuse of Logic Trees in Probabilistic Seismic Hazard Analysis", *Earthquake Spectra*, Vol. 24, No. 4, pp. 997-1009.

Bojórquez, E., I. Iervolino, A. Reyes-Salazar and S. E. Ruiz, 2012, "Comparing Vector-Valued Intensity Measures for Fragility Analysis of Steel Frames In the Case of Narrow-band Ground Motions", *Engineering Structures*, Vol. 45, pp. 472-480.

Bradley, B. A., 2010, "A Generalized Conditional Intensity Measure Approach and Holistic Ground Motion Selection", *Earthquake Engineering and Structural Dynamics*, Vol. 39, No. 12, pp. 1321-1342.

Building Seismic Safety Council (BSSC), 2009, *NEHRP Recommended Seismic Provisions for New Buildings and Other Structures (FEMA P-750)*, 2009 edition, Report prepared for the Federal Emergency Management Agency (FEMA), National Institute of Building Sciences, Washington, D.C.

Buratti, N., P. J. Stafford and J. J. Bommer, 2011, "Earthquake Accelerogram Selection and Scaling Procedures for Estimating the Distribution of Drift Response", *ASCE Journal of Structural Engineering,* Vol. 137, pp. 345–357.

Campbell, K. W. and Y. Bozorgnia, 2008, "NGA Ground Motion Model for the Geometric Mean Horizontal Component of PGA, PGV, PGD and 5% Damped Linear Elastic Response Spectra for Periods Ranging from 0.01 to 10 s", *Earthquake Spectra*, Vol. 24, No. 1, pp. 139-171.

Carballo, J. E. and C. A. Cornell, 2000, *Probabilistic Seismic Demand Analysis: Spectrum Matching and Design*, Reliability of Marine Structures Program, Department of Civil Engineering, Stanford University.

CEN, 2003, *Eurocode 8: Design of Structures for Earthquake Resistance, Part 1: General rules, seismic actions and rules for buildings, Final Draft*, Brussels, Belgium, prEN199.8.

Chadwell, C. B. and R. A. Imbsen, 2002, *XTRACT-Cross Section Analysis Software for Structural and Earthquake Engineering*, TRC, Rancho Cordova, CA.

Chiou, B., R. Darragh, N. Gregor and W. Silva, 2008, "NGA Project Strong-Motion Database", *Earthquake Spectra*, Vol. 24, No. 1, pp. 23-44.

Cimellaro, G. P., A. M. Reinhorn, A. D'Ambrisi and M. De Stefano, 2009, "Fragility Analysis and Seismic Record Selection", *Journal of Structural Engineering*, Vol. 137, No. 3, pp. 379-390.

Conte, J. P., H. Pandit, J. P. Stewart and J. Wallace, 2003, "Ground Motion Intensity Measures for Performance-Based Earthquake Engineering". *Proc. 9th ICASP*.

Cordova, P. P., G. G. Deierlein, S. S. F. Mehanny and C. A. Cornell, 2001, "Development of a Two-Parameter Seismic Intensity Measure and Probabilistic Assessment Procedure", *The Second U.S.-Japan Workshop on Performance-Based Earthquake Engineering Methodology for Reinforced Concrete Building Structures*, Sapporo, Hokkaido, pp. 187-206.

Corigliano, M., C. G. Lai, M. Rota and C. L. Strobbia, 2012, "ASCONA: Automated Selection of Compatible Natural Accelerograms", *Earthquake Spectra*, Vol. 28, No. 3, pp. 965-987.

Cornell, C. A., 1968, "Engineering Seismic Risk Analysis", *Bulletin of the Seismological Society of America*, Vol. 58, No. 5, pp. 1583-1606.

Cornell, C. A. and H. Krawinkler, 2000, *Progress and Challenges in Seismic Performance Assessment*, PEER Center News, Vol. 3, pp. 1-3.

Cornell, C. A., F. Jalayer, R. O. Hamburger and D. A. Foutch, 2002, "Probabilistic Basis for 2000 SAC Federal Emergency Management Agency Steel Moment Frame Guidelines", *Journal of Structural Engineering*, Vol. 128, No. 4, pp. 526-533.

CSI, 2014, *PERFORM-3D*, Computers and Structures, Inc., Berkeley, CA.

Cullen, A. C. and H. C. Frey, 1999, *Probabilistic Techniques in Exposure Assessment: A Handbook for Dealing with Variability and Uncertainty in Models and Inputs*, Springer Science & Business Media.

Dempster, A. P., N. M. Laird and D. B. Rubin, 1977, "Maximum Likelihood from Incomplete Data via the EM Algorithm", *Journal of the Royal Statistical Society*, Vol. 39, No. 1, pp. 1-38.

Ellingwood, B. R., O. C. Celik and K. Kinali, 2007, "Fragility Assessment of Building Structural Systems in Mid-America", *Earthquake Engineering and Structural Dynamics*, Vol. 36, No. 13, pp. 1935-1952.

FEMA 273, 1997, *NEHRP Guidelines for the Seismic Rehabilitation of Buildings*, prepared by the Building Seismic Safety Council for the Federal Emergency Management Agency, Washington, D.C, FEMA Publication No. 273.

FEMA 356, 2000, *Commentary for the Seismic Rehabilitation of Buildings*, FEMA-356, Federal Emergency Management Agency, Washington, DC.

Gasparini, D. A. and E. H. E. J. Vanmarcke, 1976, *Simulated Earthquake Motions Compatible with Prescribed Response Spectra*, Massachusetts Institute of Technology, Department of Civil Engineering, Constructed Facilities Division.

Hancock, J. and J. J. Bommer, 2006, "A State-of-Knowledge Review of the Influence of Strong-Motion Duration on Structural Damage", *Earthquake Spectra*, Vol. 22, No. 3, pp. 827-845.

Hancock, J., J. Watson-Lamprey, N. A. Abrahamson, J. J. Bommer, A. Markatis, E. M. M. A. McCOY and R. Mendis, 2006, "An Improved Method of Matching Response Spectra of Recorded Earthquake Ground Motion Using Wavelets", *Journal of Earthquake Engineering*, Vol. 10, pp. 67-89.

Hanks, T. C. and C. A. Cornell, 1994, "Probabilistic Seismic Hazard Analysis: A Beginner's Guide", *Proceedings of the Fifth Symposium on Current Issues Related to Nuclear Power Plant Structures*, Equipment and Piping.

Haselton, C. B., J. W. Baker, Y. Bozorgnia, C. A. Goulet, E. Kalkan, N. Luco, T. Shantz, N. Shome, J. P. Stewart, P. Tothong, J. Watson-Lamprey and F. Zareian, 2009, *Evaluation of Ground Motion Selection and Modification Methods: Predicting Median Interstory Drift Response of Buildings*, PEER Technical Report 2009/01, Berkeley, California, 288p.

Haselton, C. B., A. S. Whittaker, A. Hortacsu, J. W. Baker, J. Bray and D. N. Grant, 2012, "Selecting and Scaling Earthquake Ground Motions for Performing Response-History Analyses", *Proceedings of the 15th World Conference on Earthquake Engineering*.

Haselton, C. B., A. Fry, J. W. Baker, R. O. Hamburger, A. S. Whittaker, J. P. Stewart, K. J. Elwood, N. Luco, J. D. Hooper, F. A. Charney, 2014, "Response History Analysis for the Design of New Buildings: Part I - Development of Recommendations for the NEHRP Provisions and the ASCE/SEI 7 Standard", *Earthquake Spectra in review.*

Hines, E. M., L. G. Baise and S. S. Swift, 2010, "Ground-Motion Suite Selection for Eastern North America", *Journal of Structural Engineering*, Vol. 137, No. 3, pp. 358-366.

Huang, Y., A. S. Whittaker, N. Luco and R. O. Hamburger, 2011, "Scaling Earthquake Ground Motions for Performance-Based Assessment of Buildings", *Journal of Structural Engineering (ASCE)*, Vol. 137, No. 3, pp. 311–321.

IBC, 2006, *International Building Code*, International Code Council, Inc. 4051: 60478-5795.

IBC, 2012, *International Building Code*, International Code Council, Inc., Washington DC, United States.

Iervolino, I. and C. A. Cornell, 2005, "Record Selection for Nonlinear Seismic Analysis of Structures", *Earthquake Spectra*, Vol. 21, No. 3, pp. 685-713.

Iervolino, I., G. Manfredi and E. Cosenza, 2006, "Ground Motion Duration Effects on Nonlinear Seismic Response", *Earthquake Engineering and Structural Dynamics*, Vol. 35, No. 1, pp. 21-38.

Iervolino, I. and G. Manfredi, 2008, "A Review of Ground Motion Record Selection Strategies for Dynamic Structural Analysis", in O. S. Bursi and D. Wagg (eds.), *In Modern Testing Techniques for Structural Systems*, pp. 131-163, Springer Vienna.

Iervolino, I., G. Maddaloni and E. Cosenza, 2009, "A Note on Selection of Time-Histories for Seismic Analysis of Bridges in Eurocode 8", *Journal of Earthquake Engineering*, Vol. 13, No. 8, pp. 1125-1152.

Iervolino, I., C. Galasso, R. Paolucci and F. Pacor, 2011, "Engineering Ground Motion Record Selection in the ITalian ACcelerometric Archive", *Bulletin of Earthquake Engineering,* Vol. 9, No. 6, pp. 1761-1778.

Jalayer, F. and C. A. Cornell, 2003, *A Technical Framework for Probability-Based Demand and Capacity Factor (DCFD) Seismic Formats*, PEER Report, Pacific Earthquake Engineering Research Center, College of Engineering, University of California.

Jayaram, N., T. Lin and J. W. Baker, 2011, "A Computationally Efficient Ground-Motion Selection Algorithm for Matching a Target Response Spectrum Mean and Variance", *Earthquake Spectra*, Vol. 27, No. 3, pp. 797-815.

Joyner, W. B. and D. M. Boore, 1981, "Peak Horizontal Acceleration and Velocity from Strong-Motion Records Including Records from the 1979 Imperial Valley, California, Earthquake", *Bulletin of the Seismological Society of America*, Vol. 71, No. 6, pp. 2011-2038.

Kalkan, E. and A. K. Chopra, 2011, "Modal-Pushover-Based Ground Motion Scaling Procedure", *Journal of Structural Engineering (ASCE)*, Vol. 137, No. 3, pp. 298-310.

Katsanos, E. I., A. G. Sextos and G. D. Manolis, 2010, "Selection of Earthquake Ground Motion Records: A State-of-the-Art Review from a Structural Engineering Perspective", *Soil Dynamics and Earthquake Engineering*, Vol. 30, No. 4, pp. 157-169.

Katsanos, E. I. and A. G. Sextos, 2013, "ISSARS: An Integrated Software Environment for Structure-Specific Earthquake Ground Motion Selection", *Advances in Engineering Software*, Vol. 58, pp. 70-85.

Katsanos, E. I. and A. G. Sextos, 2015, "Inelastic Spectra to Predict Period Elongation of Structures under Earthquake Loading", *Earthquake Engineering and Structural Dynamics,* doi: 10.1002/eqe.2554.

Kircher, C. A., 2005, "Code Requirements for the Selection and Scaling of Ground Motion Records", *In Presentation made to the 2005 COSMOS Annual Meeting*.

Kottke, A. and E. M. Rathje, 2008, "A Semi-Automated Procedure for Selecting and Scaling Recorded Earthquake Motions for Dynamic Analysis", *Earthquake Spectra*, Vol. 24, No. 4, pp. 911-932.

Kramer, S. L., P. Arduino, and S. S. Sideras, 2012, *Earthquake Ground Motion Selection*, Washington State Transportation Center (TRAC), No. WA-RD 791.1.

Krawinkler, H., R. Medina and B. Alavi, 2003, "Seismic Drift and Ductility Demands and their dependence on ground motions", *Engineering Structures*, Vol. 25, No. 5, pp. 637-653.

Krinitzsky, E. L., 2002, "How to Obtain Earthquake Ground Motions for Engineering Design", *Engineering Geology*, Vol. 65, No. 1, pp. 1-16.

Kurama, Y. C. and K. T. Farrow, 2003, "Ground Motion Scaling Methods for Different Site Conditions and Structure Characteristics", *Earthquake Engineering and Structural Dynamics*, Vol. 32, No. 15, pp. 2425-2450.

Kwon, O. S. and A. Elnashai, 2006, "The Effect of Material and Ground Motion Uncertainty on the Seismic Vulnerability Curves of RC Structure", *Engineering Structures*, Vol. 28, No. 2, pp. 289-303.

Lin, T., C. B. Haselton and J. W. Baker, 2013, "Conditional Spectrum-Based Ground Motion Selection. Part I: Hazard Consistency for Risk-Based Assessments", *Earthquake Engineering and Structural Dynamics*, Vol. 42, No. 12, pp. 1847-1865.

Luco, N., L. Manuel, S. Baldava and P. Bazzurro, 2005, "Correlation of Damage of Steel Moment-Resisting Frames to a Vector-Valued Set of Ground Motion Parameters", *Proceedings of the 9th International Conference on Structural Safety and Reliability (ICOSSAR05)*.

Luco, N. and P. Bazzurro, 2007, "Does Amplitude Scaling of Ground Motion Records Result in Biased Nonlinear Structural Drift Responses?", *Earthquake Engineering and Structural Dynamics*, Vol. 36, pp. 1813-1835.

Luco, N. and C. A. Cornell, 2007, "Structure-Specific Scalar Intensity Measures for Near-Source and Ordinary Earthquake Ground Motions", *Earthquake Spectra*, Vol. 23, No. 2, pp. 357-392.

Mander, J. B., M. J. Priestley and R. Park, 1988, "Theoretical Stress-Strain Model for Confined Concrete", *Journal of Structural Engineering*, Vol. 114, No. 8, pp. 1804-1826.

McGuire, R. K., 2008, "Probabilistic Seismic Hazard Analysis: Early History", *Earthquake Engineering and Structural Dynamics*, Vol. 37, No. 3, pp. 329-338.

McLachlan, G. and D. Peel, 2004, *Finite Mixture Models*, John Wiley & Sons.

Naeim, F. and M. Lew, 1995, "On the Use of Design Spectrum Compatible Time Histories", *Earthquake Spectra*, Vol. 11, No. 1, pp. 111-127.

Naeim, F., A. Alimoradi and S. Pezeshk, 2004, "Selection and Scaling of Ground Motion Time Histories for Structural Design Using Genetic Algorithms", *Earthquake Spectra*, Vol. 20, No. 2, pp. 413-426.

NIST, 2011, *Selecting and Scaling Earthquake Ground Motions for Performing Response History Analysis*, NEHRP Consultants Joint Venture, NIST/GCR11-917-15.

NZS 1170.5, 2004, *Structural Design Actions. Part 5: Earthquake Actions*, New Zealand Standard, Wellington, New Zealand.

PERFORM 3D, 2006, *Nonlinear Analysis and Performance Assessment for 3D Structures*, User Guide, Version 4.

Pinho, R., M. Marques, R. Monteiro, C. Casarotti and R. Delgado, 2013, "Evaluation of Nonlinear Static Procedures in the Assessment of Building Frames", *Earthquake Spectra*, Vol. 29, No. 4, pp. 1459-1476.

Porter, K. A., 2003, "An Overview of PEER's Performance-Based Earthquake Engineering Methodology", *Proceedings of Ninth International Conference on Applications of Statistics and Probability in Civil Engineering*.

Porter, K., R. Kennedy and R. Bachman, 2007, "Creating Fragility Functions for Performance-Based Earthquake Engineering", *Earthquake Spectra*, Vol. 23, No. 2, pp. 471-489.

Prota, 2013, *Probina Orion – Bina Tasarım Sistemi 2013*, Teknik Özellikler, Ankara, Turkey.

Raghunandan, M. and A. B. Liel, 2013, "Effect of Ground Motion Duration on Earthquake-Induced Structural Collapse", *Structural Safety*, Vol. 41, pp. 119-133.

Rathje, E. M. and A. R. Kottke, 2007, "Procedures for Selection and Scaling of Earthquake Motions for Dynamic Response Analysis", *Proceedings of the First US-Italy Seismic Bridge Workshop*, Pavia, Italy.

Reiter, L., 1990, *Earthquake Hazard Analysis: Issues and Insights*, Columbia University Press, New York, 254 pp.

Reyes, J. C. and E. Kalkan, 2012, "How Many Records Should Be Used In An ASCE/SEI-7 Ground Motion Scaling Procedure?", Earthquake *Spectra*, Vol. 28, No. 3, pp. 1223-1242.

Risk Engineering, 2005, *EZ-FRISK: User's Manual*, Version 7.12, Boulder, Colorado.

Rossetto, T. and A. Elnashai, 2003, "Derivation of Vulnerability Functions for European-Type RC Structures Based on Observational Data", *Engineering Structures*, Vol. 25, No. 10, pp. 1241-1263.

Ruiz-García, J. and E. Miranda, 2006, "Residual Displacement Ratios for Assessment of Existing Structures", *Earthquake Engineering and Structural Dynamics*, Vol. 35, No. 3, pp. 315-336.

Sextos, A. G., E. I. Katsanos and G. D. Manolis, 2011, "EC8-Based Earthquake Record Selection Procedure Evaluation: Validation Study Based On Observed Damage of An Irregular R/C Building", *Soil Dynamics and Earthquake Engineering*, Vol. 31, No. 4, pp. 583-597.

Shinozuka, M., M. Q. Feng, J. Lee and T. Naganuma, 2000, "Statistical Analysis of Fragility Curves", *Journal of Engineering Mechanics*, Vol. 126, No. 12, pp. 1224-1231.

Shome, N. and C. A. Cornell, 1998, "Normalization and Scaling Accelerograms for Nonlinear Structural Analysis", *In Sixth US National Conference on Earthquake Engineering*, Seattle, WA.

Shome, N., C. A. Cornell, P. Bazzurro and J. E. Carballo, 1998, "Earthquakes, Records, and Nonlinear Responses", *Earthquake Spectra*, Vol. 14, No. 3, pp. 469-500.

Shome, N. and C. A. Cornell, 1999, *Probabilistic Seismic Demand Analysis of Nonlinear Structures,* Reliability of Marine Structures Report No. RMS-35, Department of Civil and Environmental Engineering, Stanford University.

Silva, W. J. and K. Lee, 1987, *WES RASCAL Code for Synthesizing Earthquake Ground Motions*, Department of the Army, US Army Corps of Engineers, Paper S-73-1, State-of-the-Art for Assessing Earthquake Hazards in the United States, Report 24.

Silverman, B. W., 1986, *Density Estimation for Statistics and Data Analysis*, Vol. 26, CRC press.

Stewart, J. P., S.-J. Chiou, J. D. Bray, P. G. Somerville, R. W. Graves and N. A. Abrahamson, 2001, *Ground Motion Evaluation Procedures for Performance Based Design*, Report No. PEER-2001/09, Pacific Earthquake Engineering Research Center.

TEC, 2007, *TEC-07 Specification For Buildings To Be Built In Seismic Zones*, Ministry of Public Works and Settlement, Government of Republic of Turkey, Ankara, Turkey.

Tothong, P. and Luco, N., 2007, "Probabilistic Seismic Demand Analysis Using Advanced Ground Motion Intensity Measures", *Earthquake Engineering and Structural Dynamics*, Vol. 36, No. 13, pp. 1837-1860.

Tothong, P. and C. A. Cornell, 2007, *Probabilistic Seismic Demand Analysis Using Advanced Ground Motion Intensity Measures, Attenuation Relationships, and Near-fault Effects*, PEER Report 2006/11, Pacific Earthquake Engineering Research Center, University of California, Berkeley.

Trifunac, M. D., 2012, "Earthquake Response Spectra for Performance Based Design—A Critical Review", *Soil Dynamics and Earthquake Engineering*, Vol. 37, pp. 73-83.

Turkish Standards Institute, 1997, *TS 498 Design Loads for Buildings*, Ankara, Turkey.

Turkish Standards Institute, 2000, *TS 500-2000 Requirements for Design and Construction of Reinforced Concrete Structures*, Ankara, Turkey.

Vamvatsikos, D., 2002, *Seismic Performance, Capacity and Reliability of Structures As Seen Through Incremental Dynamic Analysis*, Doctoral Dissertation, Stanford University.

Vamvatsikos, D. and C. A. Cornell, 2002, "Incremental Dynamic Analysis", *Earthquake Engineering and Structural Dynamics*, Vol. 31, No. 3, pp. 491-514.

Vamvatsikos, D. and C. A. Cornell, 2004, Applied Incremental Dynamic Analysis, *Earthquake Spectra*, Vol. 20, No. 2, pp. 523-553.

Wang, G., R. Youngs, M. Power and Z. Li, 2015, Design Ground Motion Library: An Interactive Tool for Selecting Earthquake Ground Motions, *Earthquake Spectra*, Vol. 31, No. 2, pp. 617-635.

Welch, B. L., 1947, "The Generalization of Student's' Problem When Several Different Population Variances Are Involved", *Biometrika*, Vol. 34, pp. 28-35.